Prepared for:

Rijkswaterstaat, Rijksinstituut voor Kust en Zee

Validation of a 3D temperature model for the North Sea with in-situ data and remote sensing data

February 1999

WL | delft hydraulics

Z2506.00

Validation of a 3D temperature model for the North Sea with in-situ data and remote sensing data

R.J. Vos, E.D. de Goede and R.E. Uittenbogaard

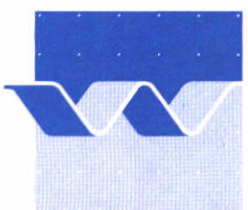

WL | delft hydraulics

WL | delft hydraulics

CLIENT:	DG Rijkswaterstaat Rijksinstituut voor Kust en Zee (RIKZ) Kortenaerkade 1 Den Haag
TITLE:	Validation of a 3D temperature model for the North Sea with in-situ data and remote sensing data

ABSTRACT:

In the present report, an important step towards full integration of temperature data and temperature modelling results is set. Hereto, the period April to December 1989 was selected. For this period accurate and continuous vertical profile temperature measurements (with a thermistor chain) are available from NERC. Remote sensing sea surface temperature data (RS SST data) of the NOAA/AVHRR satellite were obtained from KNMI as daily images. Blended data sets of sea surface temperature from ship measurements and satellite data were obtained from BSH.

A combination of in-situ measured vertical temperature profiles and RS SST data in the horizontal plane is ideal for model validation. In-situ data serve to tune the heat balance and thermocline formation (1DV models can be used efficiently hereto to reduce the calibration effort), whereas SST data can be used for synoptic validation of model results.

A previous three dimensional temperature model for the North Sea on the NSM schematization was adapted for improved representation of the thermocline thickness, the break down of the thermocline after the summer, and an improved representation of SST. A thorough sensitive analysis with a 1DV point model suggested the addition of background eddy diffusivity with a value of 7.10^{-5} m^2/s. This analysis also showed that changes in parameters like wind drag coefficients, parameters of the turbulence model and of the heat flux model are less important. Also use of depth dependent intrusion of solar irradiation is less important. The new model has improved boundary conditions, space variable wind field and initial condition.

Results for 1989 are very good with respect to the thickness of thermocline and the thermocline formation. Shortcomings were found for 2 stations with respect to thermocline breakdown at the end of summer. In general, the modelled SST is in good agreement with RS SST data although some differences were found for the western part of the North Sea. Therefore, it is recommended to investigate the effect of spatial varying meteorological input for the heat flux model on the spatial SST distribution. As an alternative for the heat flux model, the use of SST from remote sensing as a forcing function for the surface temperature in the model may be considered.

It is recommended to validate the present model with INP mooring data, RS SST data from weekly composites and other ship data for 1994.

REFERENCES: Opdrachtbonnummer 22981444 d.d 08/06/98

VER.	ORIGINATOR	DATE	REMARKS	REVIEW	APPROVED BY
2.0	R.J. Vos, R.E. Uittenbogaard	18 Februari 1998	final report	E.D. de Goede	T. Schilperoort 19/5/98

PROJECT IDENTIFICATION:		Z2506						
KEYWORDS:		3D Temperature model, North Sea, k-epsilon model, remote sensing data, in-situ data						
CONTENTS:	TEXT PAGES	30	TABLES		FIGURES	53	APPENDICES	
STATUS:	☐ PRELIMINARY		☐ DRAFT		☒ FINAL			

Contents

1 Introduction

1.1 Introduction

Recently, a project ('REST3D') for integration of satellite remote sensing sea surface temperature data, in-situ data and 3-D temperature modelling results started. The project REST3D aims at the application of a methodology named RESTWAQ (Vos and Schuttelaar, 1995) for temperature models at North Sea scale. The typical 3D behaviour of temperature (due to stratification of sea water) makes that in-situ data and remote sensing sea surface temperature data are more or less complementary.

The full integration of various temperature data sources into a 3-dimensional hydrodynamic model as done in REST3D, is different from previous applications of RESTWAQ (Vos and Schuttelaar, 1995; Vos et. al., 1998) that considered suspended particulate matter (SPM). For SPM the largest uncertainties are the reliability of the data due to a large natural variability of SPM. Therefore, full integration of SPM sources of data and SPM modelling results was primarily required in order to reduce these uncertainties. For REST3D, temperature data show a much smaller natural variability, but the complementary character of the data sources still warrants a full integration.

In the present report, a first step towards full integration of temperature data and temperature modelling results is done. Hereto, a period was selected with accurate and continuous vertical profile temperature measurements (with a thermistor chain). Such data are only available for two periods at a limited number of locations:

1. For 1989 at six locations in the North Sea (NSP data set from NERC);
2. For 1994 for one location at Oyster grounds in the North Sea (INP mooring data set from DNZ).

The 1989 in-situ data set is clearly preferable. However, the 1994 remote sensing data set is much more complete (for 1989 only 10 images were available, of which some are partially cloud covered). Due to this incompleteness of data, it was decided to test the model performance for both 1989 and 1994. For 1989 the emphasis is on the thermistor chain in-situ data. For 1994 the emphasis is more on remote sensing sea surface temperature data. The 1994 simulations are also of much interest to RWS-DNZ that supplied the INP mooring data.

The 1989 and 1994 data set were completed by use of blended data sets, supplied by Pohlmann. These blended data sets are a combination of in-situ data of the surface and remote sensing data and were made by BSH manually.

In the present report, a model validation of a North Sea temperature model for 1989 is done. The 1994 simulations will be done in a next phase of the REST3D project. Parameter settings retrieved from the 1989 simulations will serve as input for the 1994 simulations.

1.2 Background

Knowledge of water temperature is of great importance to a variety of marine issues within the North Sea. For calculating substance transport and eutrophication effects a good representation of the 3-dimensional temperature field is important. In general, vertical mixing of water and substances are limited by the existence of a thermocline. Thus, water quality and ecological processes such as nutrient transport, primary production and oxygen depletion due to mineralisation highly depend on the 3D transport for which the temperature distribution is a good indicator. The dynamics of the thermocline (depth and stability) have a profound effect on the development of nuisance algae and other negative eutrophication effects like oxygen depletion and species shifts (De Wolf and Zijlstra, 1988; Obata et al., 1996; Ruardij et al., 1997).

The development of a dynamic 3-dimensional hydrodynamic model with accurate representation of the (vertical and horizontal) temperature distribution is seen as a vital first step towards a fully 3-dimensional water quality and eutrophication model of the North Sea, for which there is great interest at 'Rijkswaterstaat' (RIKZ and DNZ). Of particular importance is the ability to model the depth of the thermocline as well as duration and areal extent of thermal stratification with a time resolution of days-weeks. The synoptic 2-dimensional remote sensing sea surface temperature (RS SST) data provide valuable information which can be used together with in-situ data (vertical profiles) for correctly modelling temperature distribution.

Additional applications of RS SST and improved knowledge of water temperature can also be considered. For use in weather forecasts, actual SST data of the North Sea are an essential boundary parameter. An upgrade of satellite data correction procedures will provide a better data product for this purpose. There are also possibilities for sea temperature use in longer term assessments of climate and ecological status of the North Sea. Sea water temperature can be considered as a key indicator for global climate change. Such changes might coincide with changes in species composition, and periods and locations for spawning and recruitment of both commercial and non-commercial fish and shellfish species. A detailed knowledge of temperature in both space and time can be very helpful in analysing long-term biological changes.

Anticipated results of the BCRS project REST3D are:

- Completion of procedures for calibration/correction of RS SST images for use by multiple end users.
- Completion of a methodology for integrating RS SST with 3-dimensional models (as started in RESTWAQ 1) with refinement of cost functions for simultaneous assimilation of RS data and in-situ data.
- Participation of various end-users in the project for reconnaissance of the applicability of results and tools, and the possibilities for future implementation; Specifically, the link to North Sea Water Quality and eutrophication models is considered as an important follow-up to this project.

1.3 Objectives of this study

The present report focuses on a validation of a 3-D temperature North Sea model for 1989 using in-situ data for temperature, and using RS SST data.

The objectives are:

1. Completion of a temperature model for the North Sea (NSM) for 1989 that was started in an earlier project (Van Kester et al., 1997). The model is based upon the special TRIWAQ/TEM source code from RWS-RIKZ for temperature simulations;
2. Comparison of the model results with in-situ data from the North Sea project.
3. Comparison of the model results with blended data sets from BSH (Loewe 1994, Pohlmann 1995).

1.4 Contents of this report

Chapter 2 of this report is about the in-situ data, the remote sensing sea surface temperature data and the blended data sets of sea surface temperature. Chapter 3 of this report describes the model calibration (based on a 1DV point model for sensitivity analysis) and the model set up. It also discusses the model performance with respect to old model results. Chapter 4 deals with the data-model comparison. Conclusions and recommendations are given in Chapter 5.

1.5 Acknowledgement

We are grateful to Hans Roozekrans (KNMI), Johan de Kok (RIKZ) and Jan Van Kester (WL | Delft Hydraulics) for their contributions to this work. Thomas Pohlmann of IfM Hamburg is kindly thanked for supplying complete model results and the blended data sets of SST. Most plots in this report where made by Dick Verploegh (WL | Delft Hydraulics).

2 Data acquisition

2.1 In-situ data

In-situ data are (nearly) continuous measurements of temperature over the vertical water column for the North Sea for 1989. These data were measured by NERC for a project named 'North Sea project' (NSP). They were put on a CD-ROM for dissemination of the project results by the Natural Environmental Research Council (NERC) and the British Oceanographic data centre (BODC) (Lowry et al., 1992).
The NSP data set of 1989 is the only one in its kind, having 6 locations on the North Sea with a series of continuous 3-dimensional temperature measurements. These in-situ data were interpolated in time and space (over depth) for the 4 most relevant stations (A,B, C and D) by Van Kester et al. (1997, Figures 4.2.a-4.2.d) and are presented here in Figures 2.2 to 2.5. Figure 2.1 gives the location of these stations on the North Sea. For station A, the original non-interpolated data are given in Figure 2.2.b. The depth of the water column according to NERC is 85 m for station A, 52 m for station B, 60 m for station C, and 30 m for station D.

2.2 Remote sensing data

2.2.1 RS SST data from KNMI

Remote Sensing data on sea surface temperature were supplied by the KNMI (Roozekrans and Prangsma, 1988). Unfortunately, only a limited amount of RS data was available for 1989, since the routine archiving of SST data by KNMI started in 1990. Daily images were available for the following (12) moments:
8 March 1989, 12:23; 8 April 1989, 12:09; 21 April 1989, 13:18; 9 May 1989 13:35; 28 May 1989 12:00; 2 June 1989 12:49; 12 June 1989, 12:47; 18 June 1989, 13:26; 19 June 1989 13:15; 18 August 1989, 12:58; 23 August 1989, 12:06; 29 November 1989 13:25

All these images come from the NOAA-11 satellite and were recorded by the AVHRR radiometer, and subsequently processed by the KNMI. All images are partially cloud covered. All images are recorded at noon. Two images (21-4-89, 28-5-89) clearly show 'hot spots' (a local strong increase in the skin temperature of the sea due to large solar radiation, see Bijlsma et al., 1989) in the Northern part of the North Sea.

The images are plotted in Figures 2.6 to 2.17 (top of page).

2.2.2 Relation between skin temperature and bulk temperature

Radiometers on board of satellites measure the skin temperature of the sea, whereas in-situ data for surface temperature are usually obtained at one to a few meters below the sea

surface. This may lead to differences between in-situ data and remote sensing data. This section will discuss these differences.

RS SST assembled at noon may be slightly overestimated with respect to in-situ data measured in the top first meter of the water column. Robinson (1984) found that the difference between skin temperate and bulk temperature amounts maximally 0.5 °C. However, images obtained during morning time may clearly underestimate the sea surface temperature considerably (1-2 °C, de Valk 1997) whereas night images are clearly in best agreement with in-situ data (de Valk, 1997). Unfortunately, no such images are available for 1989.

Borst (1995) found a very good correlation (r=0.99) between satellite data (weekly composites) and in-situ data measured by WAVEC buoys at *one location.* The WAVEC buoys generate continuous time-series of temperatures which are averaged over every 10 minutes. These values were averaged again per week to one final weekly averaged in-situ result. The satellite measurement differs on average only 0.7 °C (rms-deviation) from this weekly averaged buoy measurement. Borst also found a high correlation between the WAVEC buoy data and in-situ data measured by a ship (Holland). This gave a correlation of 0.4 °C which suggest that there is a natural variability already of 0.4 °C in the data themselves due to local fluctuations of temperature. Subtracting this rms-error of 0.4 °C from the 0.7 °C reported by Borst one obtains 0.57 °C for the remainder. This is in close agreement with the estimate of the skin effect contribution reported by Robinson (0.5 °C, 1984).

When considering a correlation between *all ship-measured in-situ data and all SST data simultaneously* the deviation (the *bias*) has been found to be higher and goes up to 2 °C. This was found both by Borst (1995) and by Bijlsma et al. (1991). Summer images are clearly warmer (up to +2 °C) whereas winter images are colder (-2 °C) than in-situ data. After the elimination of images with hot spots (although realistic physical effects, they can not be used for model validation or comparison with in-situ data), or elimination of all images with a cloud coverage > 25%, these deviations are still found (Bijlsma et al., 1991). There is no explanation given by the authors for the observed bias of 2 °C with this procedure. Use of *continuous* in-situ measurements might reduce the rms-deviation of in-situ measurements considerably. This will require further study.

Recently, KNMI (de Haan, 1998) did a thorough validation of NOAA-SST values of the NOAA-12, NOAA-14 and NOAA-15 satellites for two periods (June and September) in 1998. They have found an overestimation in weekly composites of SST from satellites compared to in-situ data of 0.3-0.5 °C. However, for three daily composites an underestimation of 0.15 °C was found. In weekly composites the overestimation follows from the higher skin temperature with respect to bulk temperature for summer periods. Furthermore, weekly composites are based on maximum values of SST to exclude cloud effects (however, when a large difference in SST is observed between night and day images the night image is preferred). The three daily composites have more pixels that are affected by clouds. Such pixels are clearly too cold, and this leads to the observed underestimation. Differences in the bias of up to 0.7°C between the various satellites were also found, and this gives an estimate of the instrumentation errors and the errors in the SST algorithms

used for retrieving SST from raw satellite data. Unfortunately, it is not clear if this also holds for the NOAA-11 satellite used in this work.

Conclusions

- Differences of up to 2°C are sometimes found when comparing in-situ data with the RS SST images used in this work. However, in practice for most locations differences turn out to be much smaller. A difference up to 0.5 °C follows from a skin effect present in satellite data, but absent in the in-situ data. About 0.4 °C follows from the natural variability in SST. Only in a few cases higher deviations than 0.7°C are observed. Such deviations will need further analysis.
- Given the fact that daily images are used one must be careful with pixels that are partially cloud covered. For such pixels the RS SST temperature is underestimated. For other pixels, an overestimation of temperature may be expected since all images are around noon. This overestimation may be about +0.7°C in summer, but is less in other periods.

Recommendations

- It is recommended to investigate the agreement/disagreement between remote sensing SST data and in-situ measured SST data further in a follow up study for the 1994 period.

2.3 Blended data

Blended data are data that are a mixture of remote sensing data and in-situ data. The Bundesambt for Schiffart und Hydrographie (BSH) integrates routinely in-situ data on SST assembled from ship measurements on the North Sea (Loewe, 1995). These data are made synoptic only by an interpolation procedure in which isolines of temperature are drawn on basis of patterns observed in weekly composites of SST. The procedure was automated at the end of 1994 (according to an algorithm of NOAA, Reynolds 1988). Before this data, the isolines were drawn manually.

For 1989, weekly composites of blended data are available for nearly all weeks of the year. They were kindly supplied to RIKZ by Thomas Pohlmann from IfM-Hamburg (Institut fur Meereskunde). Pohlmann used these data as a forcing function of surface temperature in his temperature model of the North Sea (Pohlmann, 1994).

The blended data are plotted together with the RS SST data from NOAA in Figures 2.6-2.17. The blended data are at the bottom of the page.

2.4 Comparison of blended data with RS SST data

The RS SST data and blended data are in reasonable agreement, except for June 1989. However, the following differences are noted:

- The RS SST data show more detail, especially in the vicinity of the coast line. This is due to the fact that the blended data were projected on a rather coarse grid. Good examples are the images of 8 March and 29 November.

- The RS SST images are not synoptic due too cloud cover. At the edges where clouds are, sometimes cold spots are seen that are not in the blended data.
- The RS SST images sometimes show hot spots (especially 28 May). These hot spots are absent from the blended data, and thus were recognised by BSH as being artificial.
- The RS SST images for the summer period (12 June, 18 June, 19 June, 18 August and 23 August) have higher temperatures than the blended data. Differences are most pronounced in June. For 19 June differences even go up locally to 3 °C. It is not clear what causes these large deviations. Validation with ship data is required to judge the quality of RS SST data and blended data for June 1989. This latter validation can be done with the available NERC SST data at stations A and B (see Figure 2.02 and Figure 2.03). This shows that in June 1989 the BSH data at station A are approximately 1 °C *too cold* and RS SST data from KNMI are approximately 1 °C *too hot*. However, for station B, the BSH data are approximately 2 °C too cold, whereas the KNMI data remain approximately 1 °C too hot. Since the KNMI data are daily images, it may be expected that KNMI night images probably give the correct SST for June 1989. However, all RS SST images used here were around noon and this explains the overestimation in KNMI images for June 1989. The underestimation of temperature in BSH data may follow from the type of interpolation procedure that BSH uses. This will need further study.

Daily images suffer from too much cloud cover. Unfortunately, blended data set lack detail in coastal areas and do not show properly the influx of heat through Dover Strait. These drawbacks can possibly be circumvented by use of weekly composites from satellites as produced by KNMI. Unfortunately, these composites were not available at KNMI for 1989. They will be employed in a follow up study within the REST3D project for the 1994 period.

3 Model Set Up

3.1 Introduction

In 1997, a temperature model (based on the TRIWAQ/TEM code) was set up by WL | Delft Hydraulics (Van Kester et al.,1997) for RWS-RIKZ. The model simulation was done for 1 April 1989 till 1 December 1989. The model results were satisfactory given the small calibration effort that was possible at that time. Nevertheless, some shortcomings were observed with respect to thermocline thickness, break up of thermocline and some artificial peaks in sea surface temperature. These items are further discussed in Section 3.2.

At that time, the validation of model results with RS SST satellite data was not considered yet. Using the RS SST images employed in this study we see that (for Figures 6.10-6.14 of Van Kester et al.,1997):

- The inflow of water through Dover Strait at 12 may is too cold in the model (< 7 °C in model compared to 12.5 °C in RS data for 9 May);
- The inflow of water through Dover Strait at 8 July is probably too hot in the model (18-21 °C in model compared to 15 °C in RS data for 19 June, and 17.5 °C in RS data at 18 August);
- At the beginning of November the sea is already too cold in the model.

The RS SST images suggest that the sea surface in the previous simulation heats up too fast, and cools down to fast. Also the inflow of warm and cold water through Dover Strait is not correctly simulated. This might influence the formation and break off of the stratification layer in the northern part of the North Sea, since this adds an extra influx term of heat in this part of the North Sea.

In the present study an improved model is applied for 1989. This model aims at improvement of the above mentioned shortcomings. Besides some adjustments in meteorological forcing and boundary conditions, we first studied the sensitivity of the temperature distribution in vertical for some model parameters. Since 3D calculations are too demanding for such an analysis, we employed a 1DV point model (Uittenbogaard and Van Kester, 1996). The results of this analysis are of importance for the model set up and are presented in Section 3.2. The model set up is given in Section 3.3, whereas 3D model results are given in Section 3.4.

3.2 Tuning of turbulence model parameters to observed thermocline evolution

3.2.1 Introduction

Van Kester et al. (1997) report 3D-simulations on the thermocline evolution in the North Sea using the k-ε turbulence model and with actual meteorological wind and heat forcing for 1989. Comparing their results with the NERC data set for 1989 (Lowry et al., 1992) revealed the following.

- In deeper parts, see Figure 3.1 for site A at 85 metre depth, the simulated bed temperature remains constantly 5 ^{0}C whereas a gradual increase up to about 10 ^{0}C in Sept. '89 was observed.
- The simulated thermocline depth, defined from the water surface downwards, was too shallow compared to the observed 30 to 40 metres depth in Sept. '89 in site A.
- The simulated break down of the thermocline was too slow and lasted until the end of the year.
- Finally, the simulated Sea Surface Temperature (SST) revealed significantly larger values in August than observed.

These findings as well as shortcomings of the 3D-simulations were predicted also by using a computationally more efficient *point model* that solves vertically the same set of equations for the orthogonal horizontal velocity components, heat and turbulence properties as the 3D code. The point model is driven by the depth-averaged velocity vector which is copied from the appropriately tuned Continental Shelf Model for the particular site and with the same meteorological forcing, heat model and turbulence model as in the 3D simulations, including all other parameter setting. This numerical experiment is reported in (Van Kester et al., 1997a) which also demonstrates that changing the wind drag coefficient as well as the Dalton and Stanton numbers for the various contributions to the surface-heat flux did not significantly improve the simulated thermocline evolution.

Despite the fair success of previous simulations of flows and tides in the North Sea with that 3D code, the tentative conclusion was that the applied k-ε turbulence model could form the weakest link in estimating the thermocline evolution. This tentative conclusion is supported by general studies showing that most, if not all, turbulence models do not take into account the vertical mixing induced by the shearing and the breaking actions of short and random internal gravity waves.

In principle, the inclusion of such additional internal-wave-induced mixing is possible and was proposed first in (Uittenbogaard and Baron, 1989) using an additional transport equation for Internal Wave Energy, in the following abbreviated as IWE model. Uittenbogaard (1997) shows the importance of such an IWE model, combined with the k-ε model in his *point model*, by simulating then a deeper thermocline, the proper increase of bed temperature as well as correct breakdown of the thermocline in autumn.
In addition, the study (Uittenbogaard, 1997) demonstrates that alternative corrections to the k-ε turbulence model, such as using variants based on the RNG closure, did not notably

improve the results for simulating the thermocline development. Particularly, the latter study indicates that the turbulence production in the k-ε or RNG variants is insufficient inside the thermocline. The obvious route then would be the implementation of the IWE model in the 3D code but the temporarily approach is better tuning the turbulence model or its boundary conditions. The latter objective is the subject of this chapter and the next section summarises all past and current attempts including a version of the Mellor&Yamada model that we investigated in the context of our internal research.

3.2.2 Overview and main conclusion on all investigated modifications

The following summarises all variations investigated by using the point model mainly with the k-ε model:

1. Changing Dalton and Stanton numbers in the surface-heat flux model by a factor two, see (Van Kester et al., 1997).
2. Different models for the wind-drag coefficient C_D yielding at least twofold changes of C_D, see (Van Kester et al., 1997).
3. Changing the balance between turbulence production and its dissipation rate using RNG closures in the k-ε model, see (Uittenbogaard, 1997).
4. Changing the balance between turbulence production and its conversion rate, called buoyancy flux, into potential energy by using so-called damping functions for the turbulence Prandtl/Schmidt number, see (Uittenbogaard and Van Kester, 1996).
5. Including turbulence production by short and random internal waves through the IWE model, see (Uittenbogaard, 1997).
6. Increasing the turbulence Prandtl/Schmidt σ_T number by a factor up to 40 (present study).
7. Changing surface boundary conditions for Turbulent Kinetic Energy (TKE) yielding larger near-surface mixing (present study).
8. Reducing coefficient c_μ in the k-ε model (present study), although c_μ remains flow-independent.
9. Adding buoyancy flux to the ε-equation (present study).
10. Adding a background eddy viscosity (present study) in all equations.
11. Adding a background eddy diffusivity to just heat diffusion (present study).
12. Addition of distributed absorption of solar-heat flux (present study).
13. Applying the Quasi-Equilibrium 2.5 level Mellor&Yamada turbulence model (present study).

The main conclusion of the present study and previous studies reads as follows. *The simulation of thermocline evolution in the North Sea is improved only through increasing vertical mixing of heat.* Within the limitations of this study, *we recommend the addition of a background eddy-diffusivity, just in the heat diffusion equation, of* 7.10^{-5} *m²/s to the eddy diffusivity predicted by the k-ε model.* If this increase is applied then we infer that the modelled heat flux is too small because the simulated surface temperature is below observations. The latter conclusion is tentative because horizontal advection of heat may play a role that we could not investigate with the point model. The arguments yielding the previous conclusion are presented in Section 3.2.4 which requires understanding the

essence of the applied k-ε turbulence model and, therefore, the latter is introduced first in Section 3.2.3

3.2.3 Brief overview of applied model concepts

For discussing the prominent attempts of improving thermocline simulations, first a summary of the k-ε model is given in this section.

The definitions of eddy viscosity ν_T, eddy diffusivity Γ_T and turbulence Prandtl/Schmidt number σ_T read:

$$\upsilon_T = c_\mu \frac{k^2}{\varepsilon} \quad ; \quad \Gamma_T = \frac{\upsilon_T}{\sigma_T} \quad , \tag{3.1}$$

with k turbulent kinetic energy (TKE), its dissipation rate ε and coefficient c_μ=0.09 calibrated such that near the bed holds:

$$k = \frac{u_*^2}{\sqrt{c_\mu}} \approx 3.3 u_*^2 \quad , \tag{3.2}$$

with u_* the bed-shear velocity. Detailed observations, show that, even in stably-stratified flows,

$$\sigma_T \equiv \sigma_{T,0} \approx 0.7 \tag{3.3}$$

holds for mixing of momentum and mass by turbulent motions only. The mixing coefficients (3.1) appear in the following transport equation for TKE by the k-ε model:

$$\frac{Dk}{Dt} = D_k + P - B - \varepsilon \quad ; \quad P = \upsilon_T S^2 \quad ; \quad B = \Gamma_T N^2 \quad , \tag{3.4a}$$

$$\text{with} \quad S^2 = \left(\frac{\partial U}{\partial z}\right)^2 + \left(\frac{\partial V}{\partial z}\right)^2 \quad ; \quad N^2 = -\frac{g}{\rho}\frac{\partial \rho}{\partial z} \quad . \tag{3.4b}$$

In the RHS of (3.4a), the first term D_k is diffusion of TKE, P is turbulence production proportional to shear rates squared, and B is the buoyancy flux, positive for stable stratification, with z upward. The contribution of horizontal shear rates to S^2 is not significant for the present large-scale simulations.

The most important closures of the ε-equation are scaled versions of the k-equation and then the ε-equation reads:

$$\frac{D\varepsilon}{Dt} = D_\varepsilon + P_\varepsilon - B_\varepsilon - \varepsilon_\varepsilon \quad ; \quad \omega = \frac{\varepsilon}{k} \quad ; \quad P_\varepsilon = c_{1\varepsilon} P\omega \quad ; \quad \varepsilon_\varepsilon = c_{2\varepsilon}\,\varepsilon\,\omega \quad ; \quad B_\varepsilon = c_{3\varepsilon} B\omega \quad , \text{(3.4c)}$$

with inverse time scale ω and coefficients $c_{i\varepsilon}$ calibrated for i=1,2 in neutrally-stratified flows. The role of the buoyancy flux in the ε-equation has been and still is subject of much dispute. Physical arguments suggest the following assumption:

$$N^2 > 0: \quad c_{3\varepsilon} = 0 \quad ; \quad N^2 < 0: \quad c_{3\varepsilon} = 1.0 \qquad \text{(3.4d)}$$

i.e. switching on the buoyancy flux (scaled by ω) only when the flow is unstably-stratified because then Rayleigh-Taylor instabilities grow the fastest at the small scales where ε collects most of its contribution. The closure (3.4d) is applied in our implementation of the k-ε model.

The inclusion of the IWE model involves adding to the original k-equation the transfer rate $T_{i\to t}$ (TKE source) of energy from internal waves to turbulence as well as the excitation $T_{t\to i}$ (TKE sink) of internal waves by turbulence:

$$\frac{Dk}{Dt} = D_k + P - B - \varepsilon + T_{i\to t} - T_{t\to i} \qquad \text{(3.5a)}$$

and correspondingly with the scaling of source and sinks in the ε-equation

$$\frac{D\varepsilon}{Dt} = D_\varepsilon + P_\varepsilon - B_\varepsilon - \varepsilon_\varepsilon + c_{1\varepsilon}\omega\left(T_{i\to t} - T_{t\to i}\right) \quad ; \quad \omega = \frac{\varepsilon}{k} \quad . \qquad \text{(3.5b)}$$

The transfer rate $T_{t\to i}$ is important outside the thermocline whereas the TKE-source $T_{i\to t}$ is essential at the stably-stratified levels inside the thermocline where the excited internal gravity waves attain their largest amplitude as well as the highest probability of breaking (TKE production).

This ends the introduction of our version of the k-ε turbulence model as well as the additional of internal-wave generated turbulence. The next section uses these concepts for explaining the most significant findings, announced by Section 3.2.2.

3.2.4 Discussion

The marginal sensitivity of the simulated thermocline development either by changing the heat input (points 1 and 2, Section 3.2.2) or by changing the turbulence conditions (points 2 and 7, Section 3.2.2) near the water surface indicates that the heat flux, within reasonable limits, as well as the simulated state of turbulence above the thermocline is not essential for changing its depth or changing the heat flux to the bed-boundary layer.

Changing the mutual ratio between turbulence production and dissipation by using an RNG closure (point 3, Section 3.2.2) does not improve the simulation of the thermocline either: the RNG k-ε model hardly increases the turbulence production in this particular case.

Several of these adjustments, having marginal influences on the thermocline, can be understood by the following two feedback mechanisms.

Firstly, an increase in TKE would yield a larger eddy viscosity but also a smoother velocity profile for a given wind shear stress and this smoother profile reduces the shear rates in S^2 and the TKE production is increased less than proportionally with eddy viscosity.

Secondly, changing coefficient c_μ, although still kept flow-independent, affects both the eddy viscosity and the eddy diffusivity such that the ratio:

$$\frac{B}{P} = \frac{Ri}{\sigma_T} \quad \text{with} \quad Ri = \frac{N^2}{S^2} \tag{3.6}$$

between buoyancy flux B and TKE production P remains unaltered; here Ri is the so-called gradient Richardson number. Changing c_μ is motivated by detailed analysis of the closures of the k-ε model that show a dependence of c_μ on the ratio P/ε.

In view of (3.6), the obvious influence would come from increasing the turbulence Prandtl/Schmidt number σ_T because that would reduce the buoyancy flux B, being a TKE sink under stable stratification. The argumentation for increasing σ_T under stable stratification is that not all vertical exchange of horizontal momentum is due to turbulence whereas vertical mixing of heat is due to just turbulence (and negligible molecular motions). Uittenbogaard (1995) has substantiated this classical opinion, proposed first by G.I. Taylor (1931), through estimating the contribution of internal waves in the various vertical exchange processes.

Instead of modelling this action of internal waves, a suite of supposedly-universal models, called damping functions, for σ_T as function of Ri has been proposed. The first problem of using these functions is that they induce a mathematical bifurcation i.e. yielding the creation of step-like vertical profiles of density, see the examples in (Uittenbogaard and Van Kester, 1996) for the thermocline problem and in (Van Kester et al., 1994) for other turbulence models in salt-stratified flows.

The following explains the second feedback phenomenon which is essential for thermocline problems. Neglecting molecular contributions, the vertical heat flux Q, as modelled by turbulence closures of the eddy viscosity type, reads:

$$Q = -\rho c_p \Gamma_T \frac{\partial \theta}{\partial z} = -\rho c_p \frac{\upsilon_T}{\sigma_T} \frac{\partial \theta}{\partial z} \tag{3.7}$$

with specific heat coefficient c_p. Using the thermal expansion coefficient of sea water, the vertical temperature gradient is proportional to the vertical density gradient and thus the buoyancy flux B is proportional to the local vertical heat flux Q. The latter flux, however, is prescribed at the water surface by a heat flux model. Consequently, buoyancy flux B, as TKE sink, is mainly controlled by the heat flux model and it is fairly independent of σ_T. This subject has been discussed extensively in (Uittenbogaard and Van Kester, 1996) and this concept explains the correct rate at which the thermocline deepens when there is no heat flux through the thermocline, which is a fair approximation.

For the present study, additional runs were made with significantly larger σ_T, either independent or depending on the gradient Richardson number, yet the thermocline development is not affected notably and this confirms the findings in (Uittenbogaard and Van Kester, 1996).

With reference to the list of variations given in Section 3.2.2, we now arrive at point 9 about changing the coefficient $c_{3\varepsilon}$ that controls the role of buoyancy flux in the ε-equation (3.4c). Figure 3.2 presents results with the following settings

$$N^2 > 0: \quad c_{3\varepsilon} = 0.5 \quad ; \quad N^2 < 0: \quad c_{3\varepsilon} = 1.0 \quad . \tag{3.8}$$

This choice, when applied in the ε-equation (3.4c), reduces ε under stable stratification. Figure 3.2 shows that this proposal does indeed affect the breakdown of the thermocline in autumn but it does not improve the evolution of the bed temperature nor the thermocline depth during summer. For $c_{3\varepsilon}$=0.8 the same conclusion holds, although the simulation exploded due to an unrealistically-large eddy viscosity of about 1 m^2/s just below the water surface. The latter occurred during the breakdown of the thermocline in autumn. No attempts were made to solve that problem.

In an attempt to mimic the augmented turbulence production by input from random internal waves, a background eddy-viscosity υ_0 is added to the eddy viscosity of (3.1) through

$$\upsilon_T = \upsilon_0 + c_\mu \frac{k^2}{\varepsilon} \quad ; \quad \Gamma_T = \frac{\upsilon_T}{\sigma_T} \quad . \tag{3.9a}$$

Notice that this addition is applied to all appearances of eddy viscosity/diffusivity in the momentum equations, in the heat balance as well as in all diffusion and source/sink terms of the k-ε model.

Consequently, this addition intends increasing the turbulence production P with $\upsilon_0 S^2$ that depends just weakly on the turbulence state. Notice that if no eddy viscosity were predicted directly by the k-ε model then the ratio between buoyancy flux and production is not reduced, see (3.7) which is independent of eddy viscosity. Consequently, the k-ε model response would not improve directly through the addition of the background viscosity υ_0.

Nevertheless, in case of k=0, the mixing of heat continues and (3.7) shows that the magnitude of the temperature gradient $\partial\theta / \partial z$ is limited to a maximal value which is inversely proportional to υ_0. Limiting the vertical temperature gradient has the following two consequences:
Firstly, a heat flux through the thermocline is maintained and this increases the bed temperature.
Secondly, of course, the magnitude of the vertical density gradient is limited as well and this limits the buoyancy flux as a significant drain for TKE. Conversely, limiting the buoyancy flux promotes a rapid growth of TKE mixing under moderate stratification conditions and thus a limited buoyancy flux promotes.

Figure 3.3 presents the results of (3.7) for $\upsilon_0=1.10^{-4}$ m^2/s (i.e. 1 cm^2/s), Figure 3.4 for $\upsilon_0=5.10^{-5}$ m^2/s and Figure 3.4a shows several properties, averaged over Day 240, of the simulation of Figure 3.4.

On Day 240 (Figure 3.4a), the thermocline depth, as indicated by the minimal vertical density gradient, is about 30 metres and the bed temperature is then 8^0 C. Both results correspond well the NERC data for this site. Comparing Figure 3.4a with 3.1 shows the smoothing influence of the background viscosity on turbulence properties and vertical density gradient, of course. Below we add comments to the overall heat balance.

Of all variations applied in this study, Figure 3.4 matches the NERC data the best in terms of increasing bed temperature as well as thermocline breakdown in autumn. Notice, however, that the SST responses in August (Day 240) are significantly tempered when compared with the NERC observations with SST's in August well above 15^{0}C while Figure 3.4a shows 12^{0}C instead. Compared to Figure 3.1, the surface-heat flux for Figure 3.4 is hardly changed by the addition of a background viscosity and moreover the cooler sea (Figure 3.4) would have received even more heat than in the original simulation (Figure 3.1).
The latter comparison then suggests that the heat flux model or its input underestimates the net heat flux to the sea if horizontal advection of heat may be excluded.

Figure 3.5, however, shows the temperature evolution with just a background viscosity of $\upsilon_0=5.10^{-5}$ m^2/s i.e. *excluding all contributions from a turbulence modelling*: the choice of background viscosity dominates the thermocline evolution and this choice makes the simulation highly subjective. Notice that this background viscosity corresponds to a background eddy diffusivity of 7.10^{-5} for the turbulent Prandtl/Schmidt of 0.7 applied by us.

Figure 3.6 shows the best result of this study, using the previous background eddy diffusivity in the heat diffusion equation only and with the k-ε turbulence model and momentum equations still using the eddy viscosity as predicted by the turbulence model.

An interesting point is the correspondence of the previous findings and Munk's (1966) classical estimate of the vertical mixing coefficient of heat in the oceans for matching the global heat balance. Munk's so-called *Abyssal Recipes* suggest $\upsilon_0=1$ cm^2/s which is very

close to our choice for background eddy diffusivity of 7.10^{-5} m^2/s using υ_0/σ_T with $\upsilon_0=5.10^{-5}$ m^2/s.

At this point we like to refer to the previous study (Van Kester et al., 1997) which included varying the wind drag coefficient C_D which showed a marginal effect when varied between 0.001 and 0.002. As an amplified illustration of the limited role of the wind drag coefficient, we refer to Figure 3.15 for a very large C_D of 0.004. Compared with Figure 3.1, Figure 3.15 shows a deeper thermocline while the bed temperature is not increased at all. Figure 3.15 thus underlines the importance of mixing and turbulence generation *inside* the thermocline. The latter internal mixing is capable of maintaining a heat flux through the thermocline rather than erosion from above (by the wind).

Figure 3.7, 3.8 and 3.9 show the thermocline evolution for other variations of adding a background eddy viscosity/diffusivity to just the momentum equations or k-ε model. Compared with Figures 3.4, 3.5 and 3.6, these figures demonstrate the dominance of increasing the vertical diffusion of heat in its balance equation compared to momentum of turbulence balances.

Figure 3.5 shows that adding a background eddy viscosity of 5.10^{-5} m^2/s in conjunction with a background eddy diffusivity of 7.10^{-5} m^2/s in all relevant equations yields the correct thermocline depth, the correct increase in bed temperature and the correct breakdown of the thermocline in autumn. The simulated sea-surface temperature, however, is now lower than observed and this suggests that the seasonal heat flux to this site is underestimated or that horizontal advection of heat plays a role.

Therefore, our first recommendation is adding to the vertical heat diffusion only, a background eddy diffusivity of 7.10^{-5} m^2/s to the eddy diffusivity predicted by the k-ε model.

Finally, as part of another research project, we examined the performance of the Mellor&Yamada level 2.5 model (Mellor and Yamada, 1982) using the corrections on the original stability functions as well as on truncating the length scale (ℓ) in that model as proposed by (Galperin et al., 1988). These corrections were needed for yielding realizability, robustness as well as for preventing the bifurcation problem of the creation of step-like vertical profiles of density rather than smooth profiles, see the examples in (Uittenbogaard and Van Kester, 1996) for the thermocline problem and in (Van Kester et al., 1994) for other turbulence models in salt-stratified flows.

In conjunction with the Mellor&Yamada model, the latter bifurcation problem was reported in detail by (Deleersnijder and Luyten, 1994) and the bifurcation vanished with the corrected stability functions. The corrections on the stability functions imply an assumption on quasi-equilibrium between turbulence production and buoyancy flux. The corrected model is therefore designated by Galperin et al. (1988) as the Quasi-Equilibrium Mellor&Yamada (QEMY) model.
Using our notation, below the role of the stability functions in the QEMY is explained briefly. In the QEMY, the eddy diffusivity and eddy viscosity are defined by

$$\Gamma_T = S_b \ell \sqrt{2k} \quad ; \quad \upsilon_T = S_u \ell \sqrt{2k} \quad , \tag{3.10a}$$

with stability functions S_b and S_u depending on turbulence and stratification through the quasi-equilibrium formulations

$$G_H = -\frac{N^2 \ell^2}{2k^2} \quad ; \quad S_b = \frac{c_{b1}}{1 - c_{b2} G_H} \quad ; \quad S_u = \frac{c_{u1} - c_{u2} G_H}{(1 - c_{u3} G_H)(1 - c_{u4} G_H)} \tag{3.10b}$$

and coefficients c_{bi} and c_{ui} calibrated to stably-stratified boundary layers. In addition, Galperin et al. (1988) derive the following restrictions on length scale

$$\ell^2 \le \frac{-G_{H,\min} q^2}{\max\left(0, N^2\right)} \quad , \tag{3.10c}$$

and on the stability parameter

$$G_{H,\min} \le G_H \le G_{H,\max} \text{ with } G_{H,\min} = -0.28 \quad ; \quad G_{H,\max} = 0.0233 \quad . \tag{3.10d}$$

The upper part of Figure 3.10 shows the dependence (3.10b) within the limits imposed by (3.10d) and the stability function are compared to the flow independent coefficient c_μ =0.09 of the k-ε model. An interesting subject, not considered in (Galperin et al., 1988) nor in (Deleersnijder and Luyten, 1994), is whether the QEMY allows for turbulence at larger gradient Richardson number (Ri) than the k-ε model does. The extension of (modelled) turbulence to larger Ri is considered as of the principle reasons for applying stability or damping functions.

Of importance, for this subject, are considerations about so-called local equilibrium of the turbulence equations when diffusion and advection is neglected, for stationary TKE this yields P-B-ε=0. Usually, the ratio B/P between buoyancy flux B and turbulence production P is considered while recognising that ε plays a dominant role. The ratio B/P, therefore, yields a truncation value of Ri beyond which the modelled TKE cannot exist. Experiments suggest a maximal ratio B/P of 0.25 and the truncation then follows from

$$\text{QEMY:} \quad \frac{B}{P} = \frac{S_b}{S_u} Ri \le 0.25 \quad ; \quad \text{k}-\varepsilon \text{ model:} \quad \frac{B}{P} = \frac{Ri}{\sigma_T} \le 0.25 \tag{3.11a}$$

or

$$\text{QEMY:} \quad Ri \le 0.25 \frac{S_u}{S_b} \quad ; \quad \text{k}-\varepsilon \text{ model:} \quad Ri \le 0.25 \sigma_T \tag{3.11b}$$

From the lower part of Figure 3.10 and (3.11b) follows that the truncation level of Ri is hardly increased by the QEMY. Further, the upper part of Figure 3.10 shows lesser mixing of the QEMY below the maximal Ri imposed by (3.11b). Consequently, we expect that the QEMY would yield lesser mixing than the k-ε turbulence model under stable stratification and thus a lesser performance of thermocline simulation than the k-ε turbulence model.

Nevertheless, Luyten (1996) reports good simulation performance of the QEMY for describing the thermocline evolution in the North Sea although " the erosion of the thermocline during the late summer and the autumn is clearly not represented by the (QEMY) model" (Luyten, 1996, p. 183).

Below ,the apparent contradiction with Luyten's findings is explained. Firstly, using all forcing conditions of Figure 3.1, the QEMY describes the thermocline evolution as shown in Figure 3.11a and Figure 3.11b. This figure underlines our previous analysis about the QEMY by showing a very poor downward penetration of heat supplied at the water surface. This reduced penetration is due to the reduction of mixing by the stability functions (3.10b).

The question thus reads: how could Luyten (1996) achieve a good performance with the QEMY? The essential point appears to be his description of heat input to the water. Luyten applies the following exponential distribution, based on absorption, of solar heat flux in the upper layers through:

$$H >> \lambda^{-1}: \quad \frac{dQ_{solar}(z)}{dz} = \lambda^{-1} Q_{solar}(0) \exp\left[-\lambda(H-z)\right] \quad , \tag{3.12}$$

with $Q_{solar}(0)$ the total solar-heat flux supplied to the water and Luyten (1996) selected λ=0.154 m^{-1}. The latter parameter setting corresponds to a reduction of total solar heat to 37% at a depth of 6.5 metre (e-folding depth) below the water surface.
Figure 3.12 presents the most important contributions to the total heat exchange with the water. Some of these contributions depend on SST and therefore on the performance of the simulation, including the turbulence model. Figure 3.12 is derived from the simulation of Figure 3.1 using the k-ε model. This figure clarifies the importance of the solar-heat flux in comparison to all other heat-exchange fluxes.

We applied (3.12) while keeping all other heat exchange as surface fluxes. Figure 3.13a then shows a marginal influence of (3.12) on the thermocline evolution as simulated by the k-ε turbulence model, see Figure 3.13b for the daily-average on Day 240 and compare this with Figure 3.1.

However, if the solar-heat absorption is distributed according to (3.12) and applied with the QEMY then its effect on thermocline evolution is significant, see Figure 3.14a and 3.14b and compare these with Figure 3.11. Our explanation is that due to the distributed solar-heat input the very poor mixing performance of the QEMY near the water surface is circumvented.

3.2.5 Conclusions

Until this study, our capability of modelling the evolution of the thermocline in the North Sea was:

- In deeper parts, see Figure 3.1 for site A at 85 metre depth, the simulated bed temperature remains constantly 5^{0}C whereas a gradual increase up to about 10^0 C in Sept. '89 was observed.

- The simulated thermocline depth, defined from the water surface downwards, is too shallow compared to the observed 30 to 40 metres depth in Sept. '89 in site A.
- The simulated break down of the thermocline is too slow and lasts until the end of the year.
- Finally, the simulated Sea Surface Temperature (SST) reveals significantly larger values in August than observed.

Given this status, below our conclusions, based on present as well as previous studies, all using a point model in principle with the standard k-ε model but with variations given below:

1. Changing the Dalton and Stanton numbers in the surface-heat flux model by a factor two, see (Van Kester et al., 1997), has a marginal influence on the simulated evolution of the thermocline.
2. Different models for the wind-drag coefficient C_D, yielding at least a twofold change of C_D, see (Van Kester et al., 1997), shows marginal effects. Increasing C_D dramatically up to 0.004 yields a deeper thermocline while the bed temperature remains constant.
3. Changing the balance between turbulence production and its dissipation rate using RNG closures in the k-ε model, see (Uittenbogaard, 1997), is insignificant for simulating the thermocline.
4. Changing the balance between turbulence production and its conversion rate, called buoyancy flux, into potential energy by using so-called damping functions for the turbulence Prandtl/Schmidt number, see (Uittenbogaard and Van Kester, 1996), has marginal influence on simulating the thermocline evolution. In addition, application of appropriate damping functions creates unexpected stepwise density profiles due to a mathematical bifurcation.
5. Including turbulence production by short and random internal waves through the IWE model, see (Uittenbogaard, 1997), yields the correct simulation of the thermocline at the site investigated.
6. Increasing the turbulence Prandtl/Schmidt σ_T number by a factor up to 40 (present study) is insignificant for simulating the thermocline.
7. Changing surface boundary conditions for Turbulent Kinetic Energy (TKE), yielding larger near-surface mixing (present study), is insignificant for simulating the thermocline.
8. Reducing coefficient c_μ in the k-ε model (present study), although c_μ remains flow-independent, is insignificant for simulating the thermocline.
9. Adding buoyancy flux to the ε-equation (present study) promotes the breakdown of the thermocline in autumn but it does not improve the simulation of the bed temperature nor the thermocline depth.
10. Adding a background eddy viscosity of 5.10^{-5} m^2/s as well as an eddy-diffusivity of 7.10^{-5} m^2/s in all relevant equations (present study) yields the correct thermocline depth, the correct increase in bed temperature and the correct breakdown of the thermocline in autumn. The simulated sea-surface temperature, however, is now lower than observed and this suggests that the seasonal heat flux to this site is underestimated or that horizontal advection of heat (that is not present in the 1DV model) plays a role.

11. Adding a background eddy diffusivity to just heat diffusion (present study) has practically the same effect as prescribed in point 10. Again, the simulated sea-surface temperature is now lower than observed.
12. Addition of distributed absorption of solar-heat flux (present study) hardly increases the thermocline depth using the k-ε turbulence model but adding this absorption improves the thermocline simulation when using Quasi-Equilibrium 2.5 level Mellor&Yamada turbulence model.
13. Applying the Quasi-Equilibrium 2.5 level Mellor&Yamada turbulence model (present study) with a distributed solar-heat absorption, does not yield better results than our standard simulation with the k-ε model without (or with) solar-heat absorption.

From all previous variations and their consequences we arrive at the following main conclusion of this chapter. Compared to our previous results, the thermocline simulation can be improved mainly by increasing the mixing *inside* the thermocline i.e. mixing at stably-stratified levels. Increasing the vertical mixing of heat by adding a constant 7.10^{-5} m^2/s background diffusivity yields correctly a deeper thermocline, an increasing bed temperature as well as the appropriate breakdown of the thermocline in autumn.

During the summer period, the latter fortunate results, however, yield a simulated sea-surface temperature lower than observed. Using a point model, the latter finding suggests an underestimated heat flux to the water either vertically by mixing or horizontally mainly by advection and therefore below our recommendations.

3.2.6 Recommendations

- For the site and forcing investigated, the recommended choice is 7.10^{-5} m^2/s as background eddy diffusivity, to be added to the eddy diffusivity predicted by the k-ε model, in the vertical heat diffusion of the heat balance.
- Rather than subjectively tuning the simulation we propose the objective addition of a so-called internal-wave-energy model that describes the additional turbulence production, and thus increase of turbulent mixing, inside the thermocline by breaking and shearing action of random internal waves. The latter are generated by wind, surface waves, the bed as well as more vigorous turbulence outside the thermocline.
- The simulation with the appropriately tuned background diffusivity, however, shows a simulated sea-surface temperature which is lower than observed. Therefore, we recommend an assessment of the total heat balance, both from observations as well as from 3D simulations. This assessment should clarify the importance of horizontal advection of heat to the site investigated.
- If horizontal advection of heat is marginal at the site investigated then we recommend adjusting the heat-flux model or its meteorological forcing with the purpose of increasing the seasonal heat flux to the water. This will be further discussed in the next Chapter of this report.

3.3 Set up of a 3 dimensional temperature model

The present temperature model (based on the TRIWAQ/TEM code) is an improved version of the temperature model by Van Kester et al. (1997). The model schematization is the North Sea Model (NSM), which is a grid of 105*96 computational elements using spherical co-ordinates. The model goes up to a latitude of 57 degrees and is part of the (Dutch) Continental Shelf Model (CSM8). The model uses 40 layers over depth, leading to a total of 403.200 computational elements. The number of active (not permanently dry) elements is about 200.000. The upper half of the water column consist of 26 layers with a fixed depth (1.5m) and the remainder are 14 sigma layers. However, for a depth less than 78m all layers are sigma layers (this implies that for most elements in the model only sigma layers are used). This subdivision guarantees that the top layers and layers around a thermocline are not thicker than 1.5m. The model simulation is for the period 1 April till 1 December 1989.

The hydrodynamic shallow water equations (3 momentum equations and a continuity equation for the water level) are solved in combination with transport equations for turbulent kinetic energy (k), the dissipation rate of turbulent kinetic energy (ε), and temperature (T) and salinity (S). Turbulence modelling generates the eddy viscosity (ν_T) for the momentum equations via a turbulence closure model, and gives the vertical diffusivity (Γ_T) which is employed for transport of temperature in vertical direction. The turbulence model is briefly described in Section 3.2.3.

The heat flux at the water surface is modelled according to a prescription by Proctor (see Van Kester et al., 1996 Appendix A). The heat flux model has the following meteorological input:

- wind speed (m/s);
- air temperature (°C);
- air pressure (mbar);
- humidity (%);
- cloudiness (fraction);

Solar irradiation (W/m^2) is calculated in the model as a function of latitude (for each grid point), day number and time. Time series for meteorological data for 1989 (but uniform in space) were used from the NOMADS data set (Proctor et al., 1997). These data are plotted in Van Kester et al. (1997, Fig. 4.1a-4.1e). Periods with low wind speeds (< 6 m/s) were observed for the last weeks of April and the first weeks of June. At the end of June, the mid of July and the beginning of August periods with high wind speeds (> 10 m/s) were observed. Cloudiness is low in May, but fluctuating in June (which is mostly clouded) and in July. Air temperature is smoothly changing and is in summer on average 16°C. Humidity is low at the end of April and May, but most often fluctuating around 80 %.

The most important changes with respect to the previous model (Van Kester et al., 1997) for 1989 are as follows:

1. Boundary conditions for temperature at the southern and northern boundary of the model grid are space- and time dependent temperatures specified by the user. In the previous study, temperature at the boundaries was determined by data computed with a

1DV temperature model. At present, these boundary conditions are determined from the Pohlmann model data (Pohlmann, 1996). This adaptation leads to the intrusion of relatively warm water in spring at the southern model boundary, and of relatively cold water in summer at this boundary, as observed in RS SST images (Borst 1995, in this report see Figures 2.6-2.17).

2. An initial condition for temperature at the sea surface was obtained from the blended data set of Pohlmann. Since at 1 April hardly any temperature gradients exist over the vertical of the water column, these data were also applied for all other layers. Thus, initially there is no stratification. The previous model used an initial condition which was uniformly 5 °C. The present values are closer to 6 °C for the central part of the North Sea, and show a warm plume of 7-8 °C for Dover Strait. This is as expected when linearly interpolating between satellite SST data for 8 March and 8 April 1989.
3. The background eddy diffusivity, to be added to the eddy diffusivity (as predicted by the k-ε model), was set to 7.10^{-5} m^2/s as recommended in Section 3.2. In the old model this was 1.10^{-7} m^2/s.
4. In the present study, the wind and pressure fields were taken variable in both time and space. They were taken from DNMI (for 1989), and transformed to the model grid of NSM. Note that these data were not used as input for the heat flux model. For that part of the simulation a spatial uniform wind was used.

3.4 Model results for 1989

3.4.1 Description of model results for 1989

In Chapter 4, model results will be compared to data. In this section only a short general comment on the model results is given. In this section, the data are only used in order to trace possible unrealistic errors in the model results. Figures of model results are presented in Chapter 4 for:

- vertical profiles at stations A to D: Figures 4.1 to 4.4;
- time histories for 4 layers at stations A to D: Figures 4.5 to 4.8;
- sea surface temperature distributions at the days that RS SST data are available: Figures 4.9 to 4.18.

First of all, we note that the modelled SST patterns change gradually in time from spring to summer as expected: there is a notably higher SST in Dover Strait in spring, but in summer the situation is reversed. Than there is a notably higher SST in the Central North Sea.

The time histories of temperature do not demonstrate a large difference in temperature between stations A and B (Figures 4.5 and 4.6). At station A stratification starts at the end of April. Stratification disappears at a depth of 30m (layer 20) in September, and for the total water column (layer 40 at 85m) at the end of October. Temperatures in layers 1 and 2 are similar, but both show large fluctuations during summer. Maximum temperatures are about 18-19 °C in June and July, when temperature differences between the surface and the

water column at 30m are largest. At station B (Figure 4.6) similar results are found, but stratification is somewhat less and ends about one month earlier than for station A.
The time history for station C (which is more to the south than A and B, see Figure 4.7), show smaller maximum temperatures at the surface, but higher temperatures at the bottom. This may be due too a smaller depth, and influence of advective transport of heat from Dover Strait. Station D (see Figure 4.8), which is even more to the south than C, the water column is well mixed all year, maximum temperatures are about 17 °C, and temperature fluctuations are smaller than for the other stations.

3.4.2 Comparison with old model results

Comparison with previous model results (Van Kester, 1997):

- Compared to the measured temperature profiles of the North Sea Project (NSP) data, the thickness of the thermocline for station A was too small in the previous model. The new model results for station B are very good with respect to thickness of the thermocline depth. Also results for station A, C and D are in agreement with the measured profiles.
- Compared to the old model results the unphysical jumps in temperature at the top of the water column are now absent. This is due to the increased background eddy diffusivity.
- The old model results showed at layer 20 hardly an increase in temperature for stations A, B and C. This increase is now clearly present.
- The old model results did not show any increase in temperature in the bottom layer. The present model results show an increase of temperature in the bottom layer, and a completely mixed water column in autumn which is in agreement with the data.

Conclusions:
Compared to old simulations by Van Kester et al. (1997), the increased background eddy viscosity in combination with the horizontal advection of heat from the model boundaries improved the model results significantly.

3.4.3 Comparison of 3D model and point model

Figure 3.4 shows temperatures at station A (depth 85m) obtained with the point model (1DV model) with the same parameter settings as for the 3D model. In this section, these are compared with the 3D modelling result shown in Figure 4.5. In-situ data from Figure 2.01 are shortly addressed as well. The most important difference (besides other differences) between the 3D modelling result and the 1DV model result is the horizontal advection of temperature.

Bottom temperatures are in good agreement for these simulations. Temperatures at a depth of 30m (55m above the bed) are in good agreement until the mid of July. Then, the 1DV model can no longer follow the sharp increase in temperatures that is observed in the 3D model, and the NERC in-situ data (Figure 2.2). Sea surface temperatures are too low for the point model compared with the in-situ data and the 3D model data. Maximum surface temperatures in the 3D model in summer are 13 °C, whereas the 3D model reaches sometimes even 20 °C. At the end of May, the SST is about 1 °C too cold in the point model compared to the data and the 3D model (these show 11 °C). Then, the sharp increase

of SST from 11°C to 15-17°C in the 3D model, and 14-15°C in the NERC in-situ data is not shown in the point model. The point model shows an SST of 12-13°C in June.

Most important, the 3D computation is in much better agreement with the data than the point model results for the top of the water column. These findings may suggest that the role of *advection in the heat balance of the Central North Sea is important for temperatures in the top of the water column*. This requires further study.

4 Comparison of model results with data

4.1.1 Time histories and vertical profiles

Results

Vertical profiles for stations A, B, C and D are given in Figures 4.1 to 4.4. Time histories of model results for stations A, B, C and D are given in Figures 4.5 to 4.8. Stations A to D are situated at the positions given in Figure 2.1. Results have been plotted for layers 1,2, 20 and 40. These layers are respectively (approximately) 0.75 m, 2.25 m, 30 m and just above the bed for stations A and B and C. For station D these layers are at 0.375 m, 1.1 m, 15 m and at the bed. The depth of the water column according to NERC is 85 m for station A, 52 m for station B, 60 m for station C, and 30 m for station D.

Data and model results are compared on the following items:

1. Thermocline depth: this depth is usually defined at the depth where the sharpest gradient in temperature occurs. In this study, we looked at the depth where temperatures increases from 12°C to 14°C since in that region usually the sharpest temperature gradients are found. In the colour plots (Figures 4.1-4.4) this depth can be recognised as the transition from dark blue(12°C-13°C) to red (14°C-15°C).
2. The week that stratification starts. In this study, this is defined as the week that a temperature difference of 2°C between top layer and bottom layer is found.
3. The week that stratification ends. In this study, this is defined as the week a temperature difference of less 2°C between top layer and bottom layer is found.
4. Sea surface temperatures.

Discussion of results

Station A:

- Most importantly, for station A the thickness of the thermocline is in reasonable agreement with the data. A sudden increase of temperature to 13 °C at a depth of 30m occurs in the data around 1 August. However, in the model the thermocline depth is continuously and smoothly growing. Given the original data in Figure 2.2.b the sharp lines in the data are probably due to the interpolation procedure. The location of the thermocline in the original data at 04/08/89 is at 27m below the water surface, and almost at the same depth in the model (25m below surface).
- For both model and data stratification begins after the second week of May (a temperature difference larger 2°C between top and bottom layer is found then).
- For both model and data stratification ends after the first week of October (a temperature difference less 2°C between top and bottom layer is found then).
- Sea surface temperature in June is slightly higher in the model than in the data. The raw data (Figure 2.2b) show only measurements for the 02/06/89 and 01/07/89, where a SST goes from 10.8 to 13.4°C. This indeed indicates that the model SST is too high. For 4 August the model SST and NERC SST are nearly equal (~ 15.3 °C).

- The bottom temperature in summer is between 7°C and 10°C and is in agreement with the data.

Station B:

- For station B the thickness of the thermocline is in reasonable agreement with the data. However, in the model the thermocline depth is continuously and smoothly growing, whereas in the data it varies from 30m (June) till 40m (August-September). This is probably due to the interpolation method used to get a complete data set.
- For both model and data stratification begins after the second week of May.
- For the model stratification ends in the first week of August. In the data, in August still a thermocline is found at 40m (depth is 50m).
- Sea surface temperature in June is slightly higher in the model than in the data. This can be due to interpolation of the data. At 30 July both model and data have an SST of approximately 16°C.
- The bottom temperature in August and September in the model is higher than in the data, since the model does not show any stratification after 1 August.

Station C:

- For station C the thickness of the thermocline is in reasonable agreement with the data. . However, in the model the thermocline depth is continuously and smoothly growing, whereas in the data it is about 30m (June-July). This is probably due to the interpolation method used for the data.
- For both model and data stratification begins after the third week of May.
- For the model stratification ends in the third week of August. However, in the data stratification abruptly ends for station C in the third week of July.
- Sea surface temperature in June is (only) slightly higher in the model than in the data.
- The bottom temperature in July in the model is lower than in the data, since the model does not show up the sudden break down of stratification in July. In September the model shows a higher bottom temperature.

Station D:

- For station D, during the whole simulation period the water column is well mixed in both model and data.
- Sea surface temperature in June and July is in agreement in the model and in the data.
- The bottom temperature in July in the model is lower than in the data, since the model does not show up the sudden break down of stratification in July. In September the model shows a higher bottom temperature.

Conclusions:

Given these time histories and vertical profiles, the model gives an adequate representation of the in-situ vertical temperature profiles from NERC (Lowry et al., 1992). Thermocline thickness is on average correct. However, in the model stations A, B and C the thermocline is smoothly growing, whereas in the data there is a sudden onset of stratification. Given the original data shown in Figures 2.2.b for station A this is probably due to interpolation methods used to complete the data set. The moments of onset and breakdown of the thermocline are correctly modelled, except for breakdown of stratification at stations B and C. Sea surface temperatures for model and data are in fair agreement.

4.1.2 Sea surface temperature fields

Results

Plots for model results of sea surface temperature (SST) of the North Sea are given in Figures 4.9 to 4.18. We will make a general comment on the SST compared to the data sets given from remote sensing (daily images of SST given in the top figure, KNMI data) and from the blended data (interpolated in-situ data with remote sensing patterns given in the bottom figure, BSH data) in Figures 2.07 to 2.17.

Discussion

- Figure 2.07 (8 April) and Figure 2.08 (21 April): the plot is in reasonable agreement with the data, but does not show the fine structures observed in the KNMI data.
- Figure 2.09; 9 May 1989: the resemblance between model and data is good. However, the north east side of the plot (containing station B) is too cold by about 2°C compared to the blended data, but seems to be consistent with the RS data from KNMI.
- Figure 2.10; 28 May 1989: SST in the model is 1-2°C warmer than the blended data. Unfortunately, there is a hot spot in the RS data.
- Figure 2.11-2.12; 2 June 1989 and 12 June 1989:SST in the model is again 1-2°C warmer than for the blended data. Compared to the RS SST data this is also the case for the western part of the North Sea, but not for the eastern part of the Central North Sea. There, the RS SST images seem to be consistent with the model.
- Figure 2.13-2.14; 18 June 1989 and 19 June 1989: The sharp increase in temperature observed in the RS SST data is produced by the model. The model is again, somewhat too hot in the eastern part of the Central North Sea. The blended data from BSH are not showing the sharp temperature increase observed in these data. The blended data are about 3-5°C cooler than the RS SST data from KNMI and the model for the Central North Sea.
- Figure 2.15 and 2.16:; 18 August 1989 and 23 August 1989: like 2.14. The blended data and model data are in fair agreement, except that the model shows some cold water at the English coast that is not seen in the blended data. RS SST data show a little bit lower temperatures in August (~1°C).
- Figure 2.17; 29 November 1989: like 2.15 and 2.16. The model is somewhat warmer in the western part of the Central North Sea than blended data (RS data are not given there due too cloudiness). The blended data show less detail than the model data in general, especially concerning the intrusion of relatively warm water from Dover Strait. This intrusion is clearly observed in the RS SST data.

Conclusions

- Model data for SST are in good agreement with RS SST data (daily images) from KNMI. However, differences of 1-2°C are found in the western part of the Central North Sea in summer.
- Model data for SST are in good agreement with blended data, but not for June 1989. Then, the model data are clearly 3-5°C warmer than the blended data. However, for this period the model data are in good agreement with KNMI data.
- In general, the model SST data are in better agreement with KNMI data than with the blended BSH SST data for 1989.

5 Conclusions and recommendations

5.1 Conclusions

Data:

- A bias of about ±0.7 °C. may be expected when comparing in-situ data with the RS SST images when in-situ data have a high time resolution (Borst, 1995; de Haan, 1998).
- Given the fact that daily images are used one must be careful with pixels that are partially cloud covered. For such pixels the RS SST temperature is underestimated. For other pixels, an overestimation of temperature may be expected since all images are around noon. This overestimation may be about +0.7 °C in summer, but is less in other periods.
- The RS SST data show more detail than the blended data set of BSH, especially in the vicinity of the coast line. This is due to the fact that the blended data were projected on a rather coarse grid. Good examples are the images of 8 March and 29 November.
- Blended data sets are free of hot spots.
- The RS SST images for the summer period (12 June, 18 June, 19 June, 18 August and 23 August) ahead higher temperatures then the blended data. Differences are most pronounced in June. For 19 June differences even go up locally to 4 °C. It is not clear what causes such large deviations. Validation with ship data is required to judge the quality of RS SST data and blended data for June 1989.

Model:

- An improved model was set up with an improved background eddy diffusivity for the k-ε model. This parameter was set to 7.10^{-5} m^2/s as recommended from the sensitivity analysis of Section 3.2, in order to get a correct thickness of the thermocline compared to observations.
- The new model contains improved initial conditions, boundary conditions and meteorological forcing by wind.
- 1 DV point models are an efficient and reliable device to tune the vertical transport of large 3-dimensional transport models.
- In the old model results the thickness of the thermocline for station A, B and C was too small. The new model simulates a proper thickness for the thermocline (see below)
- Compared to old simulations by Van Kester et al. (1997), the increased background eddy viscosity in combination with the horizontal advection of heat from the model boundaries improved the model results significantly.

Data-model comparison, in-situ data vs. model:

- Given these time histories and vertical profiles (and the original non-interpolated in-situ data), the model gives a very good representation of the NERC vertical profile (in-situ measured) chain data. Results for stations A, B, C and D are very good with respect to thickness of the thermocline depth. The onset of stratification is correctly modelled.

Shortcomings are that for station B and C, the breakdown of stratification happens too early.

Data-model comparison, remote sensing SST data vs. model SST data:

- Model data for SST are in good agreement with RS SST data (daily images) from KNMI. However, differences of 1-2°C are found in the western part of the Central North Sea in summer.
- Model data for SST are in good agreement with blended data, but not for June 1989. Then, the model data are clearly 3-5°C warmer than the blended data. However, for this period the model data are in good agreement with KNMI data.
- In general, the model SST data are in better agreement with KNMI SST data than with the blended BSH SST data for 1989. However, daily images of SST from KNMI demonstrate too much cloud cover. Probably weekly composites (like the blended sets presented here) must be preferred.

General conclusions:

- The present 3D model results for 1989 are in good agreement with NERC in-situ data and RS SST data from daily images.
- A combination of in-situ data over vertical and RS SST data in the horizontal plane is ideal for model validation. In-situ data serve to tune the heat balance and thermocline formation (1DV models can be used efficiently hereto to reduce the calibration effort). RS SST data contain reliable information.

5.2 Recommendations

- It is recommended to validate the 3D model with the 1994 data set of the North Sea.
- Interpolation procedures on ship data used in this study (on vertical profiles, and on SST ship data) in general show shortcomings and must be improved.
- The present calculations are very promising but still show some shortcomings for SST in the western part of the Central North Sea in summer compared to remote sensing data (differences of 1-2°C were found). It is recommended to investigate the effect of using space-varying meteorological input in the heat flux model. Unfortunately, except for wind speed (DNMI) reliable space-varying data are not available. Cloudiness may be obtained from full analysis of all (NOAA/AVHRR and other) satellite imagery. It must be investigated if forthcoming satellites and/or meteorological models can deliver detailed spatial information on humidity and air temperature.
- As an alternative for the heat flux model, SST forcing at the sea surface may be considered. It is recommended to exploit this possibility in a follow up project.
- In this model an background eddy diffusivity was added. Rather than subjectively tuning the simulation we propose (in the future) the objective addition of a so-called internal-wave-energy model that describes the additional turbulence production, and thus increase of turbulent mixing, inside the thermocline by breaking and shearing action of random internal waves. The latter are generated by wind, surface waves, the bed as well as more vigorous turbulence outside the thermocline.

References

Bijlsma A.C, van den Boogaard H.F.P. and de Smet A.C. '*The assimilation of satellite and in-situ data in a temperature model of the North Sea*', BCRS report 91-24, Delft, 1991

Borst H.C, '*Calibration and Validation of NOAA/AVHRR Satellite data*', RWS-RIKZ report IT 95.172X, 1995.

Deleersnijder, E. and P. Luyten 1994 '*On the practical advantages of the quasi-equilibrium version of the Mellor and Yamada level 2.5 turbulence closure applied to marine modelling*'. Appl. Math. Modelling, vol. 18, May, pp. 281-287.

Galperin B., L.H. Kantha, S. Hasid and A. Rosati 1988 '*A quasi-equilibrium turbulent energy model for geophysical flows*'. J. Atmos. Sc., vol. 45, no. 1, Jan., pp. 55-62.

Haan de S, '*Validation of NOAA-SST',preprint of KNMI report for HIRLAM-SST project of BCRS'*. De Bilt 1998

Kester J.A.Th.M van., R.E. Uittenbogaard and E.D. de Goede,'*Onderzoek naar thermocliene effecten op de Noordzee*', WL|Delft Hydraulics Report Z2034, Oktober 1997.

Kester J.A.Th.M.van, R.E. Uittenbogaard and G.S. Stelling 1994 *Gevoeligheidsonderzoek 3D-NOORDWIJKRAAI-model.* WL | Delft Hydraulics, report Z-691, two parts text and figures, March (in Dutch).

Kester J.A.Th.M.van, R.E. Uittenbogaard and E.D. de Goede 1997 *Onderzoek naar numerieke modellering van thermocliene effecten op de Noordzee.* WL | Delft Hydraulics, report Z-2034.30, (in Dutch).

Loewe P.; 'Surface temperatures of the North Sea in 1994', Deutsch Hydrographische Zeitschrift, 42, p.145-152, 1995

Lowry R.K. R.N. Cramer and L.J. Richards 1992 *North Sea Project NERC CD-ROM.* British Oceanographic Data Centre.

Luyten P.J.;'*An analytical and numerical study of surface and bottom boundary layers with variable forcing and application to the North Sea*', J. of Marine Systems 8, p 171-189, 1996

Obata A., Ishizaka J. and Endoh M.; '*Global verification of critical depth theory for phytoplankton bloom with climatological in-situ tempearture and satellite ocean color data*', J. Geophysical Res., 101, p20,657-20,667, 1996

Pohlmann T.; '*Predicting the thermocline in a circulation model of the North Sea-PART I: model description, calibration and verification*', Cont. Shelf Res, 16,p131-146, 1996

Proctor (editor), 'NOMADS-North sea Model Advection-Dispersion Study', Final Report of MAST contract MAS2-CT94-0105, POL Internal Document N0. 108, 1997

Roozekrans J.N.and Prangsma G.J., '*Processing and application of digital AVHRR-imagery for alnd and sea surfaces*'. BCRS report 88-08, Delft, 1988

Reynolds R.W.; 'A Real-Time Global Sea Surface Temperature Analysis', J.of Climate, vol 1, p.75-86, 1988

Ruardij P., van Haren H., Ridderinkhof H.; '*The impact of thermal stratification on phytoplankton and nutrient dynamics in shelf seas: a model study*', J. of Sea Research, 38, p.311-331, 1997

Robinson I.S., Wells N.C. and Charnock H.,'*The sea surface thermal boudary layer and its relevance to the measurement of sea surface temperature by airborne and spaceborne radiometers'*, Int.J. Remote Sensing 5, pp19-45, 1984

Uittenbogaard R.E., and Van Kester J.A.Th.M., '*Modelling seasonal temperature stratification with TRIWAQ. A preliminary study based on one-dimensional computations'*. WL|delft Hydraulics report Z978, 1996.

de Valk C.,'*Case study 2: validation of the prediction of coastal upwelling during summer*', Chapter 5 of report for ERS-2 AO (ESYS-96140-RPT-3), November 1997

Mellor G.L. and T. Yamada 1982 *Development of a turbulence closure model for geophysical fluid problems.* Rev. Geophys. Space Phys., vol. 20, no. 4, Nov., pp.851-875.

Munk W. 1966 Abyssal recipes. *Deep Sea Res.*, vol. 13, pp. 707-730.

Taylor G.I. 1931b *Internal waves and turbulence in a fluid of variable density.* Proc. Roy. Soc. A, vol. 132 (Aug.), pp. 35-43. Reprinted in: *The scientific papers of Sir Geoffrey Ingram Taylor, vol. II Meteorology, oceanography and turbulent flows*, G.K. Batchelor (ed.), Cambridge Un. Press, 1960, pp. 240-246.

Uittenbogaard R.E. and F. Baron 1989 *A proposal: extension of the k-ε model for stably stratified flows with transport of Internal Wave Energy.* In 7th Turbulent Shear Flows Symp., Stanford, August, paper 18.4, pp. 21-23.

Uittenbogaard R.E. 1995 *The importance of internal waves for mixing in a stratified estuarine tidal flow.* Ph.D. Thesis, Delft University.Uittenbogaard, R.E. and J.A.Th.M. Van Kester 1996 *Modelling seasonal temperature stratification with TRIWAQ. A preperatory study based on one-dimensional computations.* WL|Delft Hydraulics, March 1996.

Uittenbogaard R.E. 1997 *Temperatuurstratificatie in Noordzee berekend met standaard k-ε, RNG k-ε, Extended k-ε model en standaard k-ε model uitgebreid met model voor interne golven.(vooronderzoek met 1DV model).* WL|Delft Hydraulics, note Z-2393, Febr. 1998 (in Dutch).

Vos R.J., and Schuttelaar M.'RESTWAQ: *Data assessment, data-model integration and application to the Sotuhern North Sea*', BCRS report 95-19, Delft, 1995

Vos R.J., Villars M., Roozekrans J.N., Peters S.W.M. and van Raaphorst W., 'RESTWAQ 2, Part I: *Integrated monitoring of total suspended matter in the Dutch coastal zone*', BCRS report 98-08, Delft, 1998

Wolf P. de, and Zijlstra J.J., '*The Ecosystem*', (Figures 1a,b and 2a,b). Appeared in 'Pollution of the North Sea, An Assessment', edited by W.Salomons, B.L. Bayne, E.K. Duurma, U. Forstner, Springer-Verlag, Heidelberg, 1988

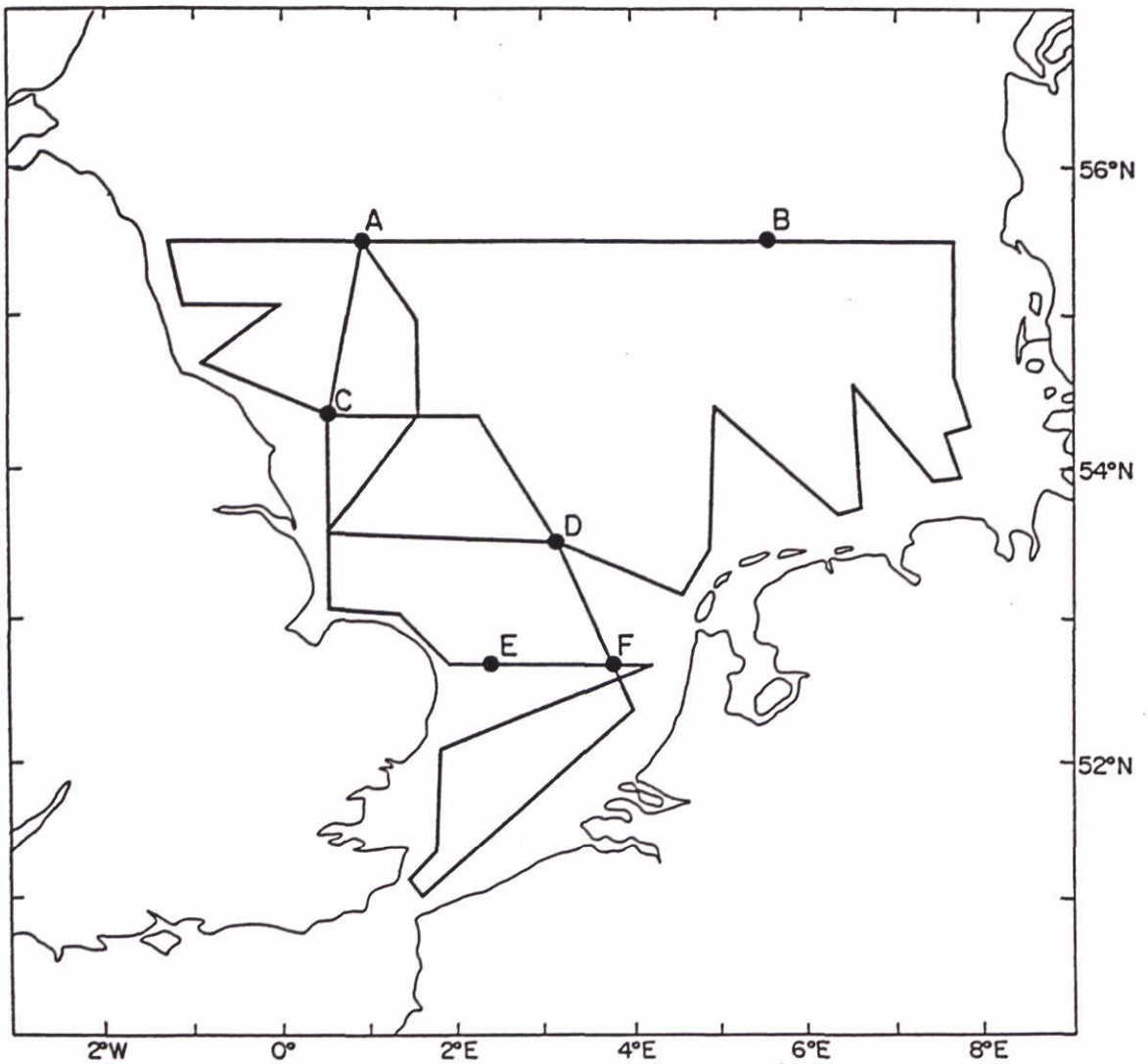

North Sea Survey cruise track
North Sea Project NERC.

DELFT HYDRAULICS | Z-2034 | **Fig 2.01**

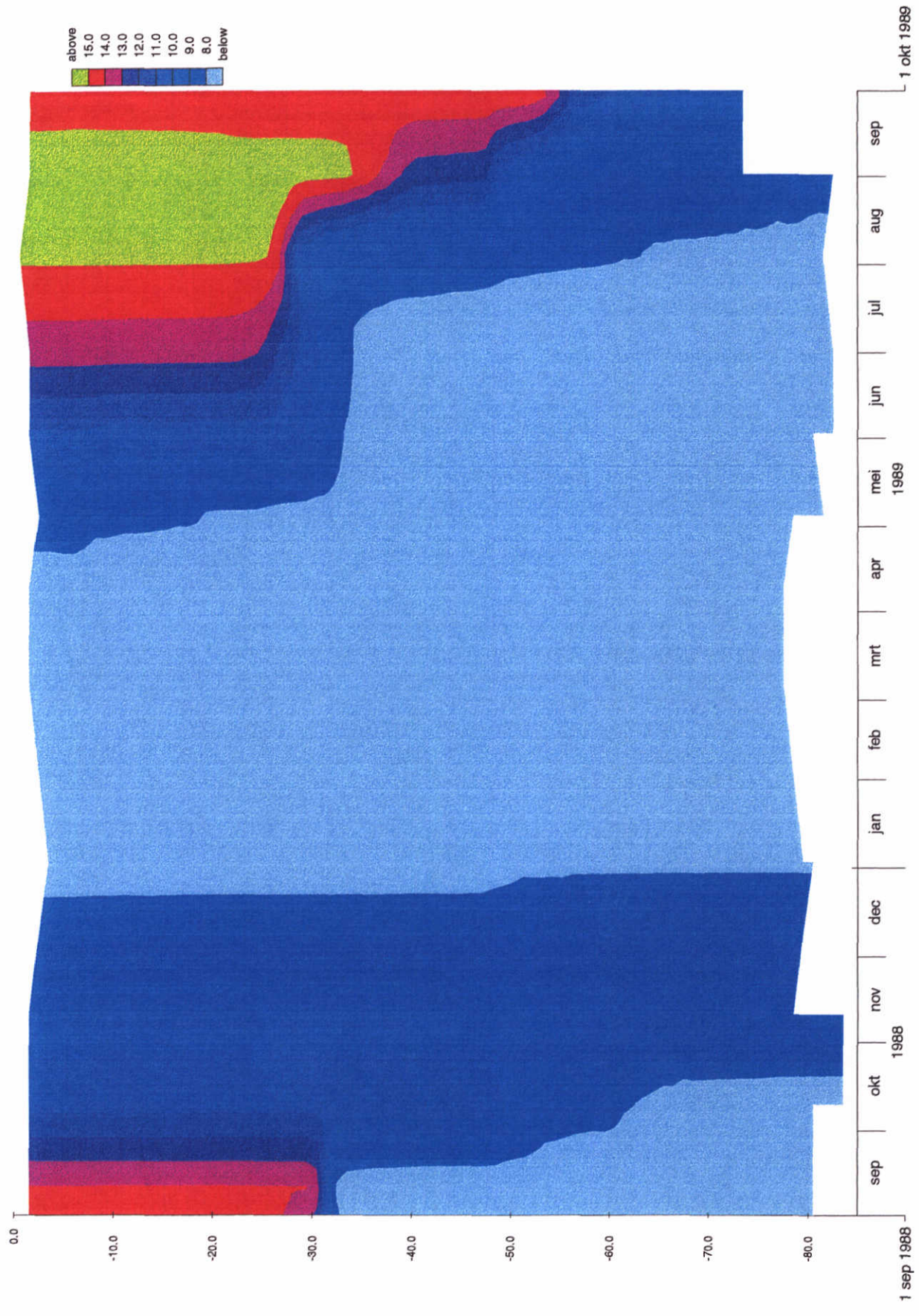

Evolution thermal stratification
Site A (55>o30'N; 0>o54'E) , depth 85 (m)
Dataset North Sea Project NERC.

DELFT HYDRAULICS | Z-2034 | Fig. 2.2

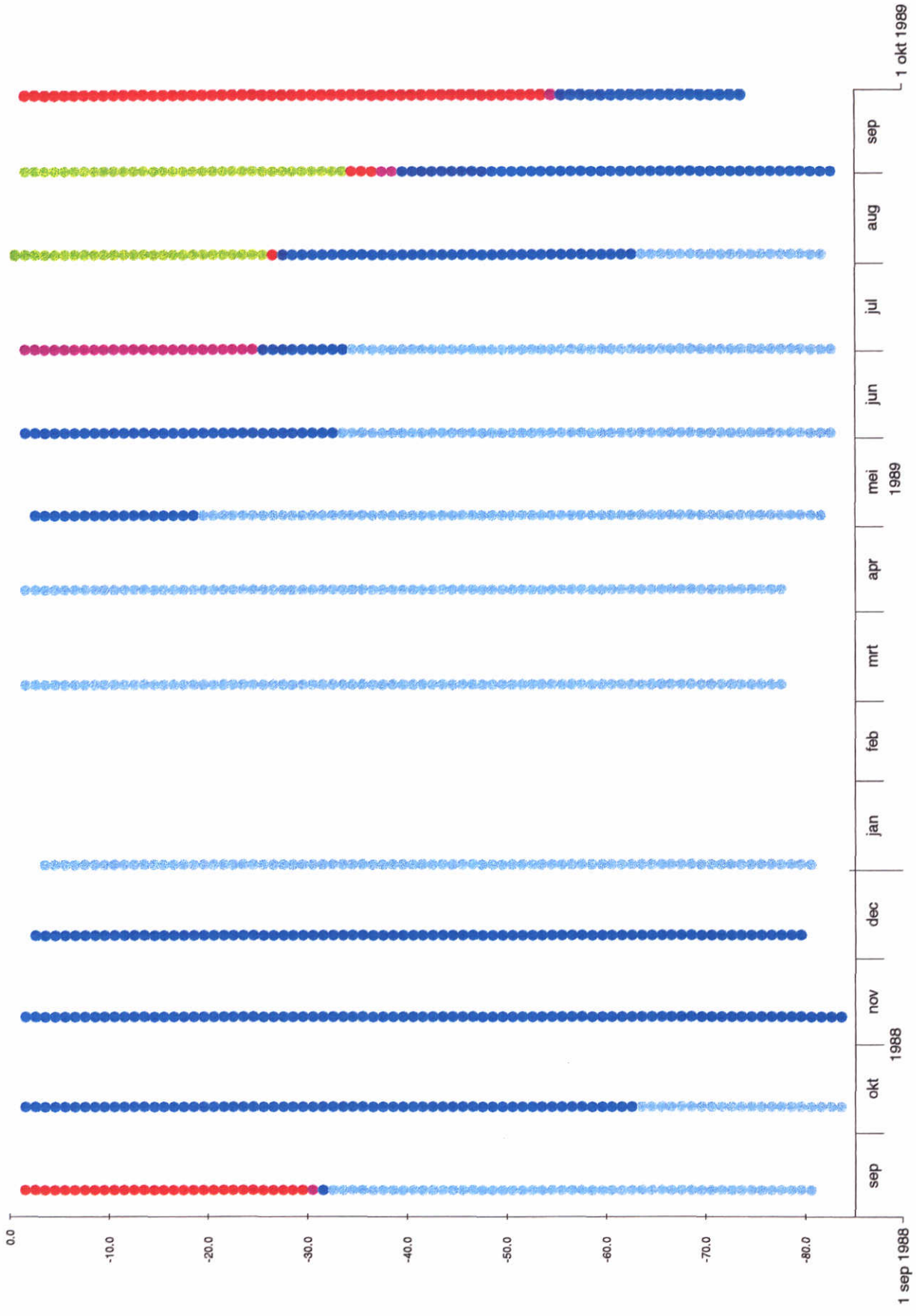

Evolution thermal stratification
Site A (55>o30'N; 0>o54'E) , depth 85 (m)
Dataset North Sea Project NERC.

DELFT HYDRAULICS | Z-2034 | Fig. 2.2b

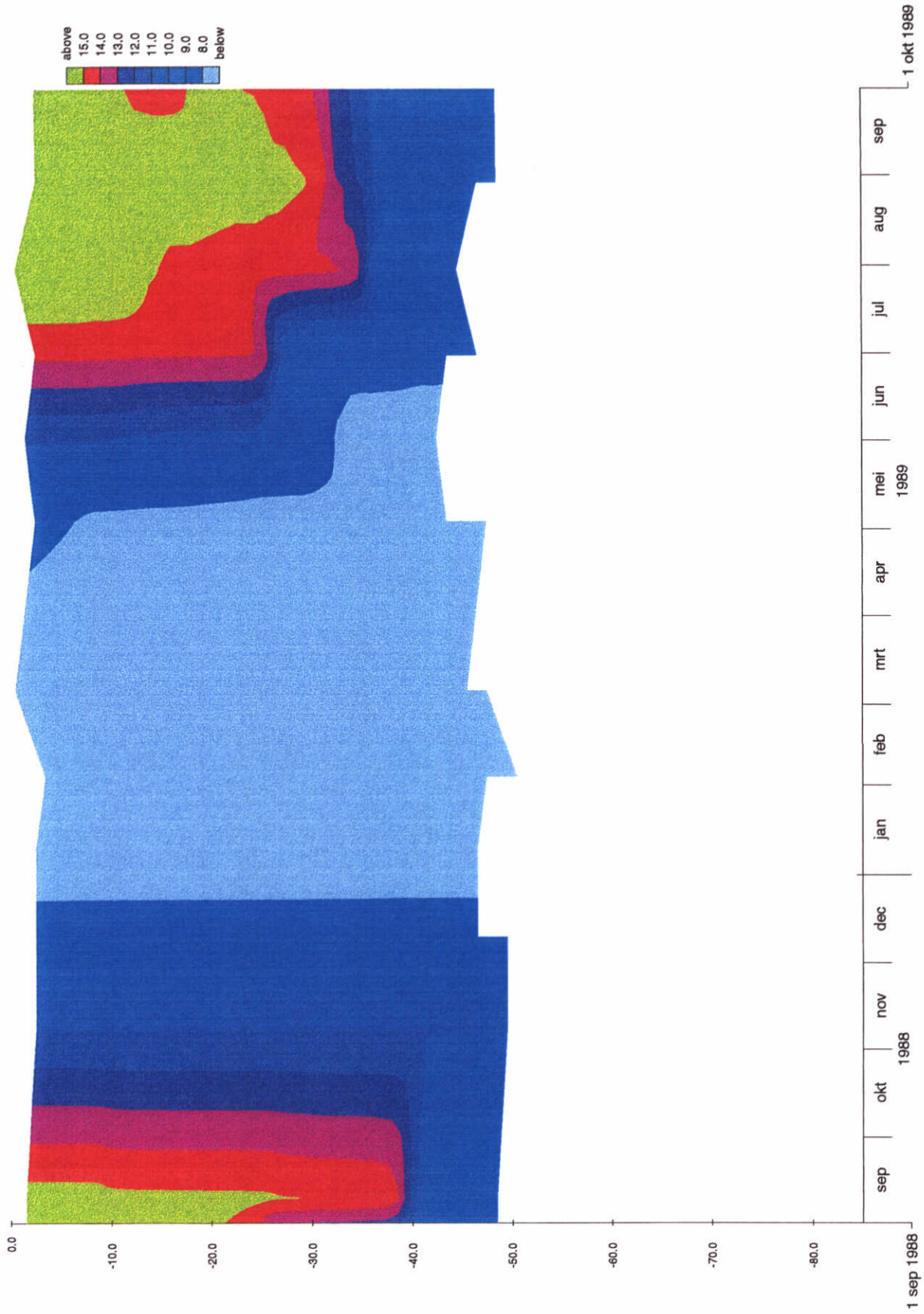

Evolution thermal stratification
Site B (55>o30'N; 5>o31'E) , depth 52 (m)
Dataset North Sea Project NERC.

DELFT HYDRAULICS | Z-2034 | Fig. 2.3

Evolution thermal stratification
Site C (54>o20'N; 0>o24'E) , depth 60 (m)
Dataset North Sea Project NERC.

DELFT HYDRAULICS | Z-2034 | Fig. 2.4

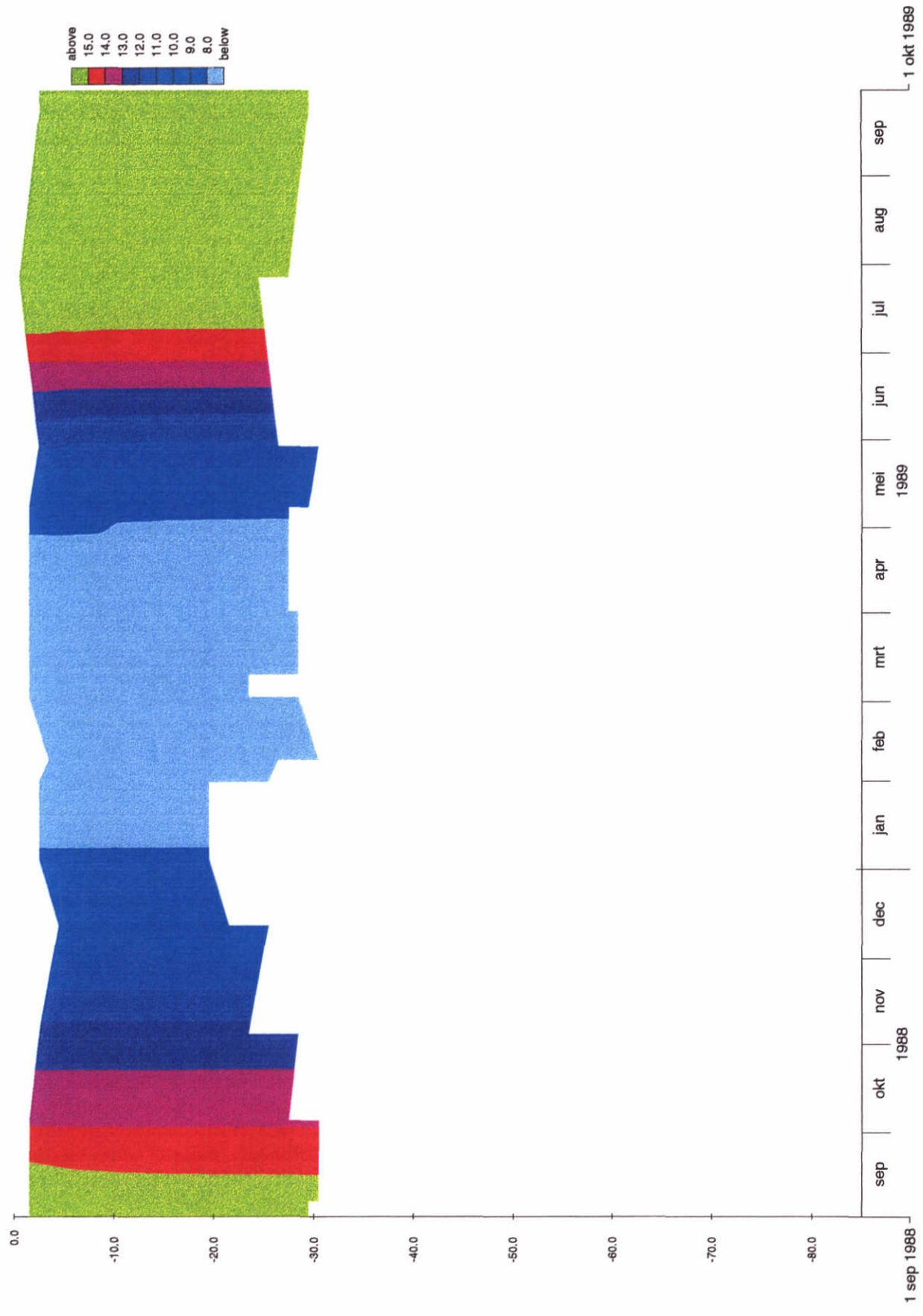

Evolution thermal stratification
Site D (53>o30'N; 3>o 0'E) , depth 30 (m)
Dataset North Sea Project NERC.

DELFT HYDRAULICS | Z-2034 | Fig. 2.5

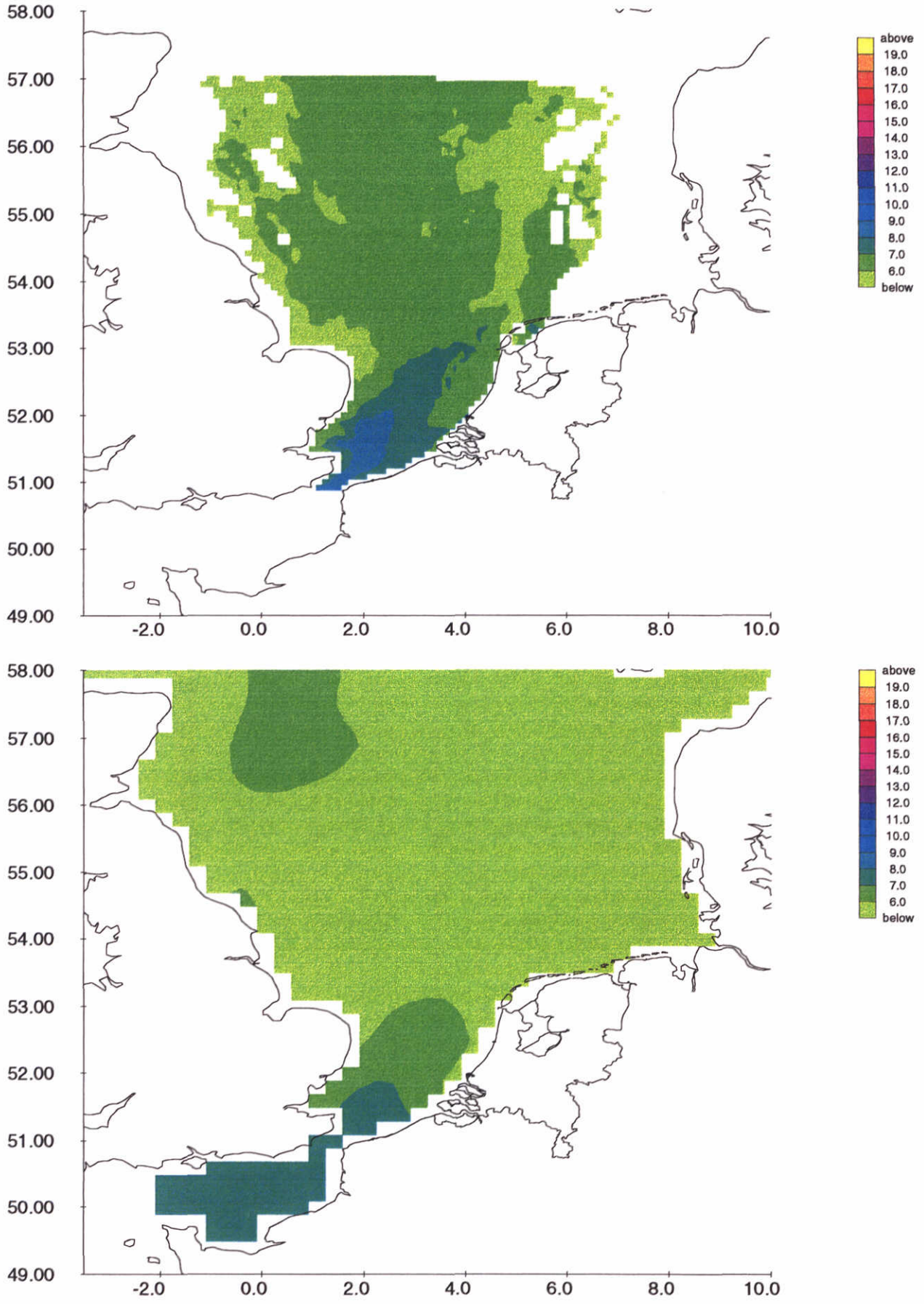

Remote sensing SST data (top) versus blended SST data (below
Date : March 08 1989

1998-11-12
11:41:51

DELFT HYDRAULICS | Z-2506 | Fig. 2.06

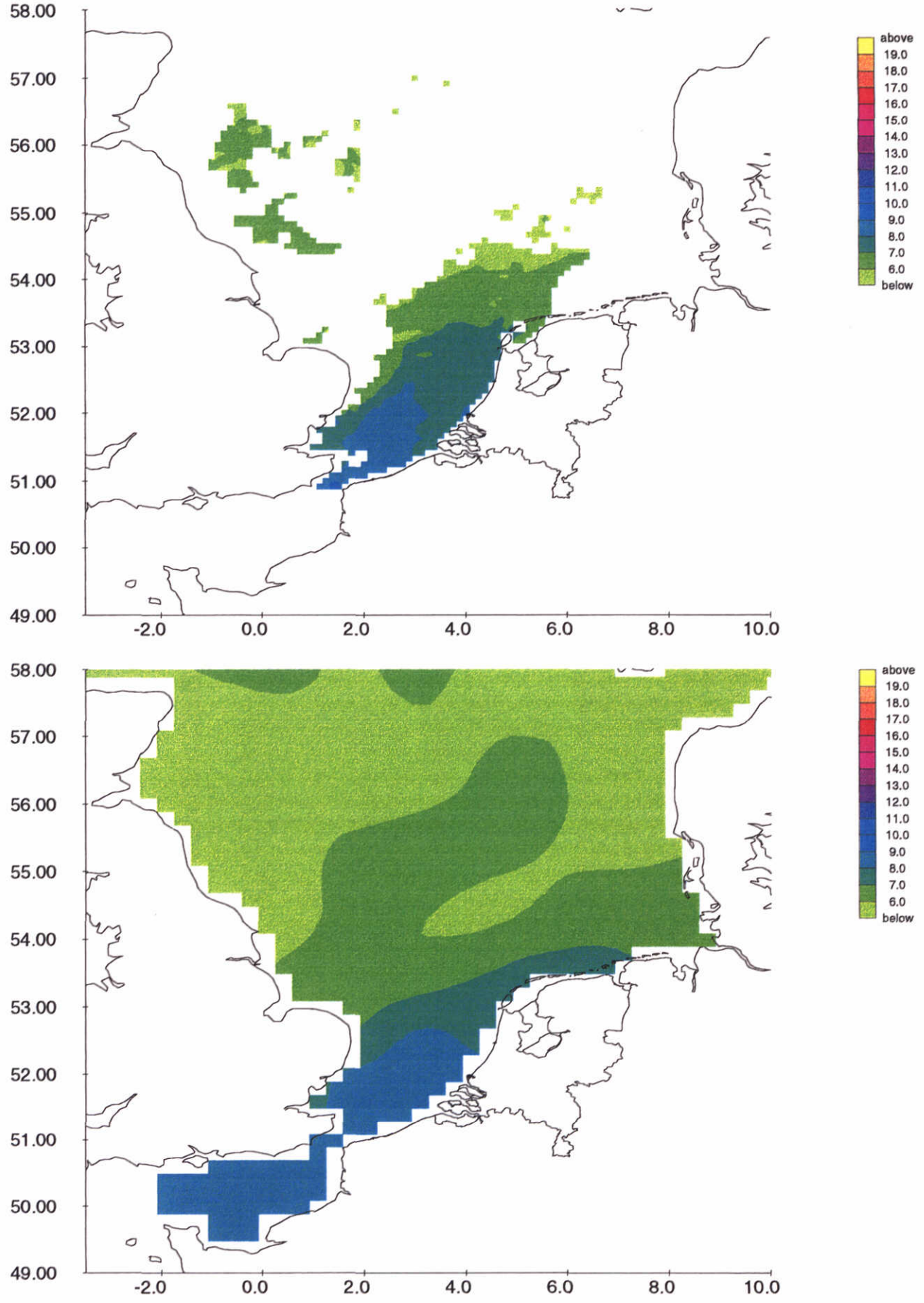

Remote sensing SST data (top) versus blended SST data (below
Date : April 08 1989

1998-11-12
11:41:53

DELFT HYDRAULICS | Z-2506 | Fig. 2.07

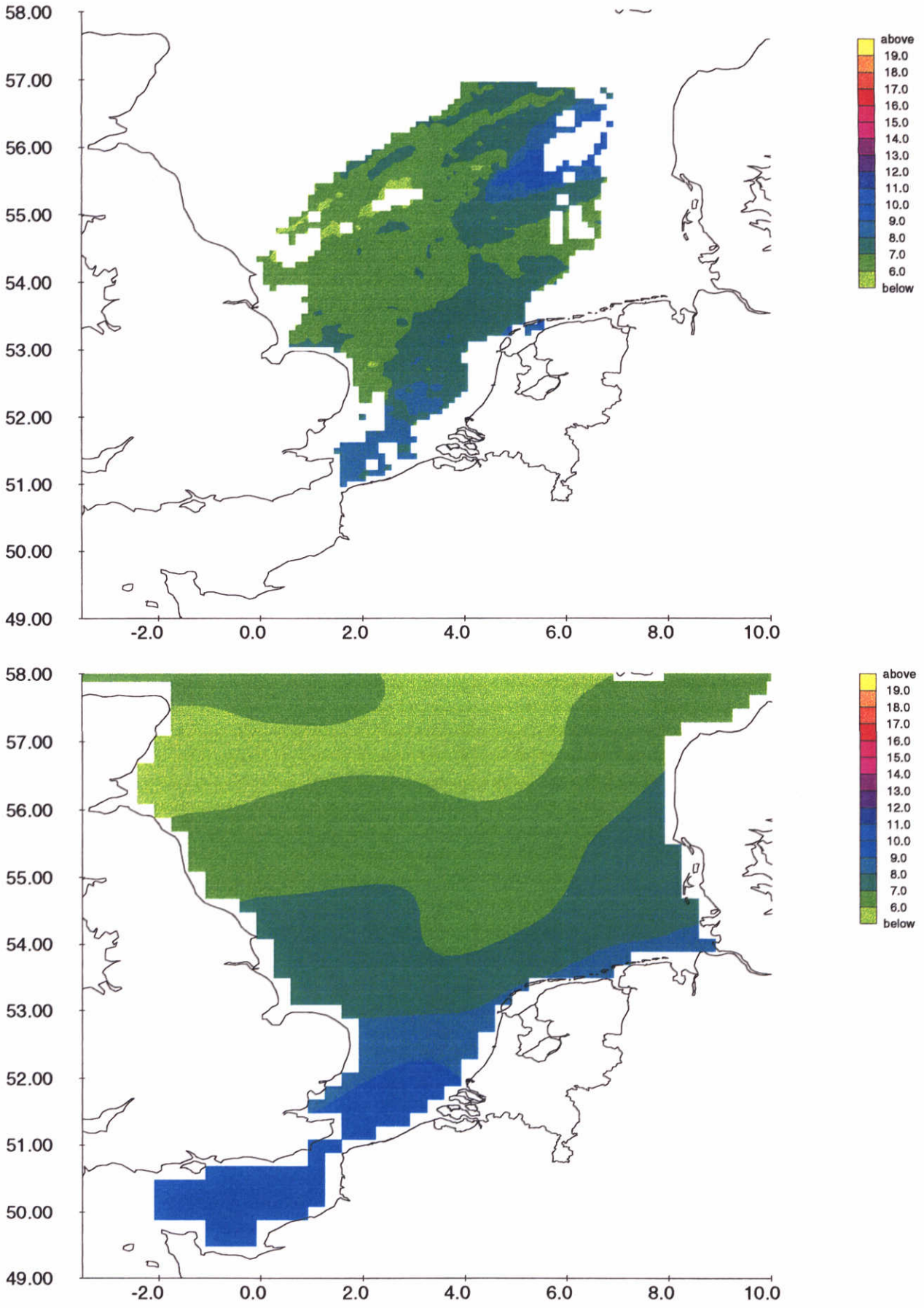

Remote sensing SST data (top) versus blended SST data (below
Date : April 21 1989

1998-11-12
11:41:55

DELFT HYDRAULICS | Z-2506 | Fig. 2.08

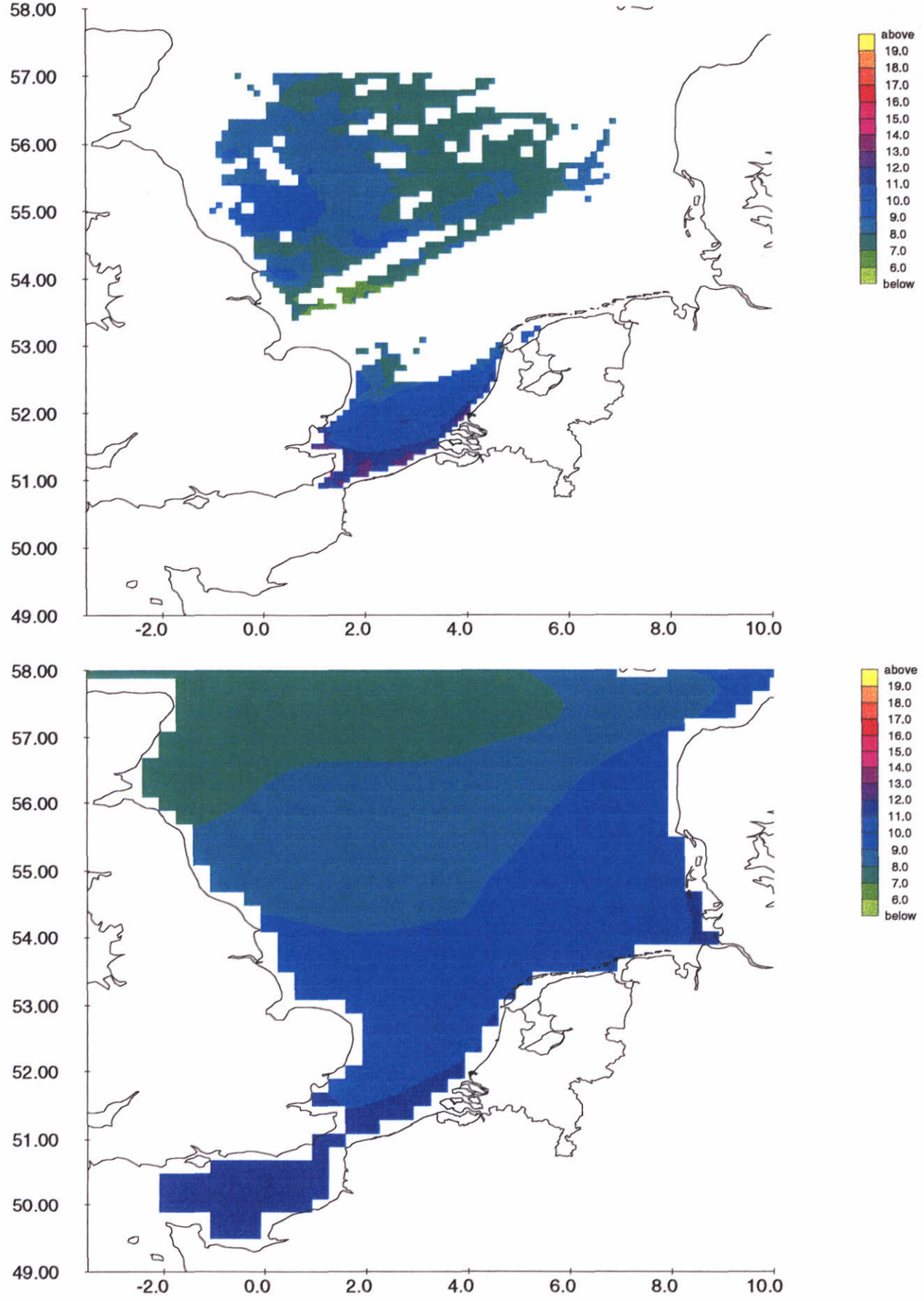

Remote sensing SST data (top) versus blended SST data (below
Date : May 09 1989

1998-11-12
11:41:57

DELFT HYDRAULICS | Z-2506 | Fig. 2.09

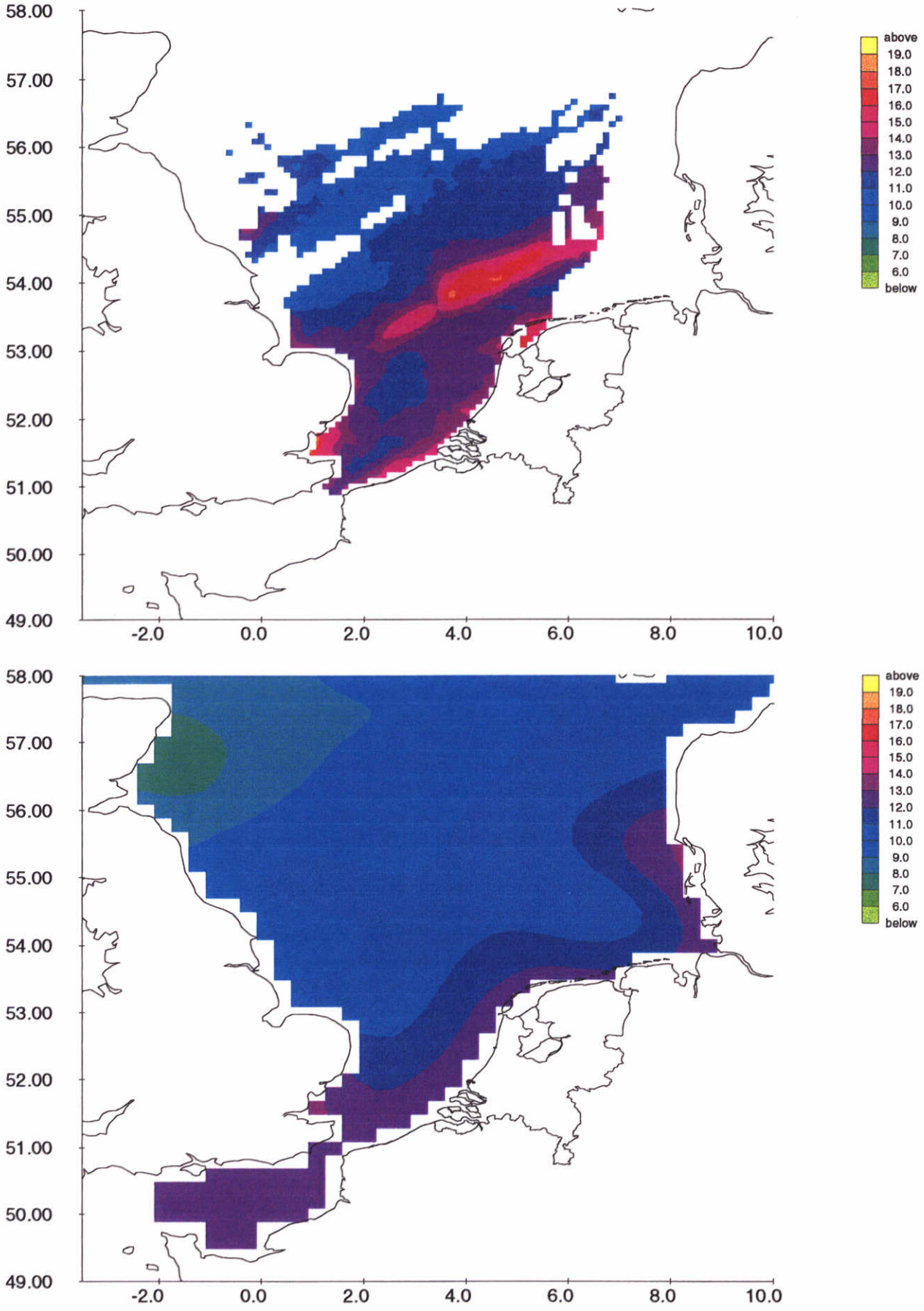

Remote sensing SST data (top) versus blended SST data (below
Date : May 28 1989

1998-11-12
11:41:59

DELFT HYDRAULICS | Z-2506 | Fig. 2.10

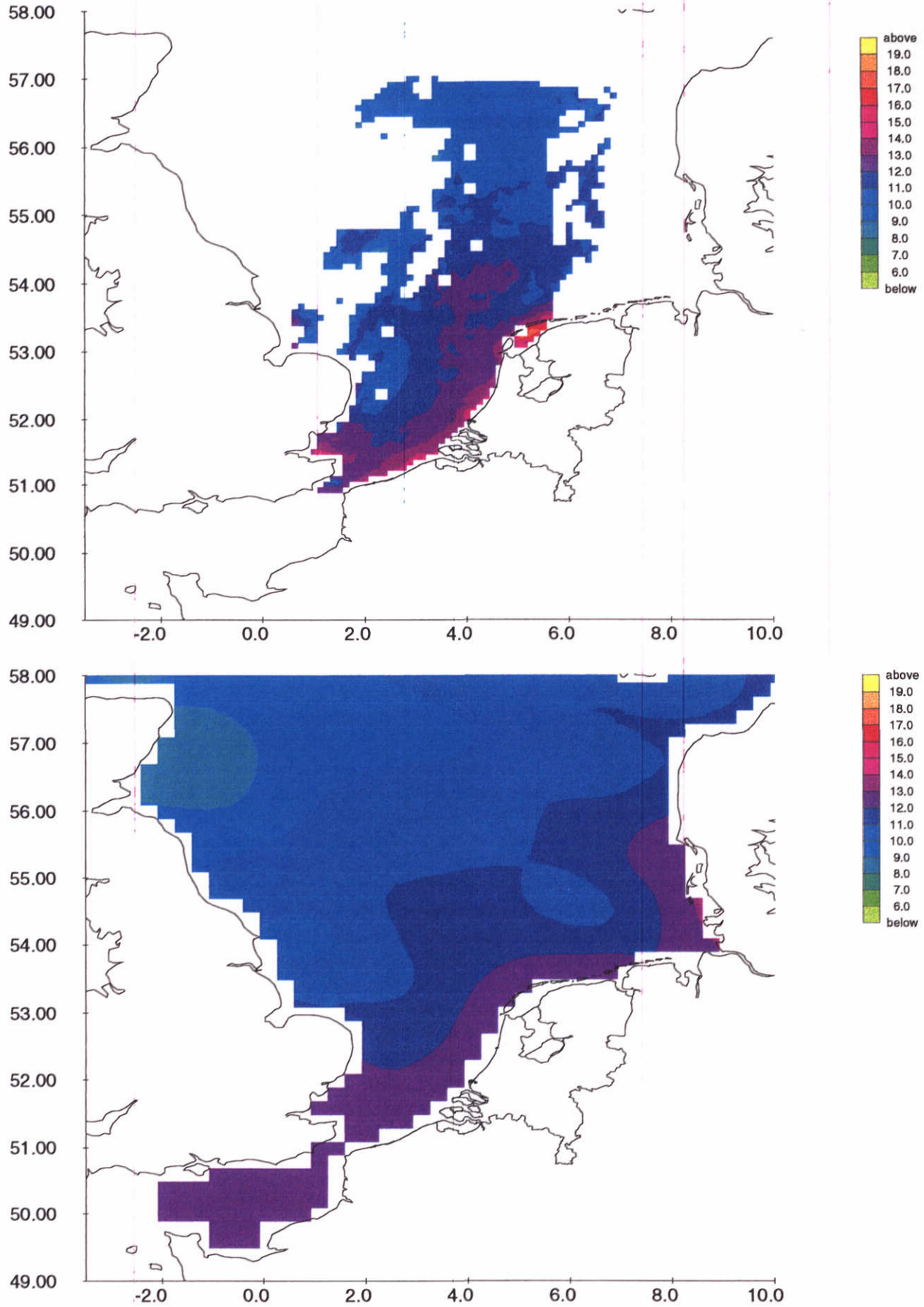

Remote sensing SST data (top) versus blended SST data (below

Date : June 02 1989

1998-11-12
11:42:01

DELFT HYDRAULICS

Z-2506

Fig. 2.11

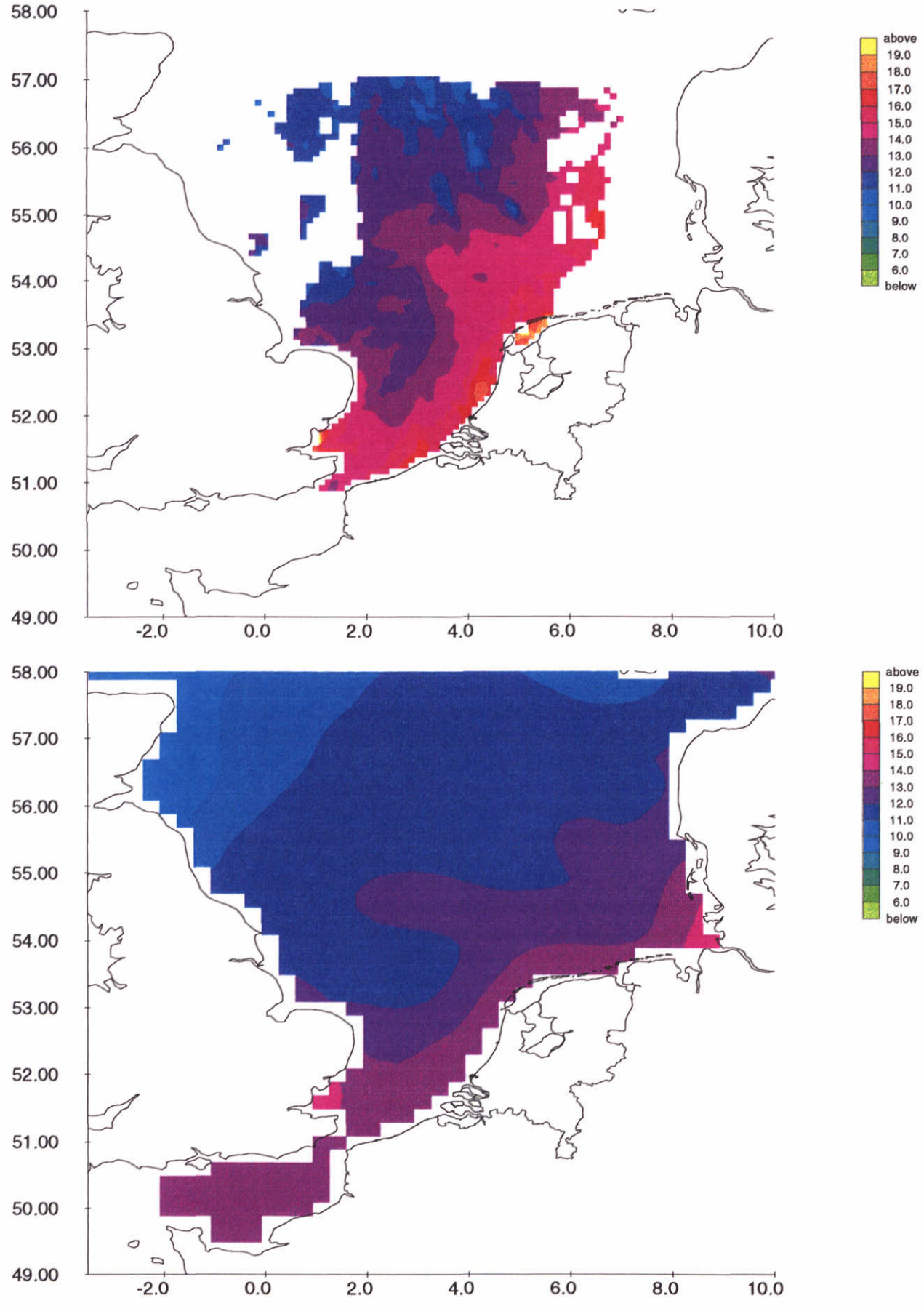

Remote sensing SST data (top) versus blended SST data (below
Date : June 12 1989

1998-11-12
11:42:03

DELFT HYDRAULICS | Z-2506 | Fig. 2.12

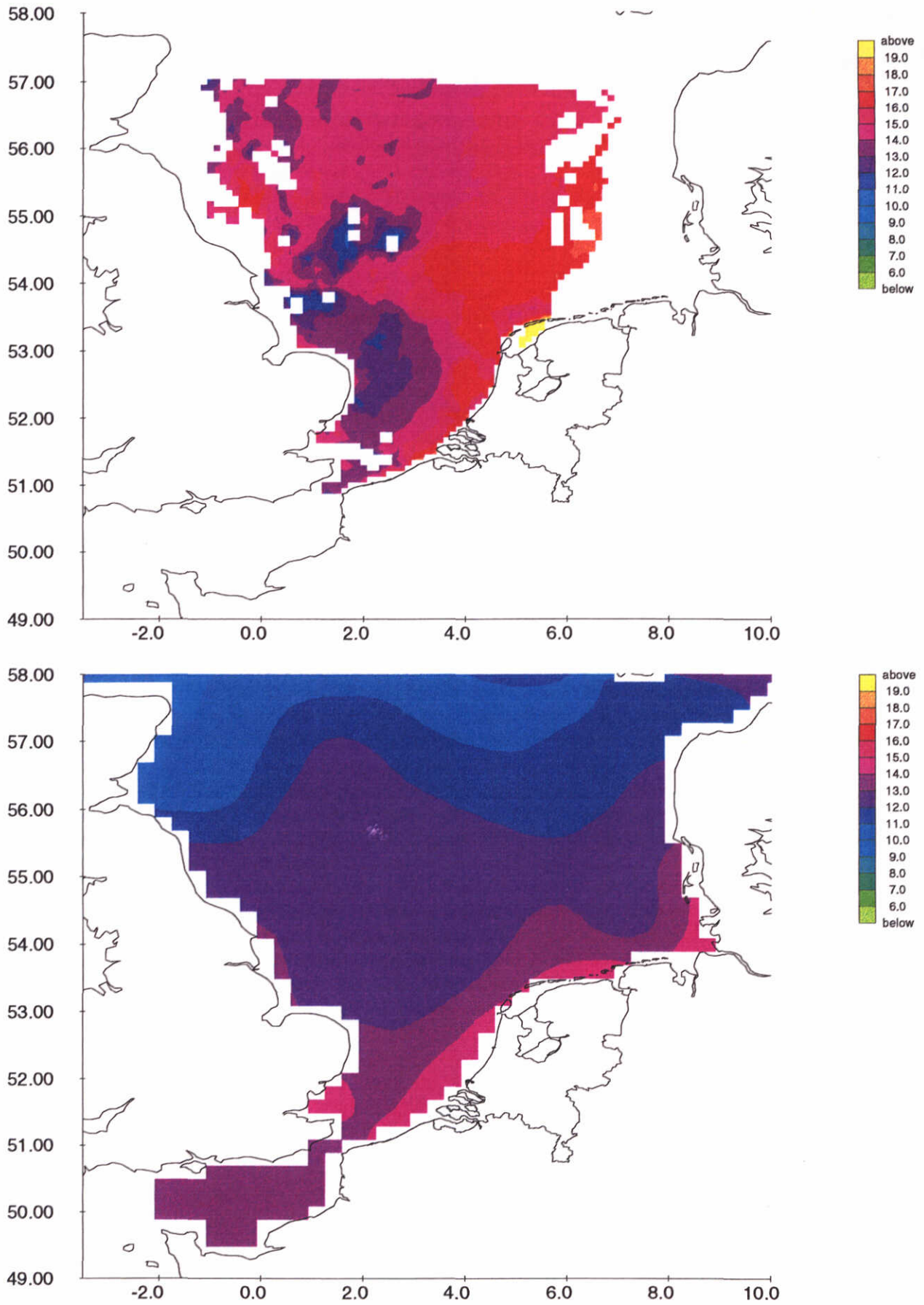

Remote sensing SST data (top) versus blended SST data (below
Date : June 18 1989

1998-11-12
11:42:05

DELFT HYDRAULICS | Z-2506 | Fig. 2.13

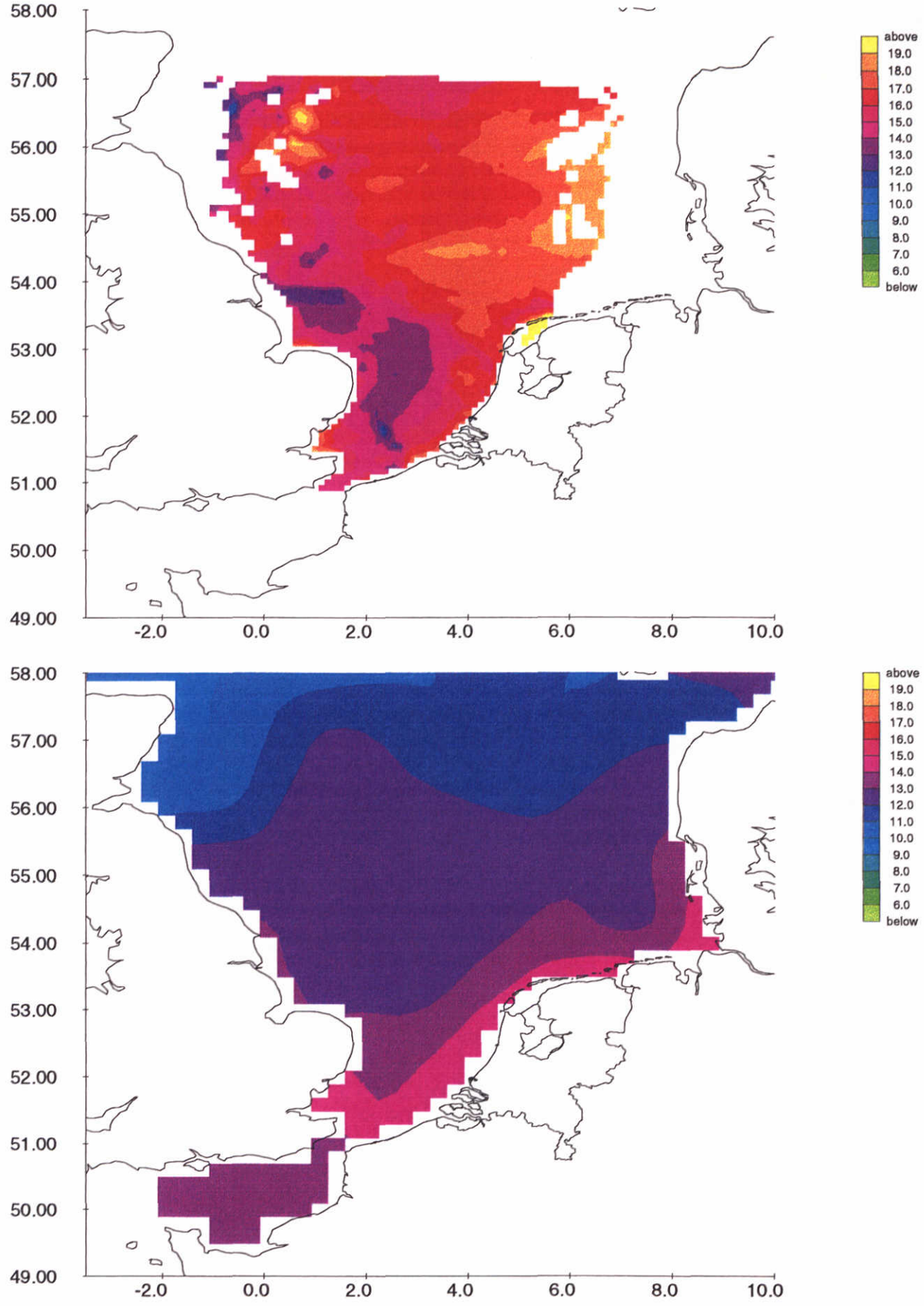

Remote sensing SST data (top) versus blended SST data (below
Date : June 19 1989

1998-11-12
11:42:07

DELFT HYDRAULICS | Z-2506 | Fig. 2.14

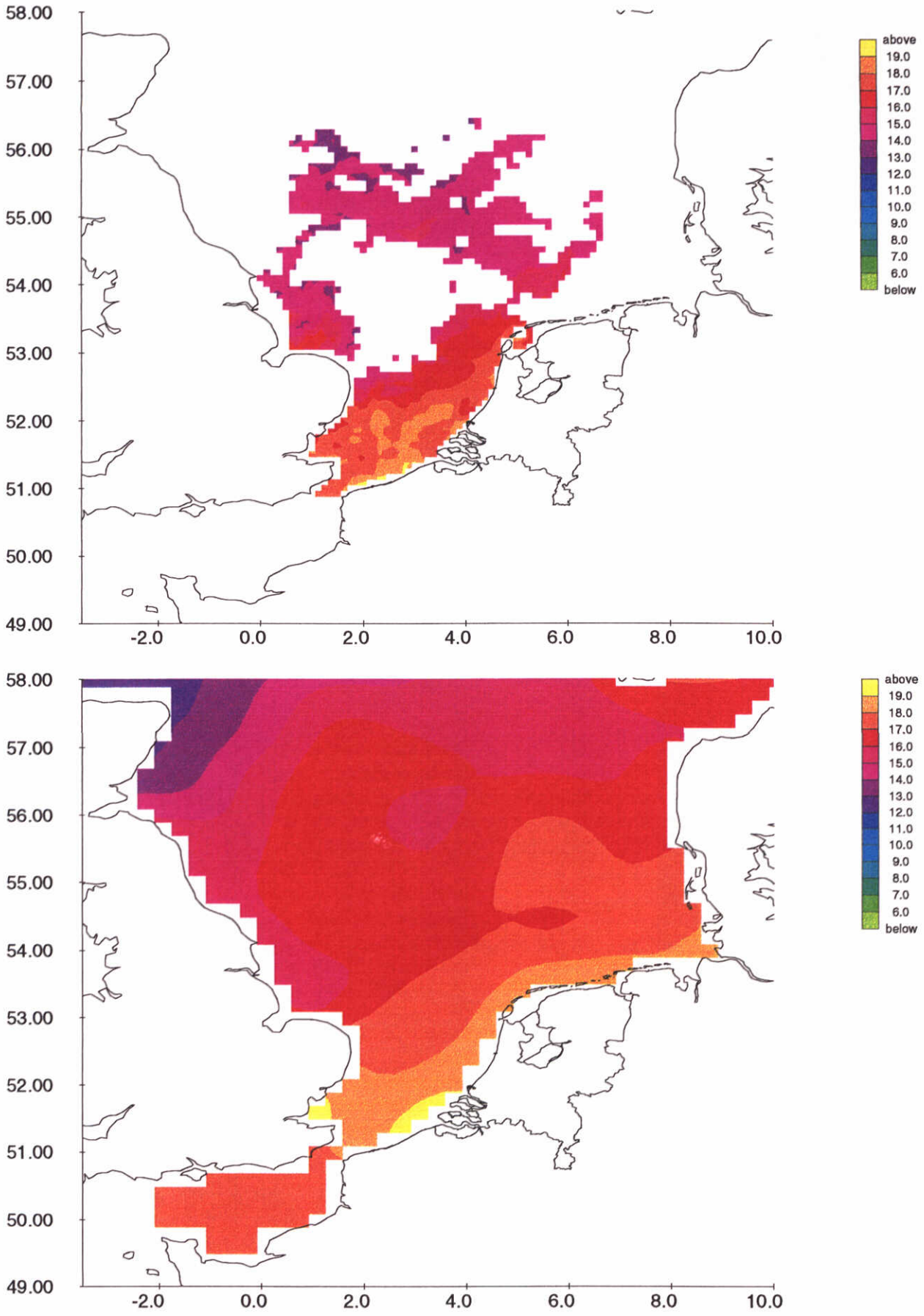

Remote sensing SST data (top) versus blended SST data (below
Date : August 18 1989

1998-11-12
11:42:09

DELFT HYDRAULICS | Z-2506 | Fig. 2.15

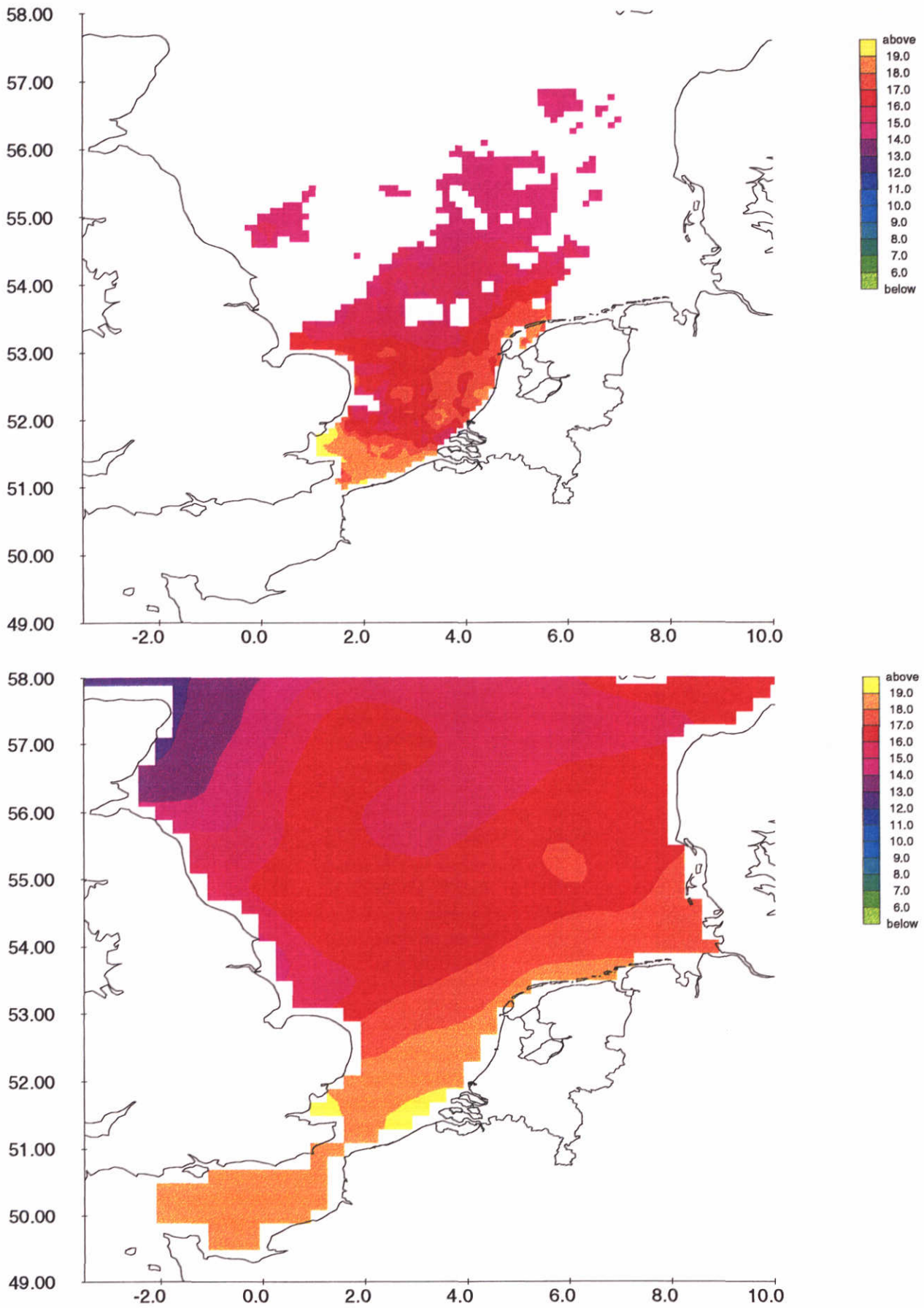

Remote sensing SST data (top) versus blended SST data (below
Date : August 23 1989

1998-11-12
11:42:11

DELFT HYDRAULICS | Z-2506 | Fig. 2.16

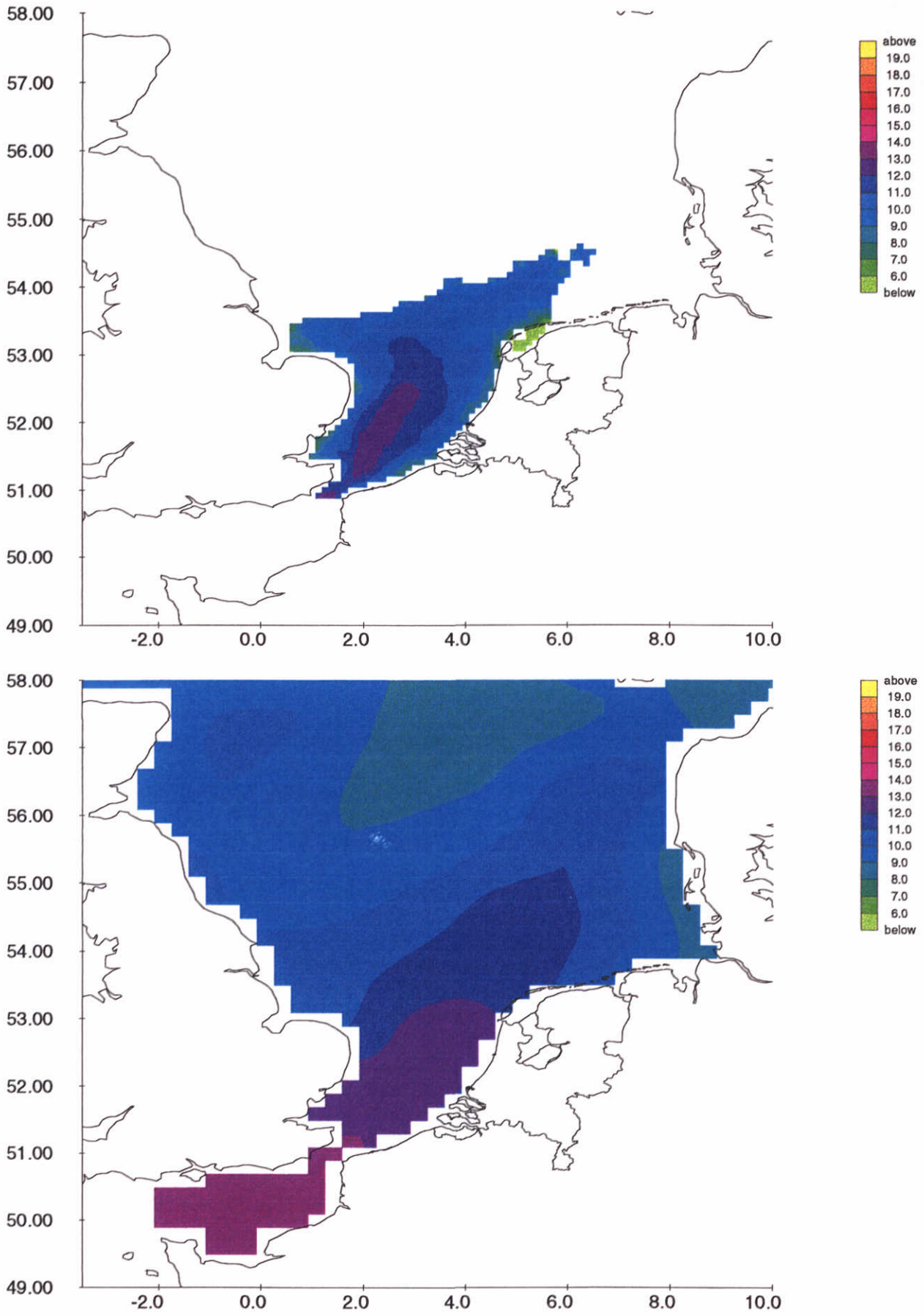

Remote sensing SST data (top) versus blended SST data (below
Date : November 29 1989

1998-11-12
11:42:13

DELFT HYDRAULICS | Z-2506 | Fig. 2.17

Reference simulation, see (Van Kester et al., 1997)

Directional Point Model. Formation of seasonal thermocline in North Sea. Site A : H=85 [m] ; 40 non-equidistant layers ; forcing by tide (CSM8) ; Lane's heat-flux model driven by observations of wind, cloud cover, air temperature, atmospheric pressure and humidity.		
	thermo.a40	
DELFT HYDRAULICS	Z 2506	Fig 3.1

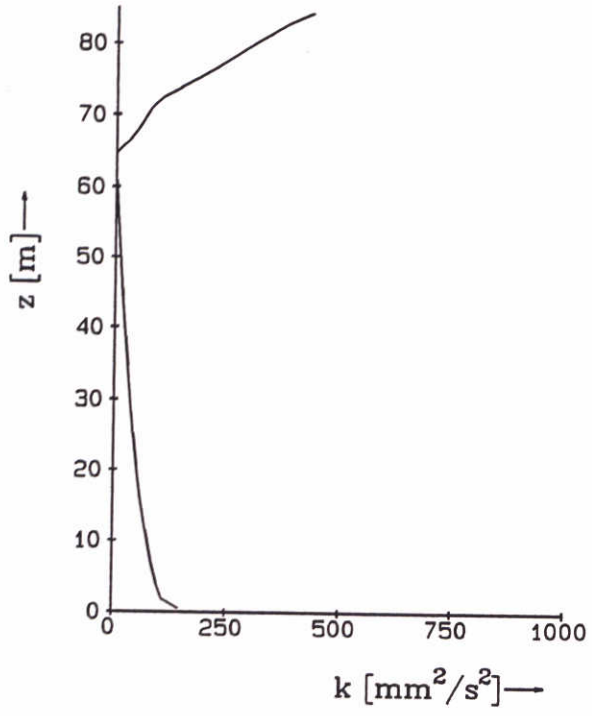

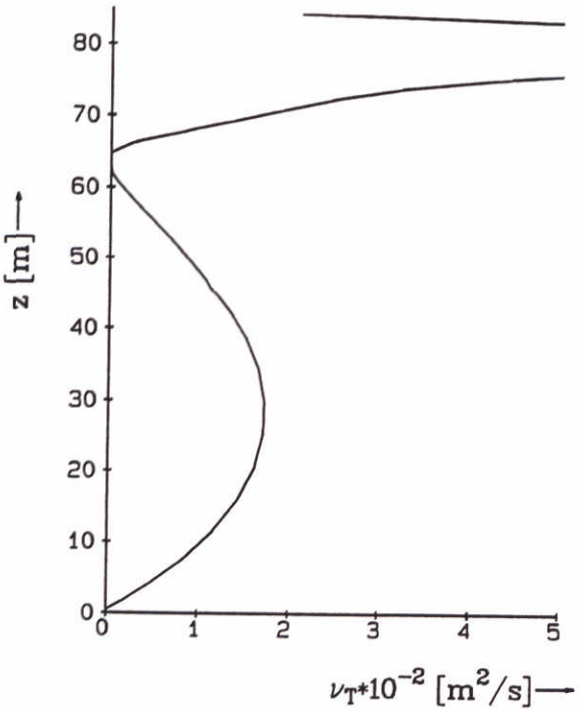

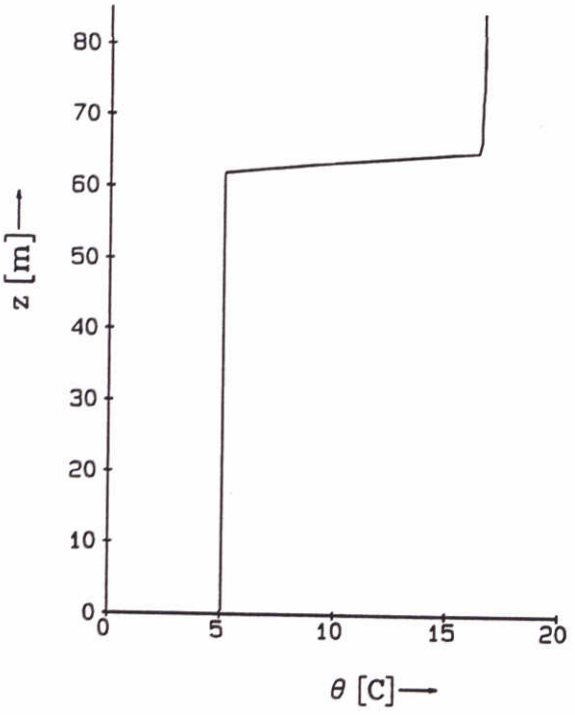

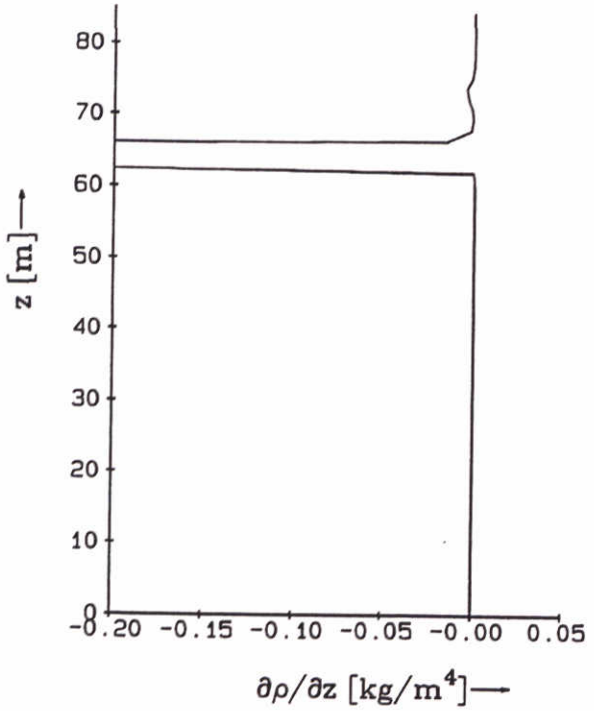

Day 240 ; Site A ($55^0$30'N,$0^0$54'E) ; H=85 [m].

Directional Point Model. Formation of seasonal thermocline in North Sea. Site A : H=85 [m] ; 100 equidistant layers ; forcing by tide (CSM8) ; Proctor's heat-flux model driven by observations of wind, cloud cover, air temperature, atmospheric pressure and humidity.	Day 240	
	selpro.a40	
DELFT HYDRAULICS	Z 2506	Fig 3.1a

For positive buoyancy: c_{3e}=0.5

Directional Point Model. Formation of seasonal thermocline in North Sea. Site A : H=85 [m] ; 40 non-equidistant layers ; forcing by tide (CSM8) ; Lane's heat-flux model driven by observations of wind, cloud cover, air temperature, atmospheric pressure and humidity.		
	thermo.a40	
DELFT HYDRAULICS	Z 2506	Fig 3.2

Background eddy viscosity: 1.10^{-4} [m^2/s]

Directional Point Model. Formation of seasonal thermocline in North Sea. Site A : H=85 [m] ; 40 non-equidistant layers ; forcing by tide (CSM8) ; Lane's heat-flux model driven by observations of wind, cloud cover, air temperature, atmospheric pressure and humidity.		
	thermo.a40	
DELFT HYDRAULICS	Z 2506	Fig 3.3

Background eddy viscosity: 5.10^{-5} [m^2/s]

Directional Point Model. Formation of seasonal thermocline in North Sea. Site A : H=85 [m] ; 40 non-equidistant layers ; forcing by tide (CSM8) ; Lane's heat-flux model driven by observations of wind, cloud cover, air temperature, atmospheric pressure and humidity.		
	thermo.a40	
DELFT HYDRAULICS	Z 2506	Fig 3.4

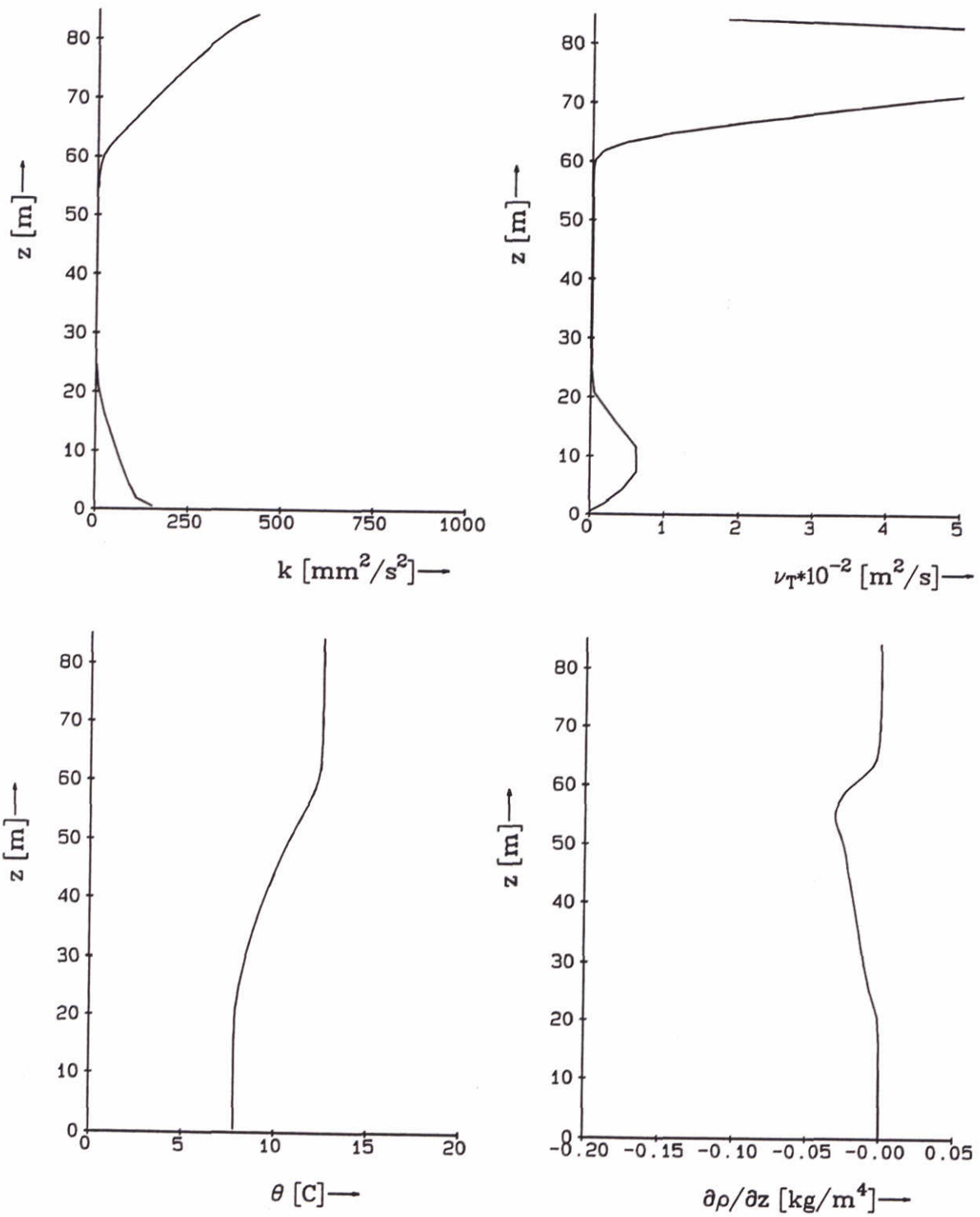

Day 240 ; Site A ($55^0 30'N, 0^0 54'E$) ; H=85 [m].

Directional Point Model. Formation of seasonal thermocline in North Sea. Site A : H=85 [m] ; 100 equidistant layers ; forcing by tide (CSM8) ; Proctor's heat-flux model driven by observations of wind, cloud cover, air temperature, atmospheric pressure and humidity.	Day 240	
	selpro.a40	
DELFT HYDRAULICS	Z 2506	Fig 3.4a

Constant 5.10^{-5} [m^2/s] diffusion for heat.

Directional Point Model. Formation of seasonal thermocline in North Sea. Site A : H=85 [m] ; 40 non-equidistant layers ; forcing by tide (CSM8) ; Lane's heat-flux model driven by observations of wind, cloud cover, air temperature, atmospheric pressure and humidity.		
	thermo.a40	
DELFT HYDRAULICS	Z 2506	Fig 3.5

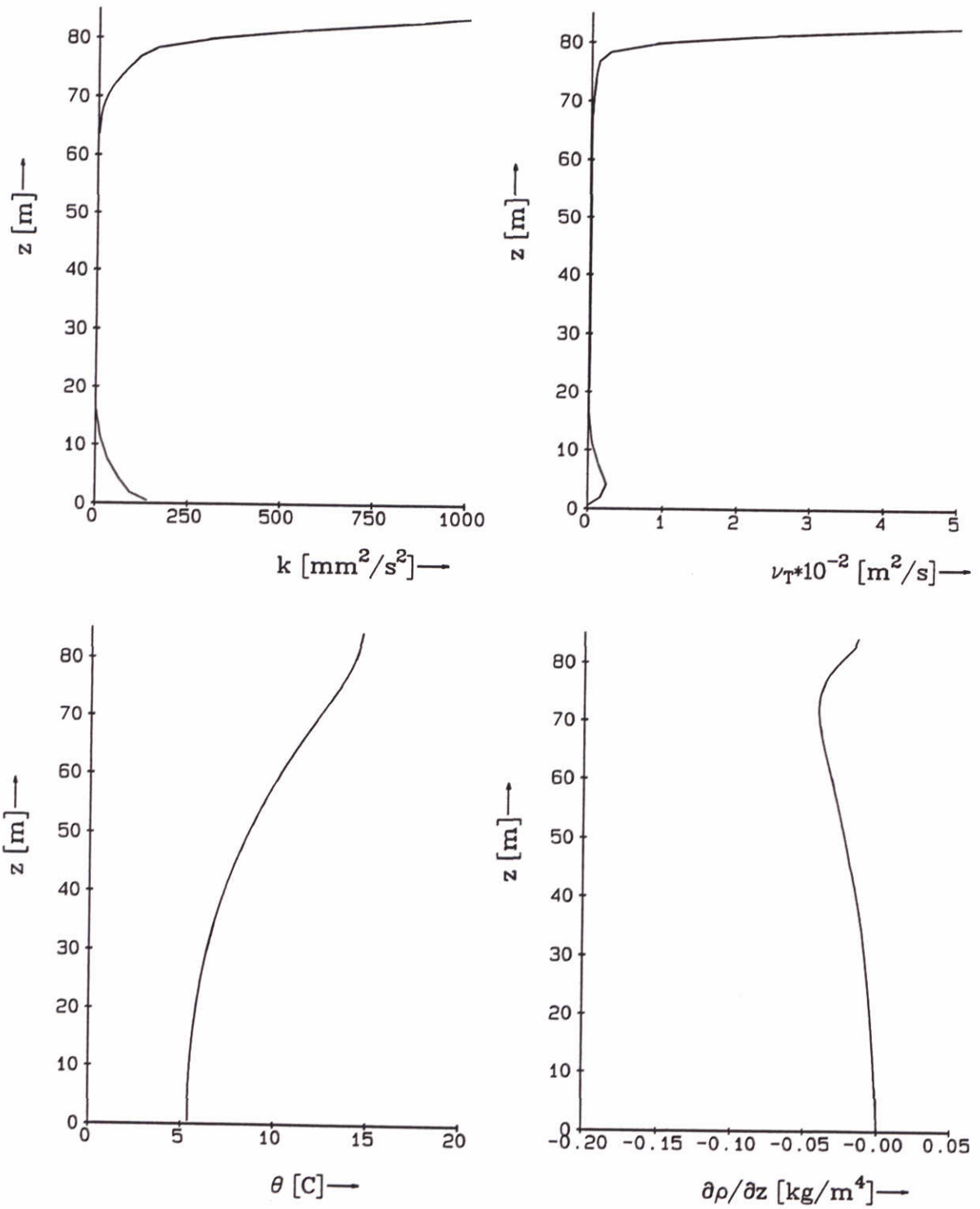

Day 240 ; Site A ($55^0$30'N,$0^0$54'E) ; H=85 [m].

Directional Point Model. Formation of seasonal thermocline in North Sea. Site A : H=85 [m] ; 100 equidistant layers ; forcing by tide (CSM8) ; Proctor's heat-flux model driven by observations of wind, cloud cover, air temperature, atmospheric pressure and humidity.	Day 240	
	selpro.a40	
DELFT HYDRAULICS	Z 2506	Fig 3.5a

Background eddy diffusivity of 7.10^{-5} [m^2/s] for heat added to eddy diffusivity estimated by k−ε model.

Directional Point Model. Formation of seasonal thermocline in North Sea. Site A : H=85 [m] ; 40 non-equidistant layers ; forcing by tide (CSM8) ; Lane's heat-flux model driven by observations of wind, cloud cover, air temperature, atmospheric pressure and humidity.	thermo.a40	
DELFT HYDRAULICS	Z 2506	Fig 3.6a

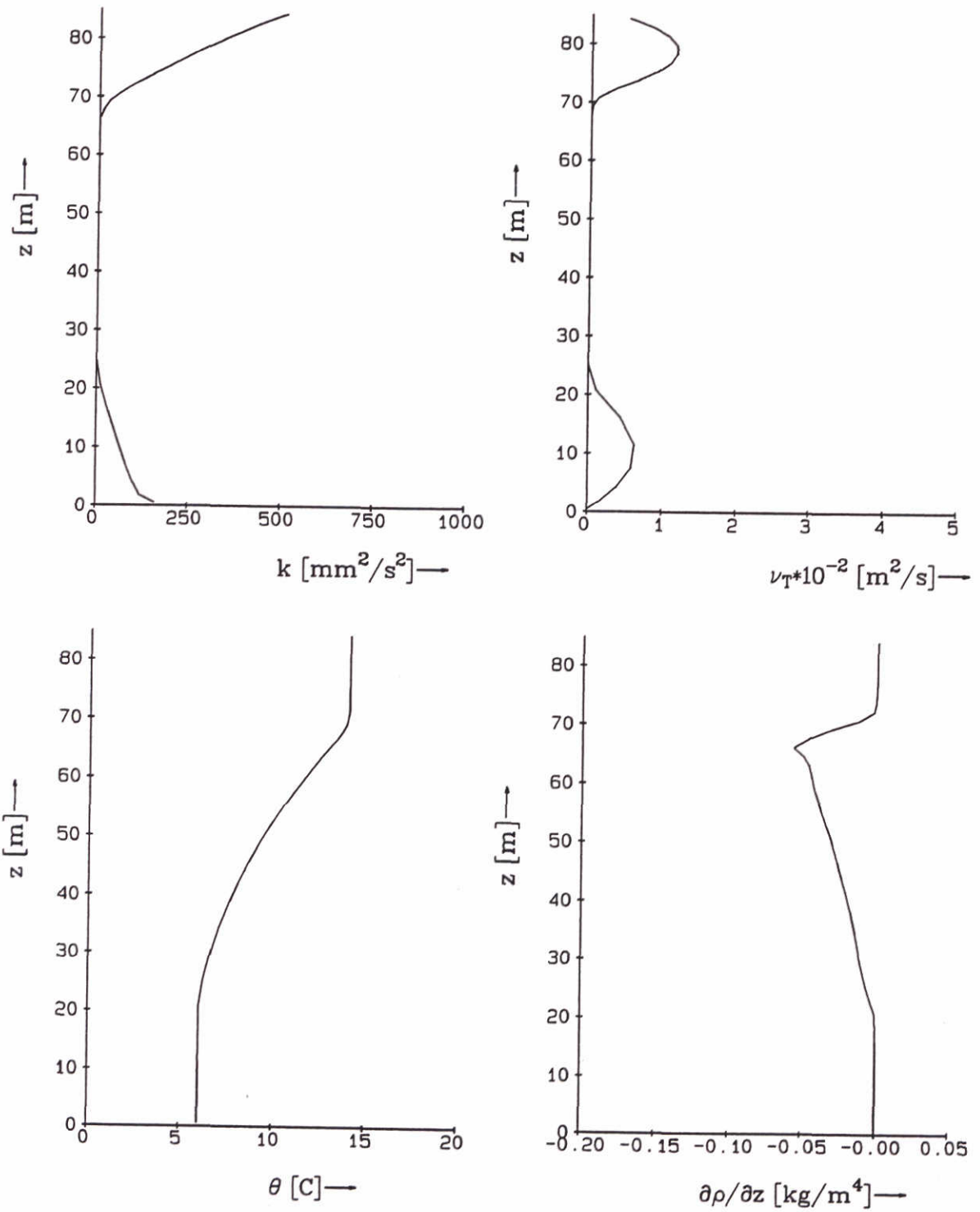

Background eddy diffusivity of 7.10^{-5} [m^2/s] for heat added to eddy diffusivity estimated by k–ε model.

Directional Point Model. Formation of seasonal thermocline in North Sea. Site A : H=85 [m] ; 40 non–equidistant layers ; forcing by tide (CSM8) ; Lane's heat–flux model driven by observations of wind, cloud cover, air temperature, atmospheric pressure and humidity.	Day 240	
	selpro.a40	
DELFT HYDRAULICS	Z 2506	Fig 3.6b

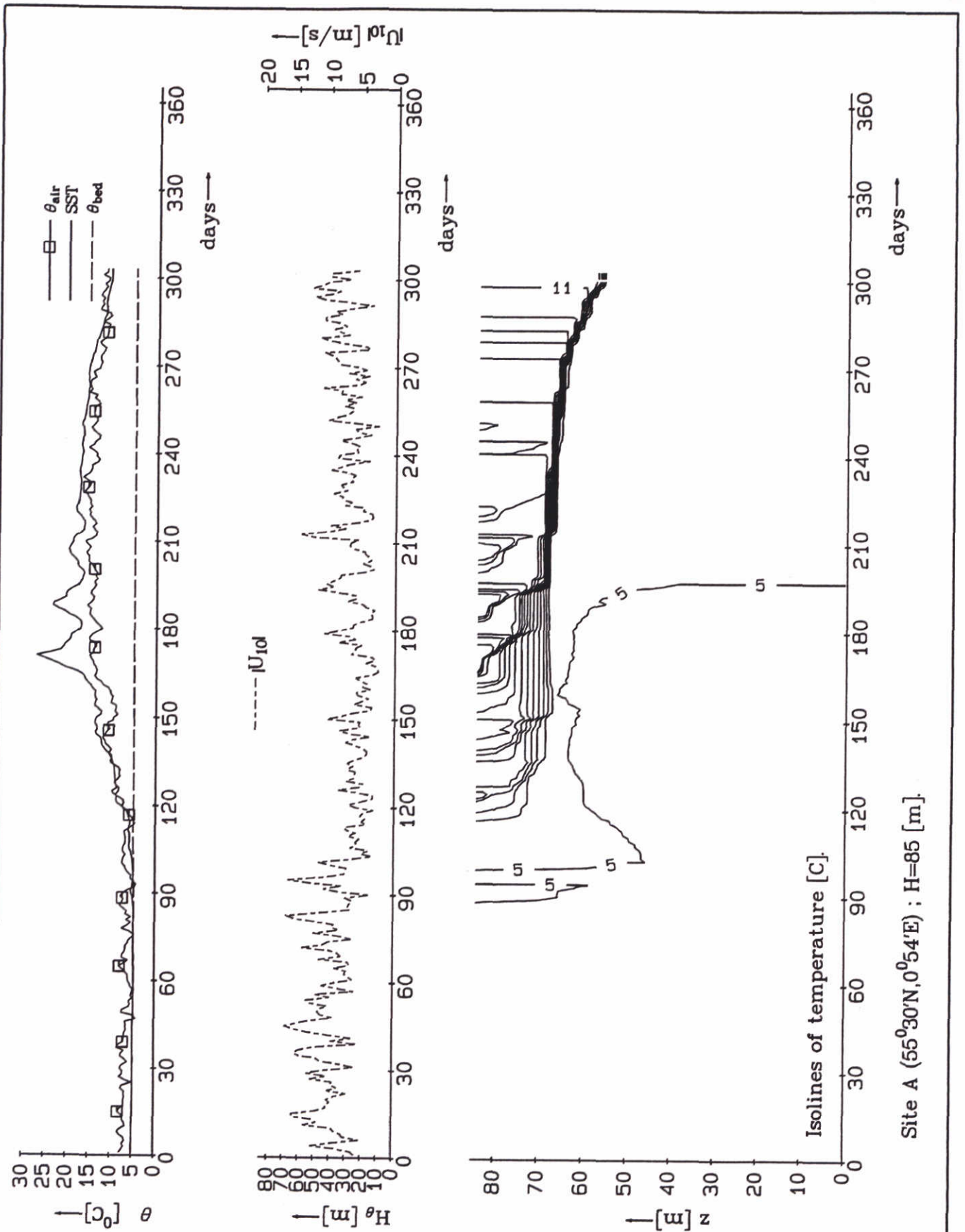

Background eddy viscosity of 1.10^{-4} [m^2/s] added to momemtum equations only.

Directional Point Model. Formation of seasonal thermocline in North Sea. Site A : H=85 [m] ; 40 non-equidistant layers ; forcing by tide (CSM8) ; Lane's heat-flux model driven by observations of wind, cloud cover, air temperature, atmospheric pressure and humidity.		
	thermo.a40	
DELFT HYDRAULICS	Z 2506	Fig 3.7

Background eddy viscosity of 1.10^{-4} [m^2/s] added to momemtum equations and k and ε shear production.

Directional Point Model. Formation of seasonal thermocline in North Sea. Site A : H=85 [m] ; 40 non-equidistant layers ; forcing by tide (CSM8) ; Lane's heat-flux model driven by observations of wind, cloud cover, air temperature, atmospheric pressure and humidity.		
	thermo.a40	
DELFT HYDRAULICS	Z 2506	Fig 3.8

Background eddy viscosity of 5.10^{-4} [m^2/s] added to momemtum equations and k and ε shear production.

Directional Point Model. Formation of seasonal thermocline in North Sea. Site A : H=85 [m] ; 40 non–equidistant layers ; forcing by tide (CSM8) ; Lane's heat–flux model driven by observations of wind, cloud cover, air temperature, atmospheric pressure and humidity.	thermo.a40	
DELFT HYDRAULICS	Z 2506	Fig 3.9

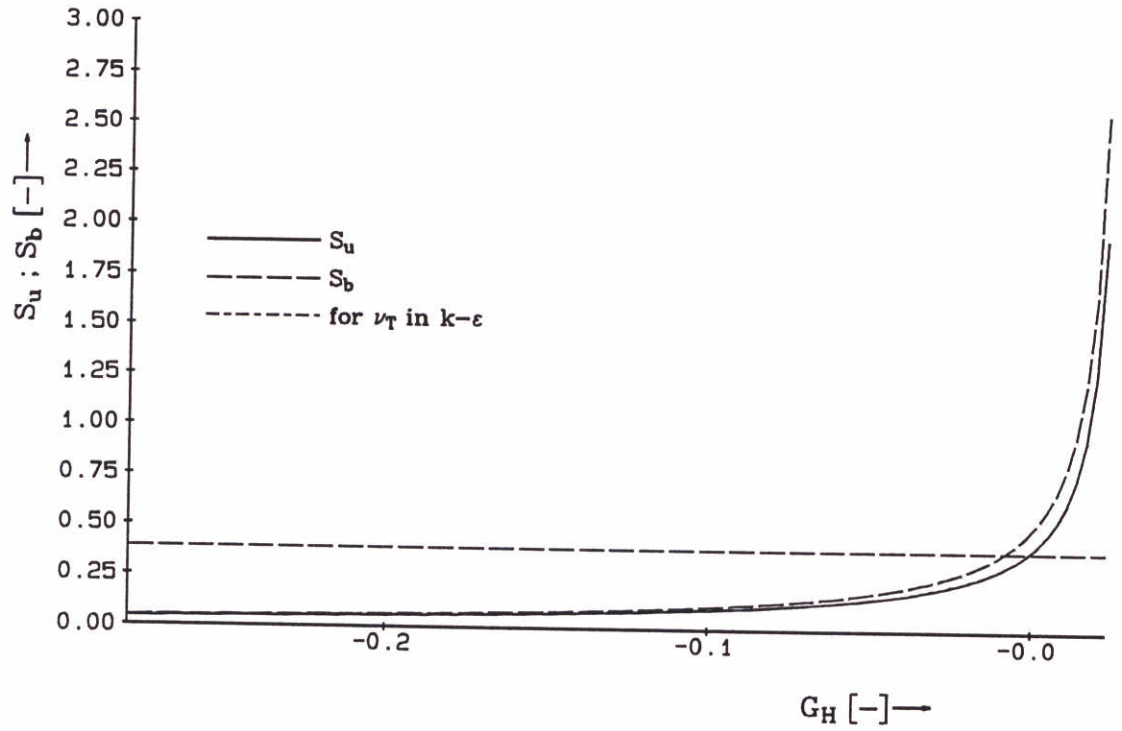

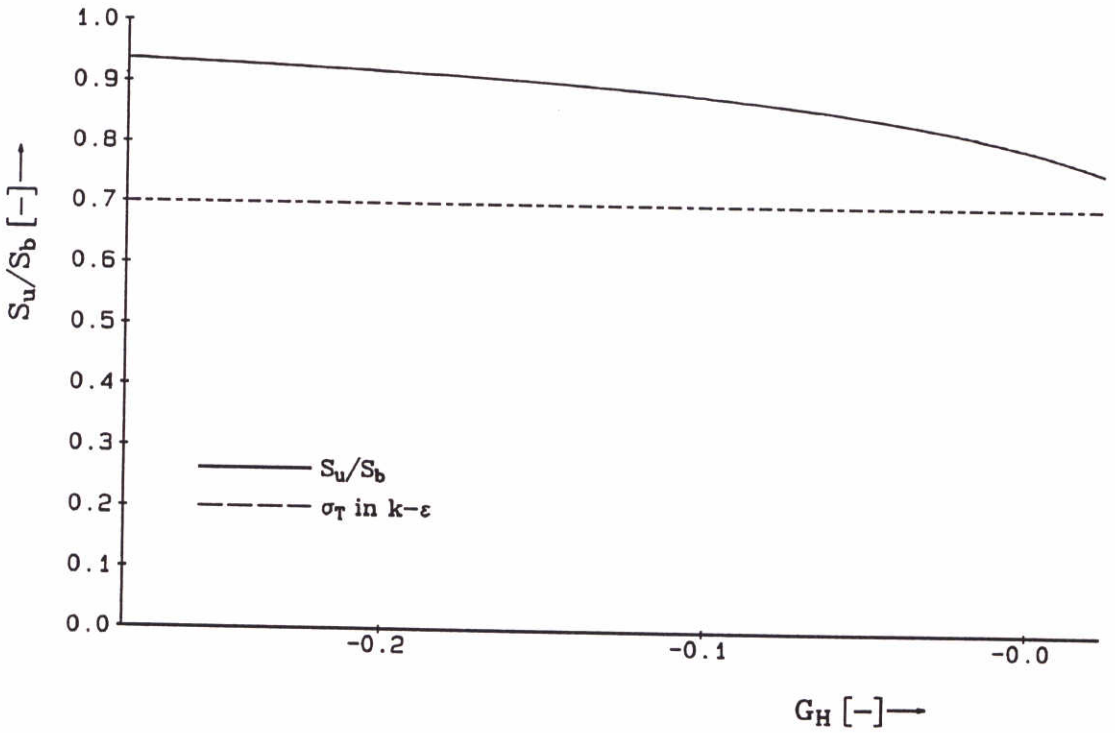

Damping functions S_b and S_u (Galperin et al., 1988) for the Quasi-Equilibrium version of the 2.5 level Mellor-Yamada model ; $G_H=-(Nl/q)^2$.

susb.inv

DELFT HYDRAULICS

Z 2506

Fig 3.10

Application of the Quasi-Equilibrium Mellor-Yamada model level 2.5, with same forcing as for Figure X.1.

Directional Point Model. Formation of seasonal thermocline in North Sea. Site A : H=85 [m] ; 40 non-equidistant layers ; forcing by tide (CSM8) ; Lane's heat-flux model driven by observations of wind, cloud cover, air temperature, atmospheric pressure and humidity.		
	thermo.a40	
DELFT HYDRAULICS	Z 2506	Fig 3.11a

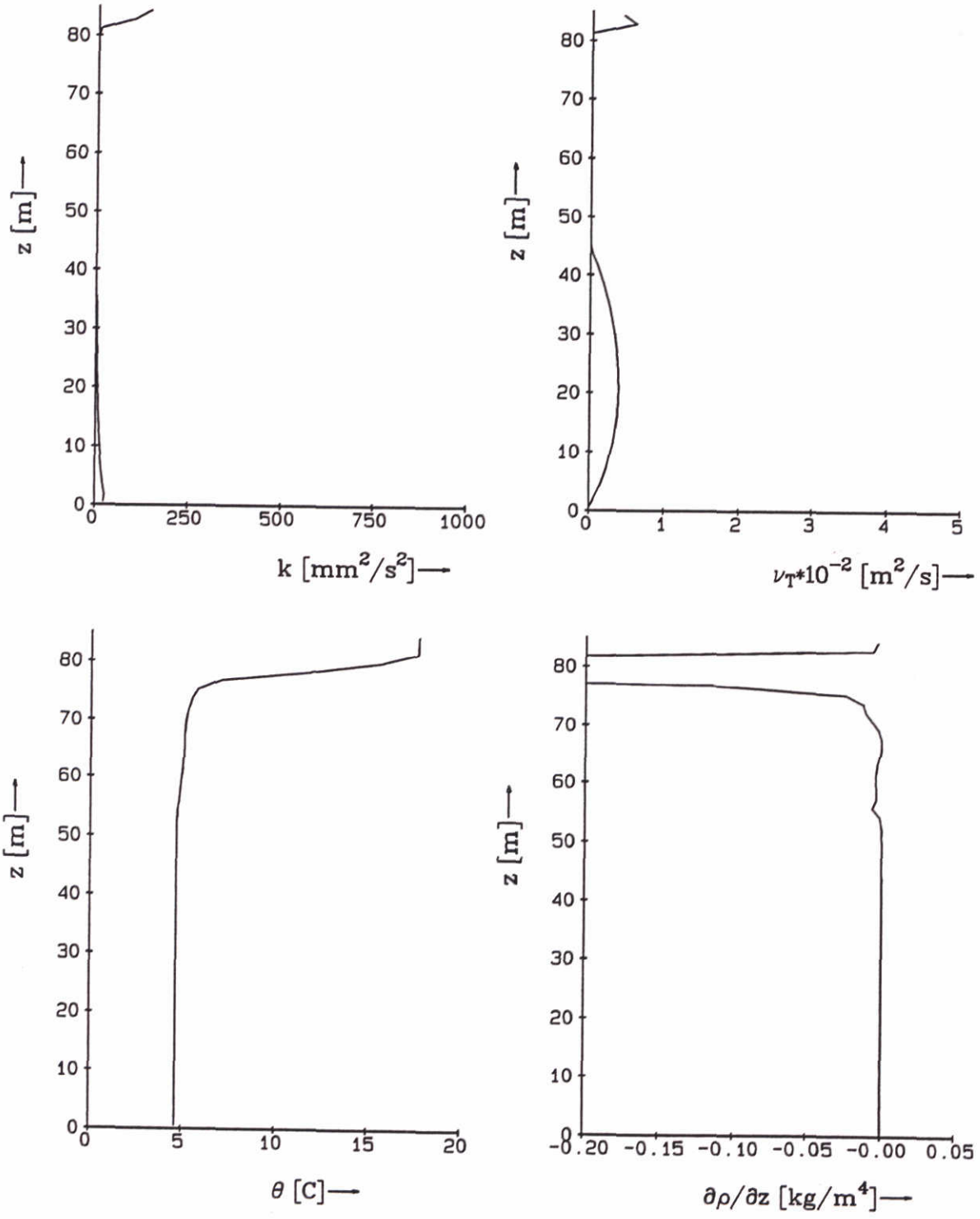

Application of the Quasi-Equilibrium Mellor-Yamada model level 2.5, with same forcing as for Figure X.1.

Directional Point Model. Formation of seasonal thermocline in North Sea. Site A : H=85 [m] ; 40 non-equidistant layers ; forcing by tide (CSM8) ; Lane's heat-flux model driven by observations of wind, cloud cover, air temperature, atmospheric pressure and humidity.	Day 240	
	selpro.a40	
DELFT HYDRAULICS	Z 2506	Fig 3.11b

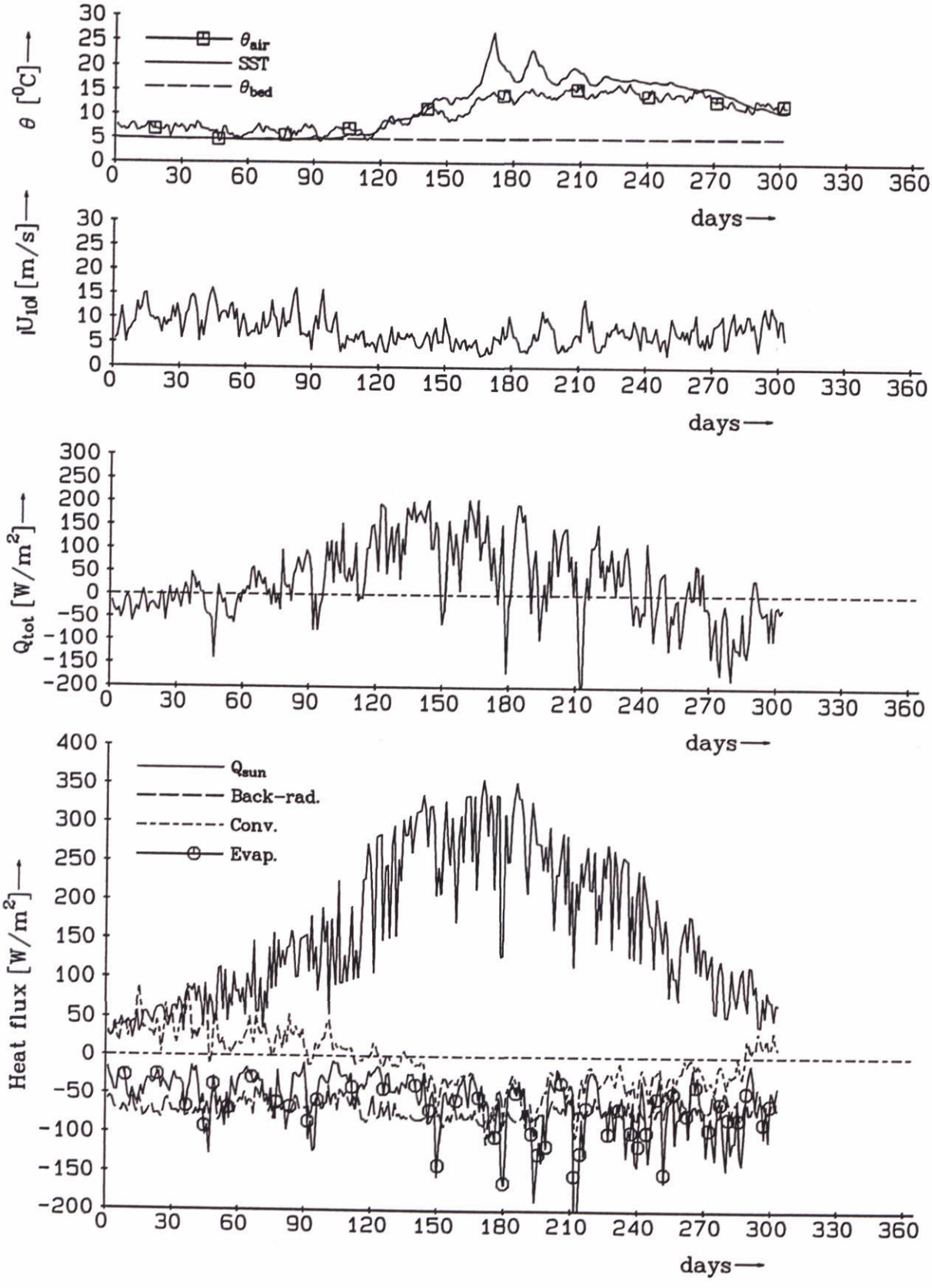

Directional Point Model. Formation of seasonal thermocline in North Sea. Site A : H=85 [m] ; 40 non-equidistant layers ; forcing by tide (CSM8) ; Lane's heat-flux model driven by observations of wind, cloud cover, air temperature, atmospheric pressure and humidity.

heat.csm

DELFT HYDRAULICS

Z 2034.30

Fig 3.12

Application of the k−ε model and solar−heat flux $Q_{sol}.\exp(-\lambda z)$; λ=0.154.

Directional Point Model. Formation of seasonal thermocline in North Sea. Site A : H=85 [m] ; 40 non−equidistant layers ; forcing by tide (CSM8) ; Lane's heat−flux model driven by observations of wind, cloud cover, air temperature, atmospheric pressure and humidity.	thermo.a40	
DELFT HYDRAULICS	Z 2506	Fig 3.13a

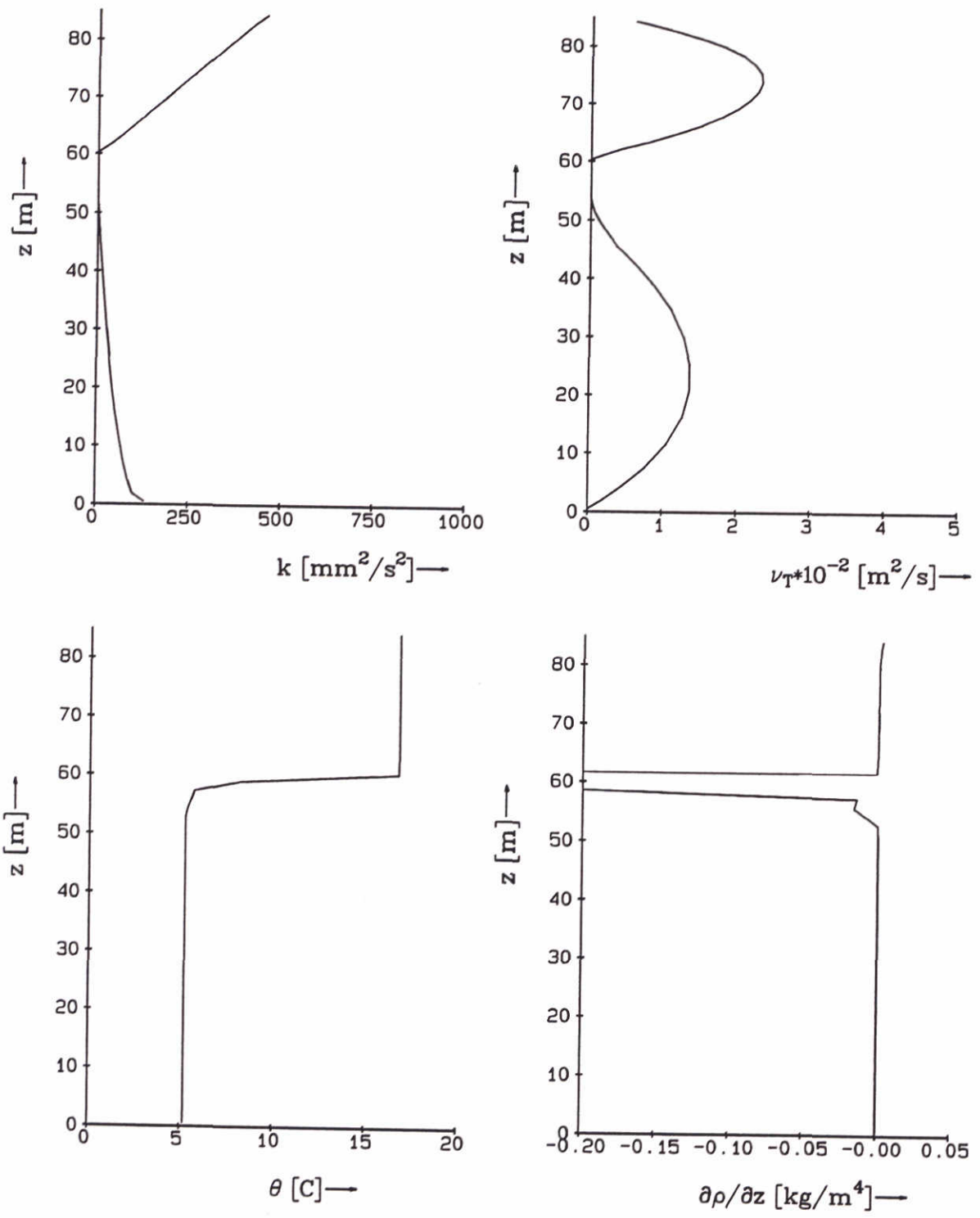

Application of the k−ε model and solar−heat flux $Q_{sol}.\exp(-\lambda z)$; λ=0.154.

Directional Point Model. Formation of seasonal thermocline in North Sea. Site A : H=85 [m] ; 40 non−equidistant layers ; forcing by tide (CSM8) ; Lane's heat−flux model driven by observations of wind, cloud cover, air temperature, atmospheric pressure and humidity.	Day 240	
	selpro.a40	
DELFT HYDRAULICS	Z 2506	Fig 3.13b

Quasi–Equilibrium Mellor–Yamada model ; solar–heat flux $Q_{sol}.\exp(-\lambda z)$; λ=0.154.

Directional Point Model. Formation of seasonal thermocline in North Sea. Site A : H=85 [m] ; 40 non–equidistant layers ; forcing by tide (CSM8) ; Lane's heat–flux model driven by observations of wind, cloud cover, air temperature, atmospheric pressure and humidity.

thermo.a40

DELFT HYDRAULICS

Z 2506

Fig 3.14a

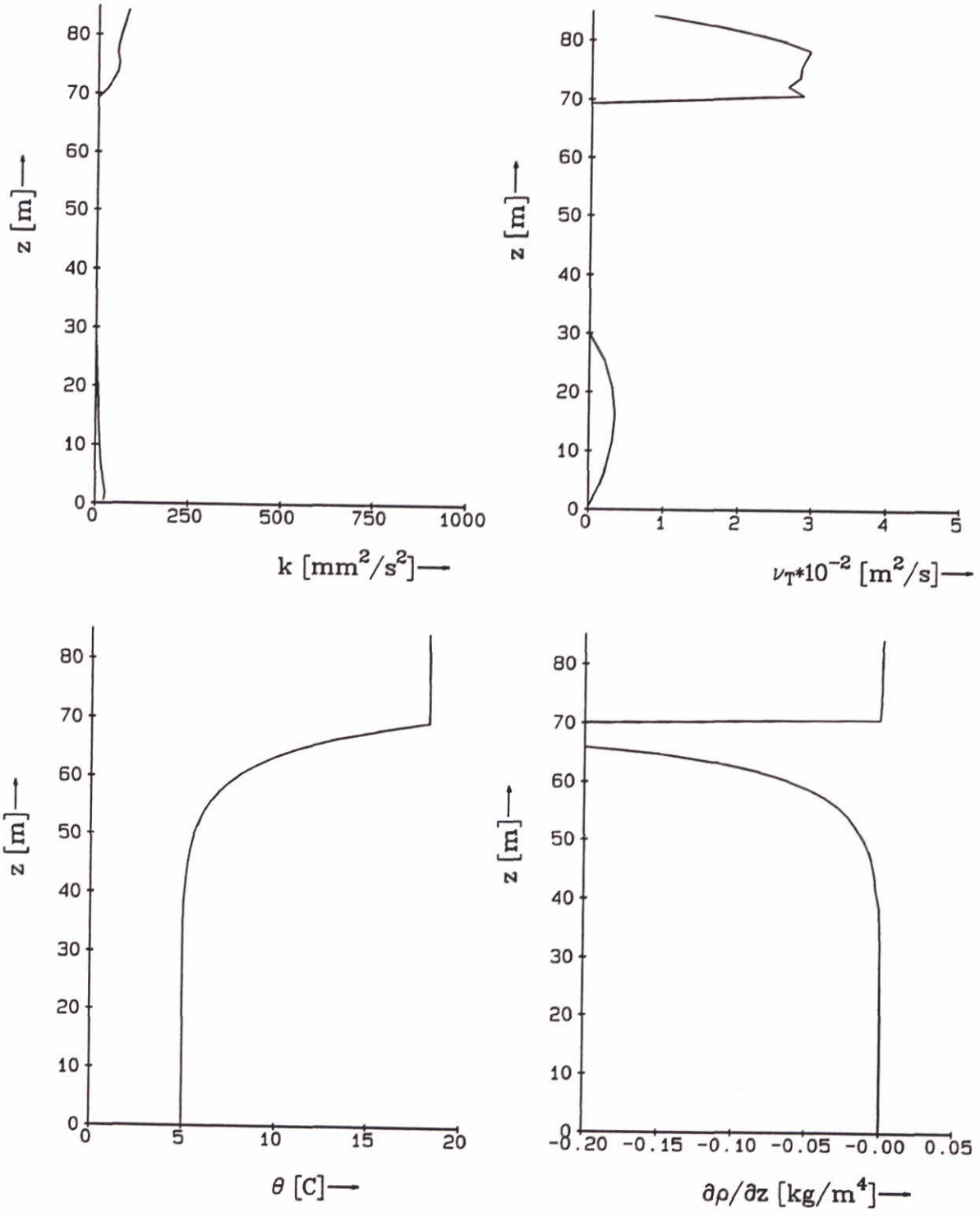

Quasi–Equilibrium Mellor–Yamada model ; solar–heat flux $Q_{sol}.\exp(-\lambda z)$; λ=0.154.

Directional Point Model. Formation of seasonal thermocline in North Sea. Site A : H=85 [m] ; 40 non–equidistant layers ; forcing by tide (CSM8) ; Lane's heat–flux model driven by observations of wind, cloud cover, air temperature, atmospheric pressure and humidity.	Day 240	
	selpro.a40	
DELFT HYDRAULICS	Z 2506	Fig 3.14b

Wind-drag coefficient C_D=0.004 .

Directional Point Model. Formation of seasonal thermocline in North Sea. Site A : H=85 [m] ; 40 *non-equidistant* layers ; forcing by tide (CSM8) ; Lane's heat-flux model driven by observations of wind, cloud cover, air temperature, atmospheric pressure and humidity.		
	thermo.a40	
DELFT HYDRAULICS	Z 2506	Fig 3.15a

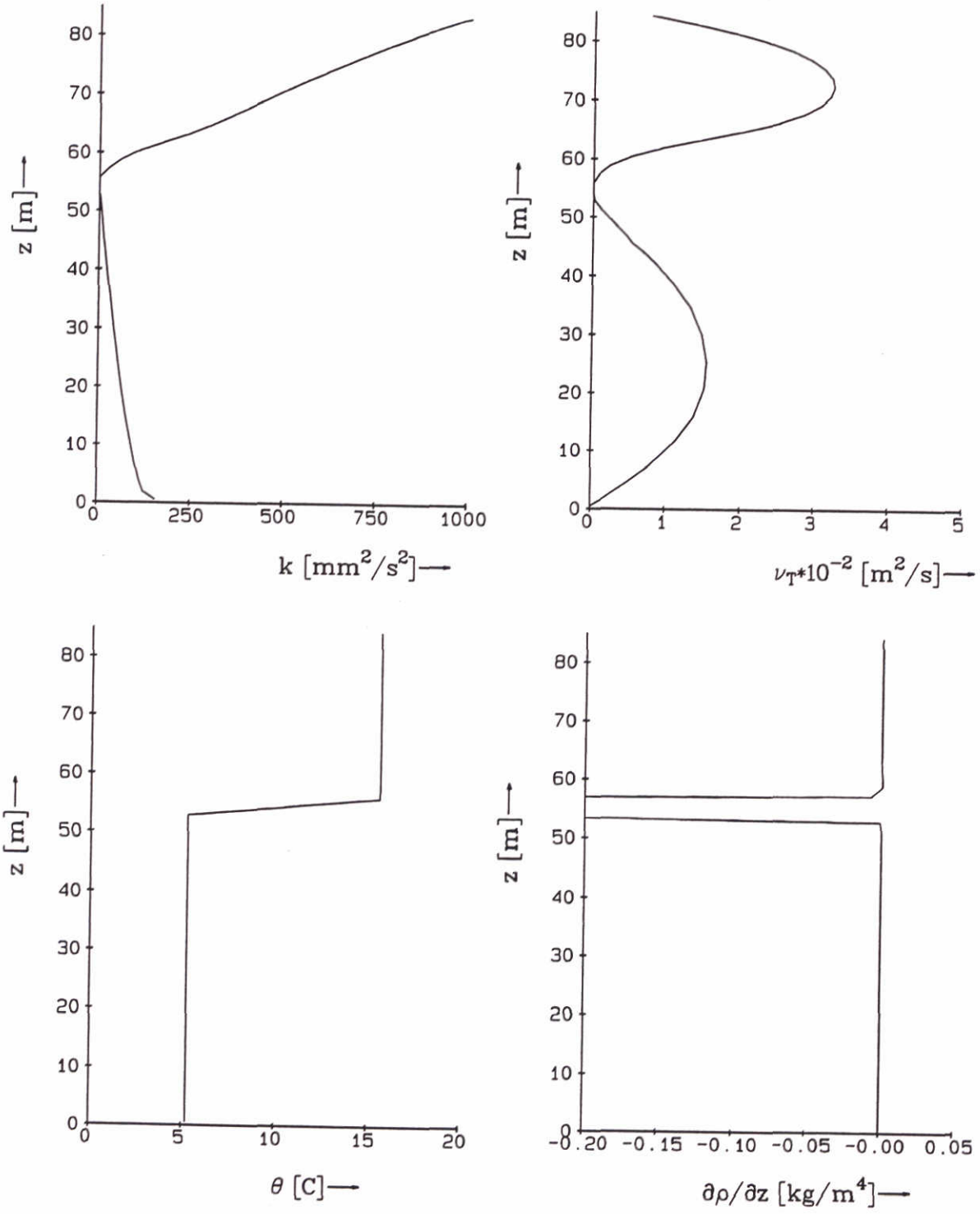

Wind-drag coefficient C_D=0.004 .

Directional Point Model. Formation of seasonal thermocline in North Sea. Site A : H=85 [m] ; 40 non-equidistant layers ; forcing by tide (CSM8) ; Lane's heat-flux model driven by observations of wind, cloud cover, air temperature, atmospheric pressure and humidity.	Day 240	
	selpro.a40	
DELFT HYDRAULICS	Z 2506	Fig 3.15b

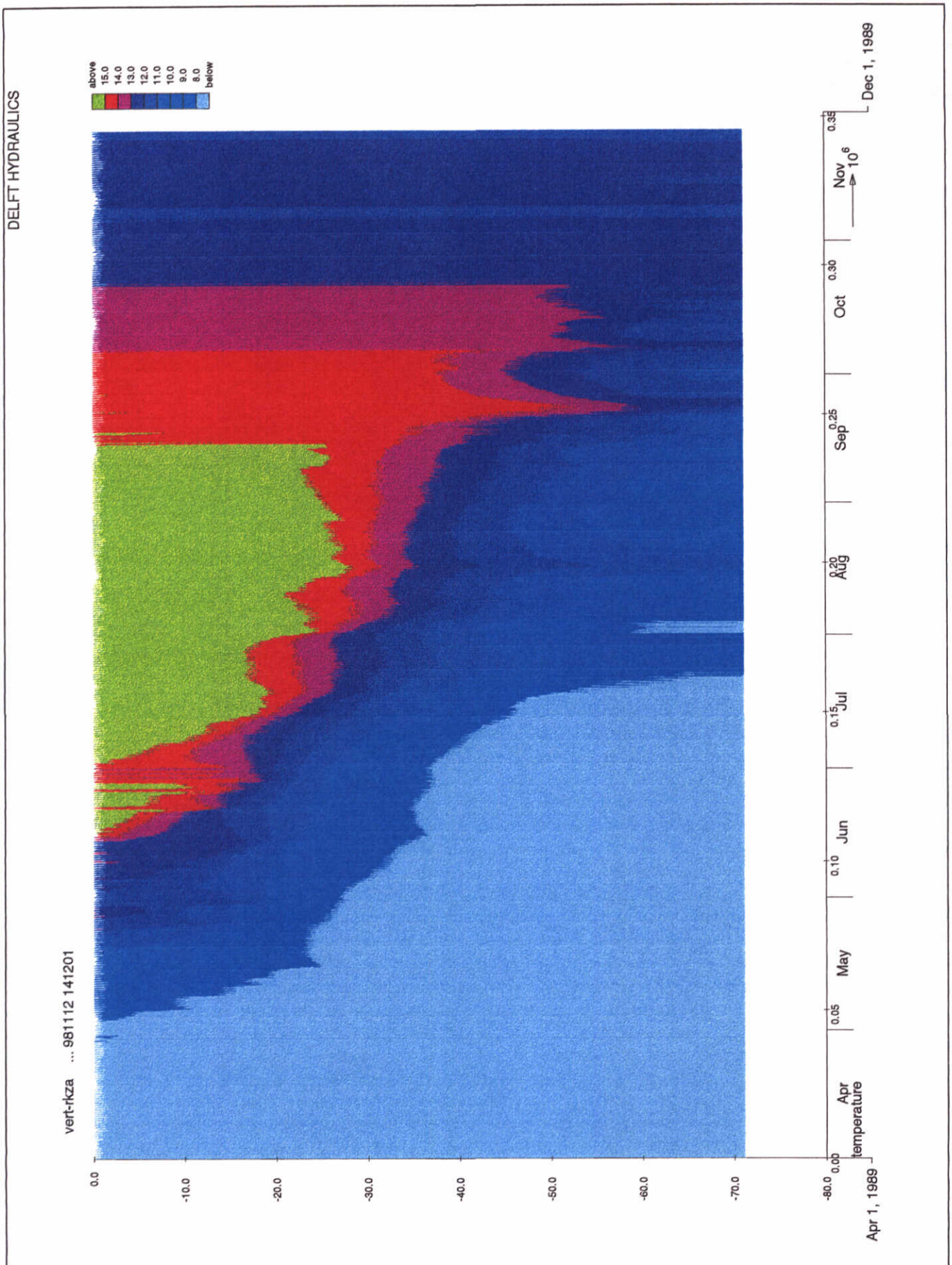

Evolution thermal stratification; 3D model 40 layers
at Site A (55.30 N, 0.54 E)
Forcing by NERC data

1998-11-12
14:17:38

DELFT HYDRAULICS

Fig. 4.1

DELFT HYDRAULICS

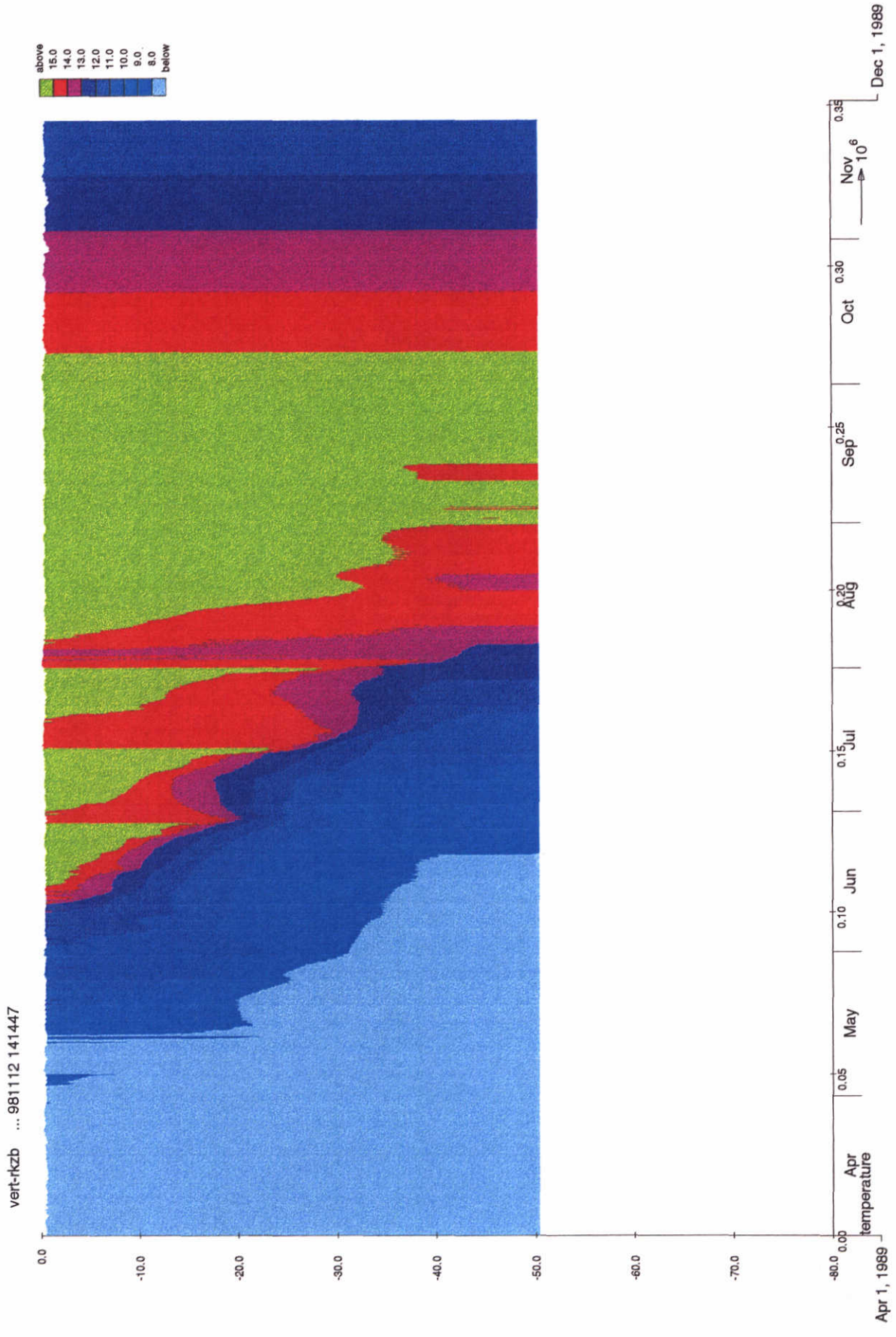

Evolution thermal stratification; 3D model 40 layers
at Site B (55.30 N, 5.31 E)
Forcing by NERC data

1998-11-12
14:18:33

DELFT HYDRAULICS

Fig. 4.2

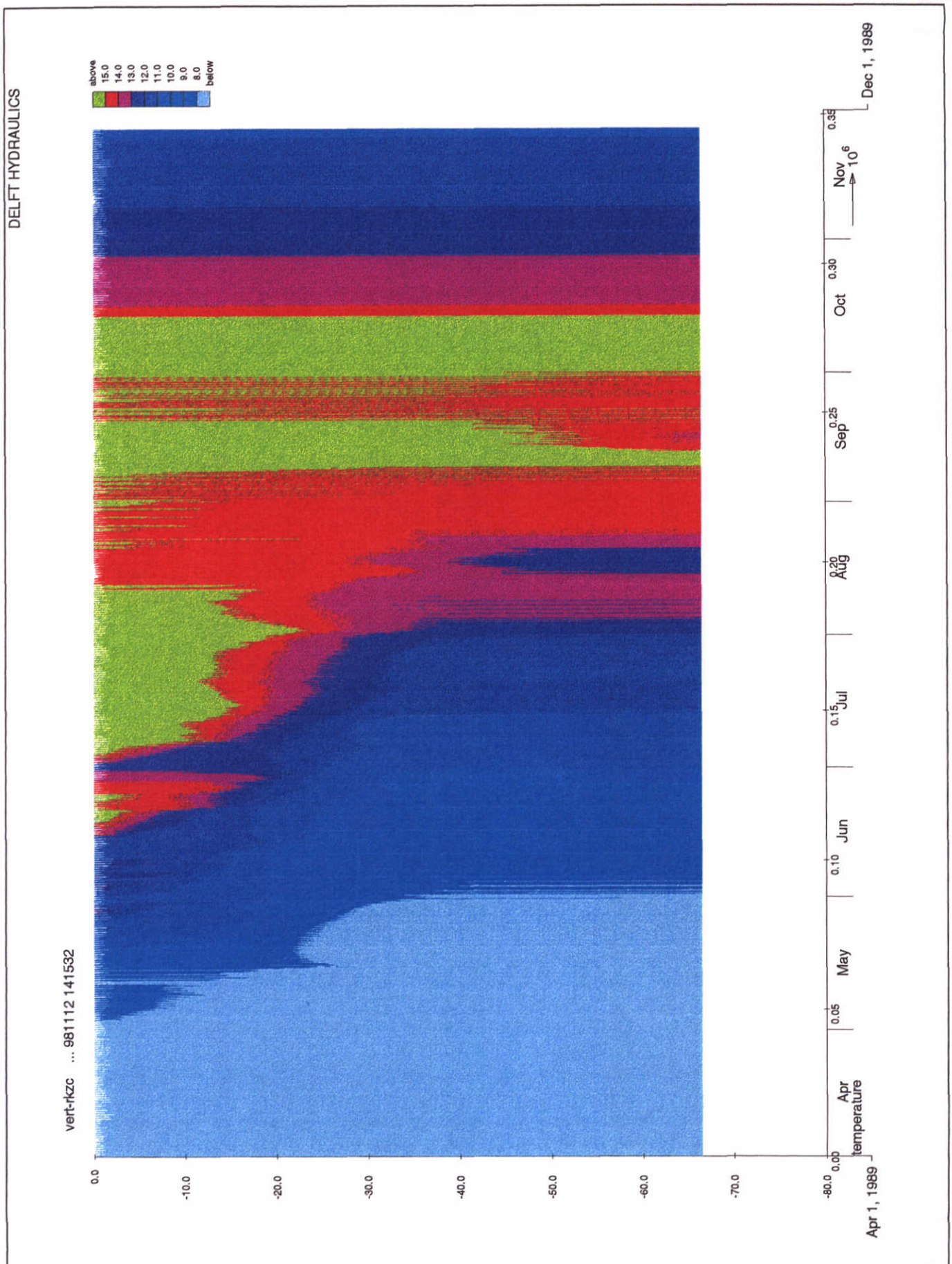

Evolution thermal stratification; 3D model 40 layers
at Site C (54.20 N, 0.24 E)
Forcing by NERC data

1998-11-12
14:19:29

DELFT HYDRAULICS

Fig. 4.3

DELFT HYDRAULICS

Evolution thermal stratification; 3D model 40 layers
at Site D (53.30 N, 3.0 E)
Forcing by NERC data

1998-11-12
14:20:31

DELFT HYDRAULICS

Fig. 4.4

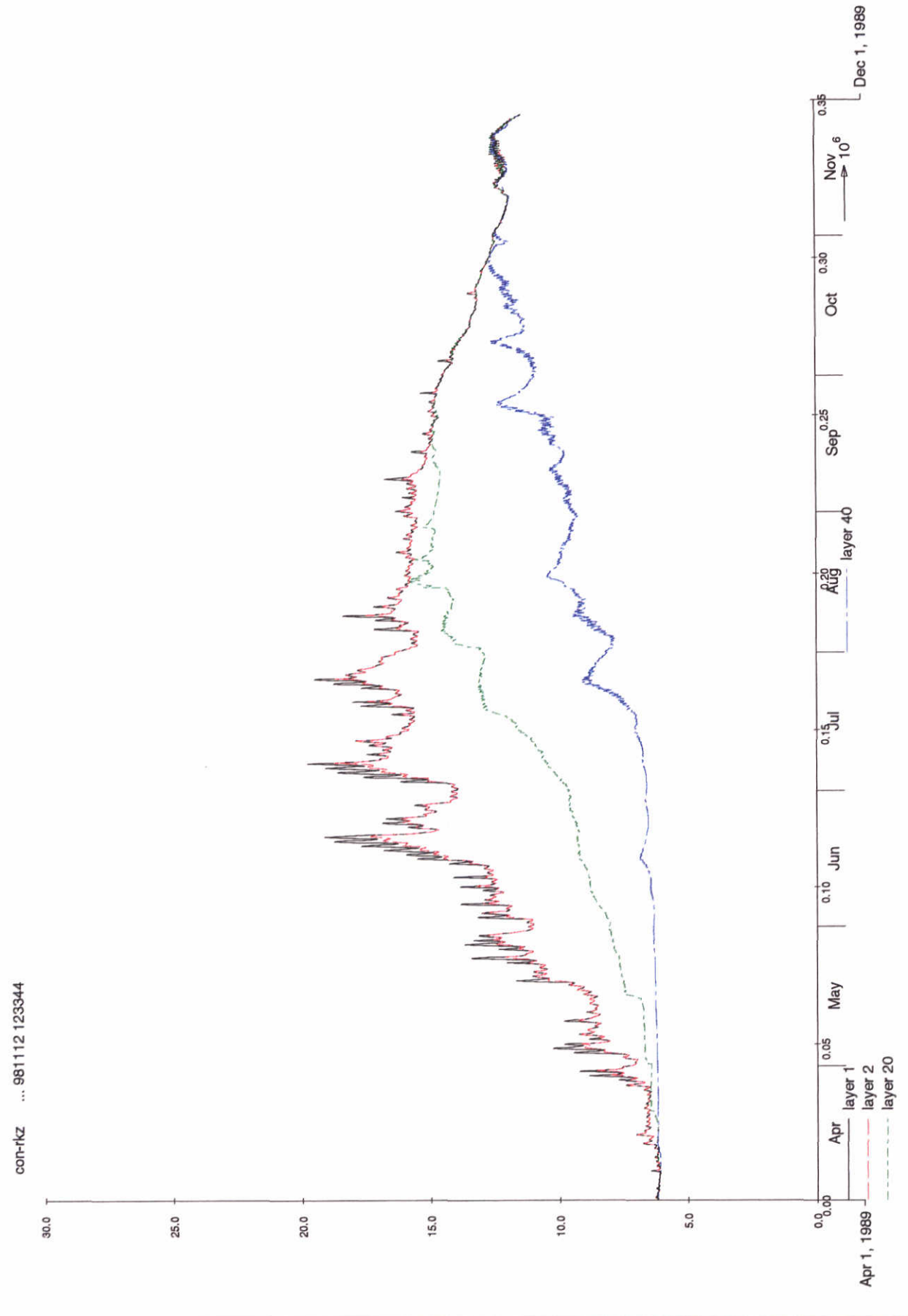

Long term simulation; 40 layers
Time histories of temperature at Measurement point A
Forcing by NERC data

1998-11-12
12:39:21

DELFT HYDRAULICS

Fig. 4.5

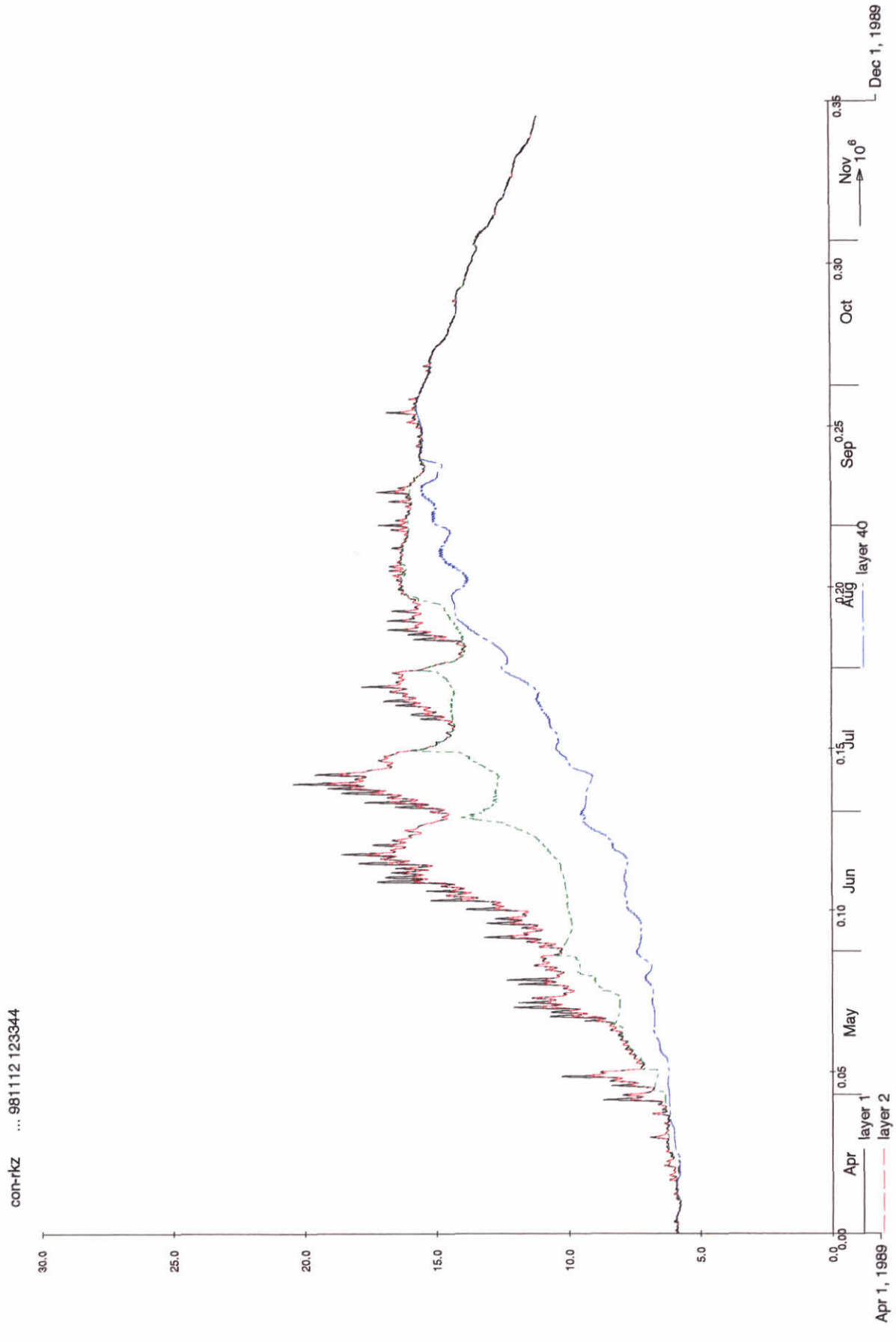

Long term simulation; 40 layers
Time histories of temperature at Measurement point B
Forcing by NERC data

1998-11-12
12:39:45

DELFT HYDRAULICS

Fig. 4.6

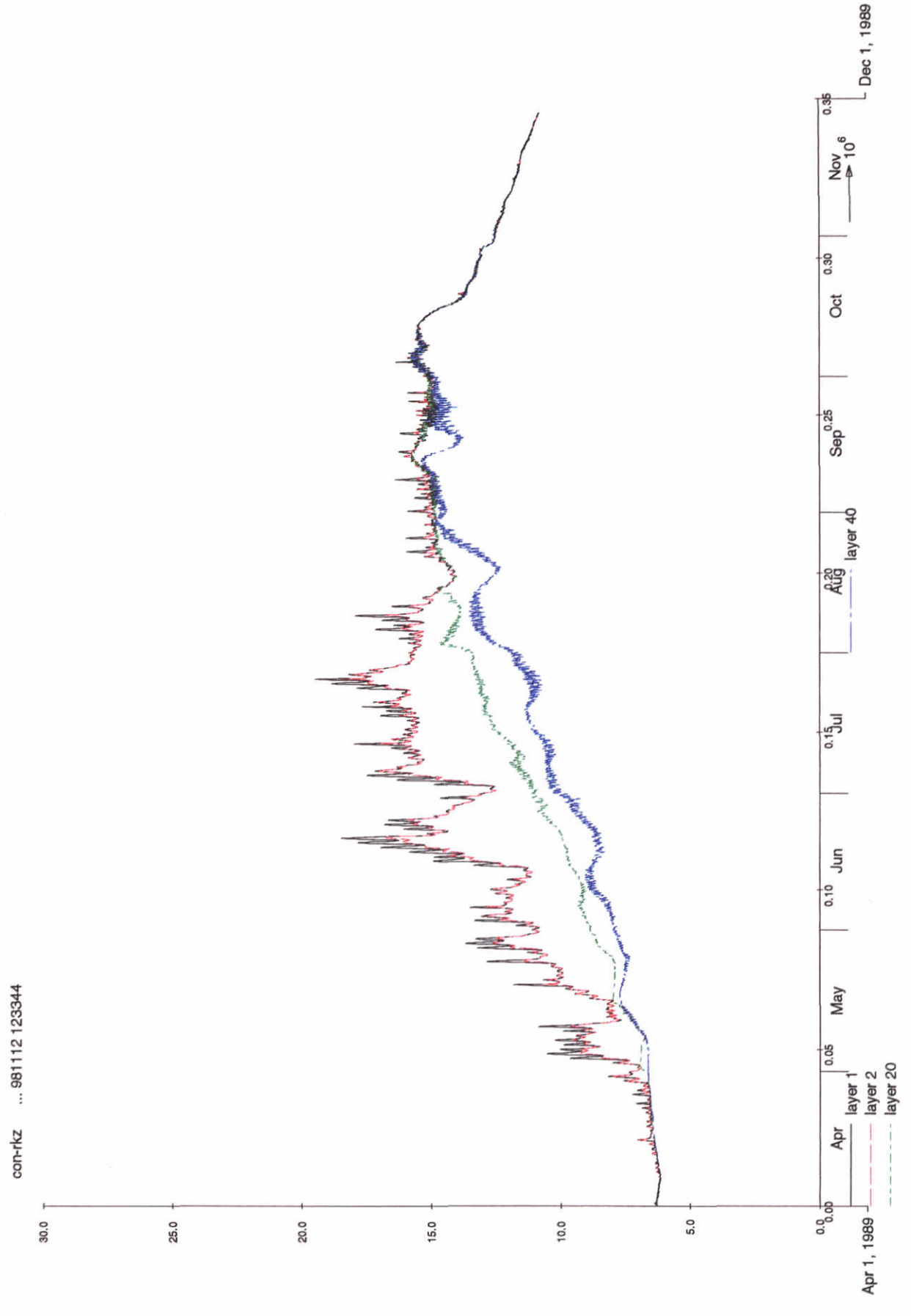

Long term simulation; 40 layers
Time histories of temperature at Measurement point C
Forcing by NERC data

1998-11-12
12:40:02

DELFT HYDRAULICS

Fig. 4.7

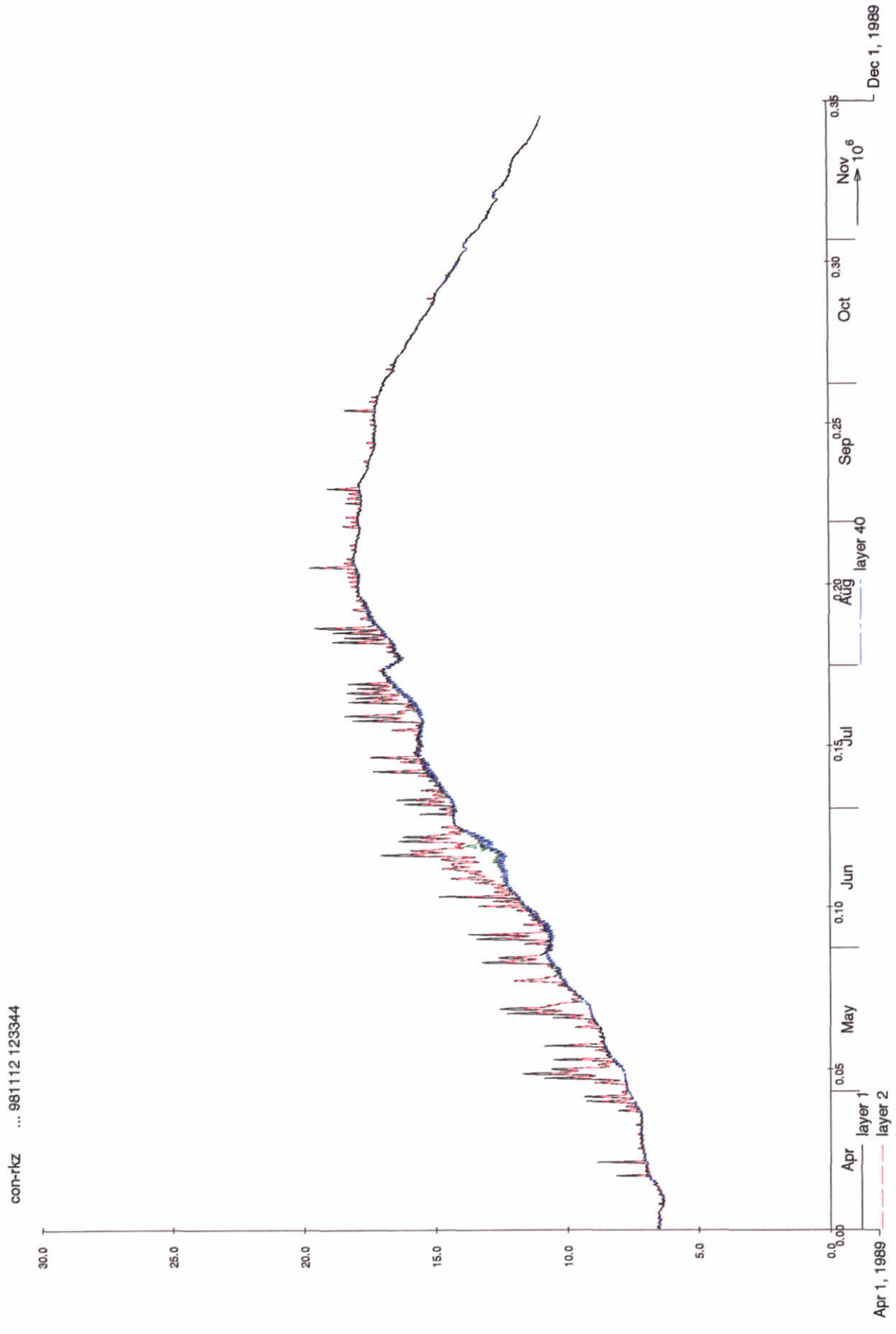

Long term simulation; 40 layers
Time histories of temperature at Measurement point D
Forcing by NERC data

1998-11-12
12:40:25

DELFT HYDRAULICS

Fig. 4.8

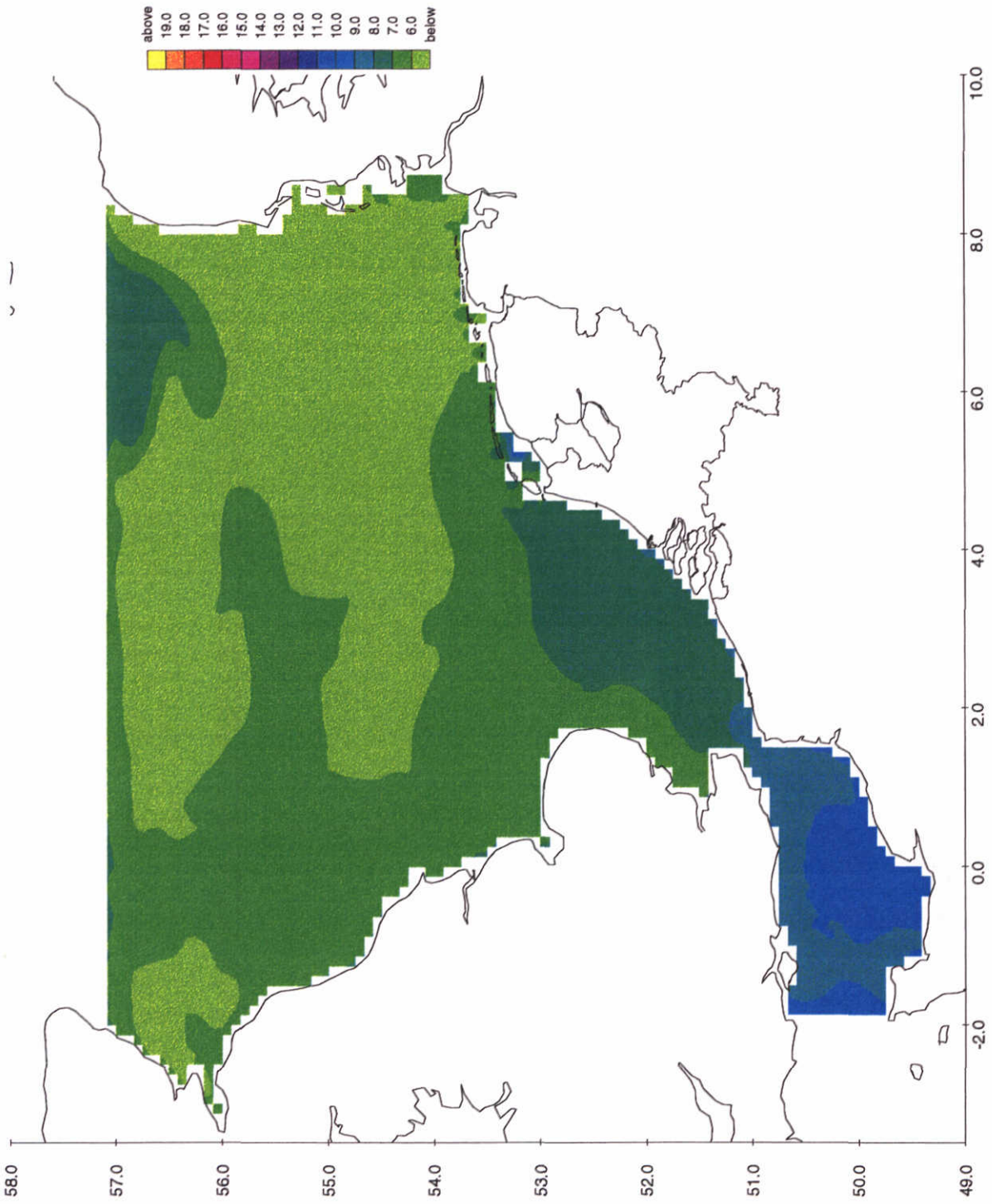

Model results of SST obtained with TRIWAQ/TEM
Date : 1989/04/08 13:00

1998-12-14
12:35:38

DELFT HYDRAULICS

Z-2506

Fig. 4.09

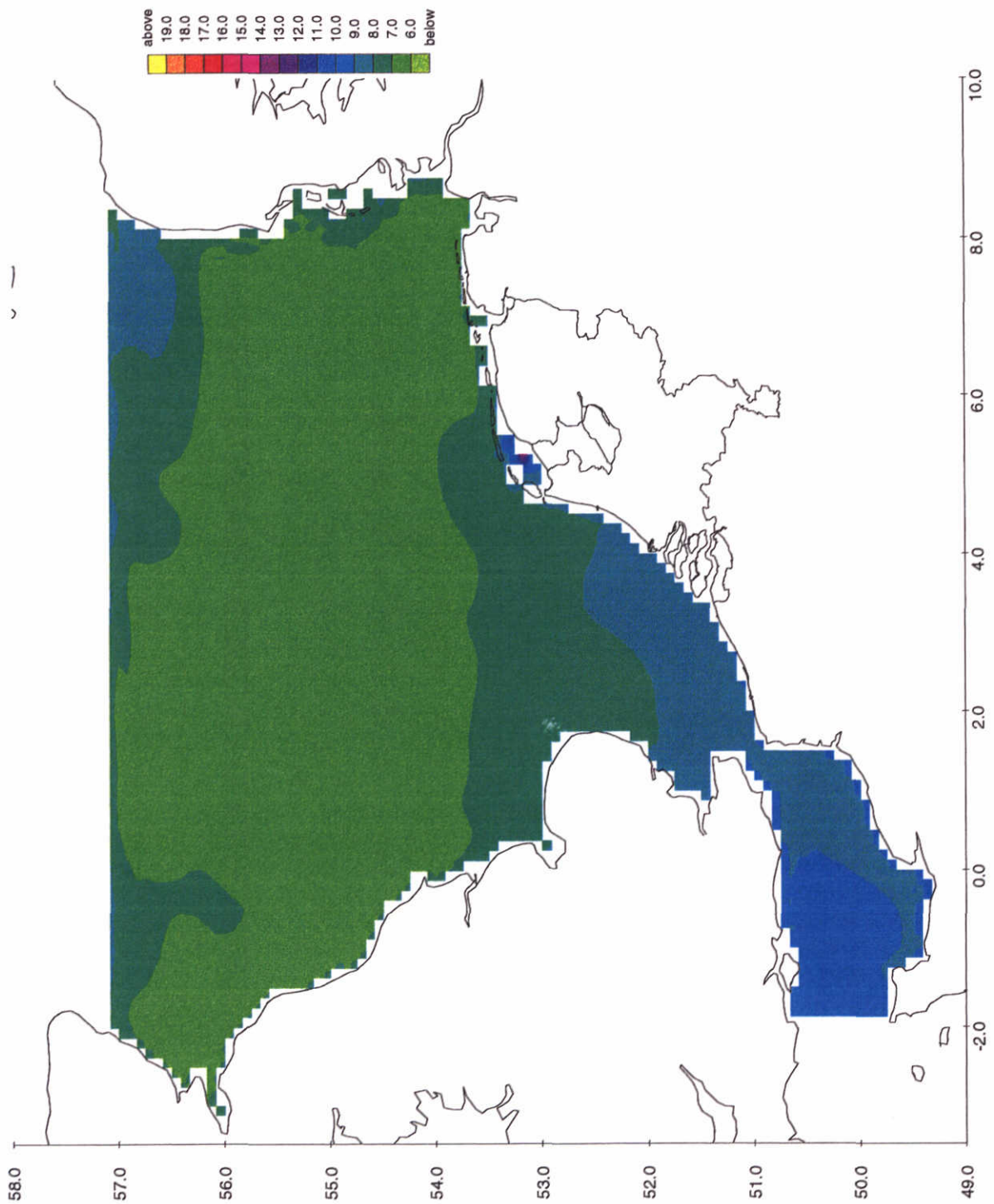

Model results of SST obtained with TRIWAQ/TEM
Date : 1989/04/21 13:00

1998-12-14
12:35:40

DELFT HYDRAULICS

Z-2506

Fig. 4.10

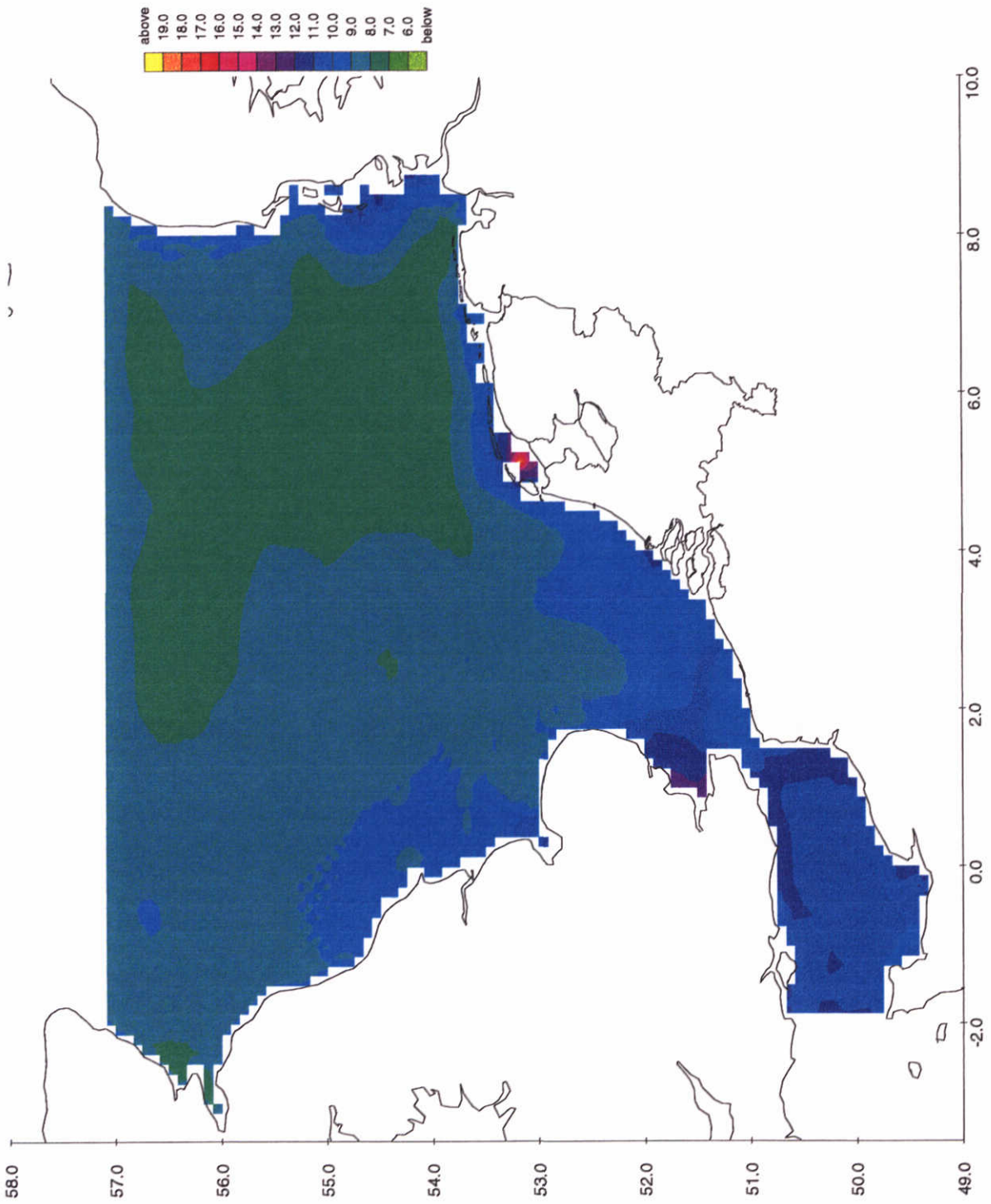

Model results of SST obtained with TRIWAQ/TEM
Date : 1989/05/09 13:00

1998-12-14
12:35:43

DELFT HYDRAULICS

Z-2506

Fig. 4.11

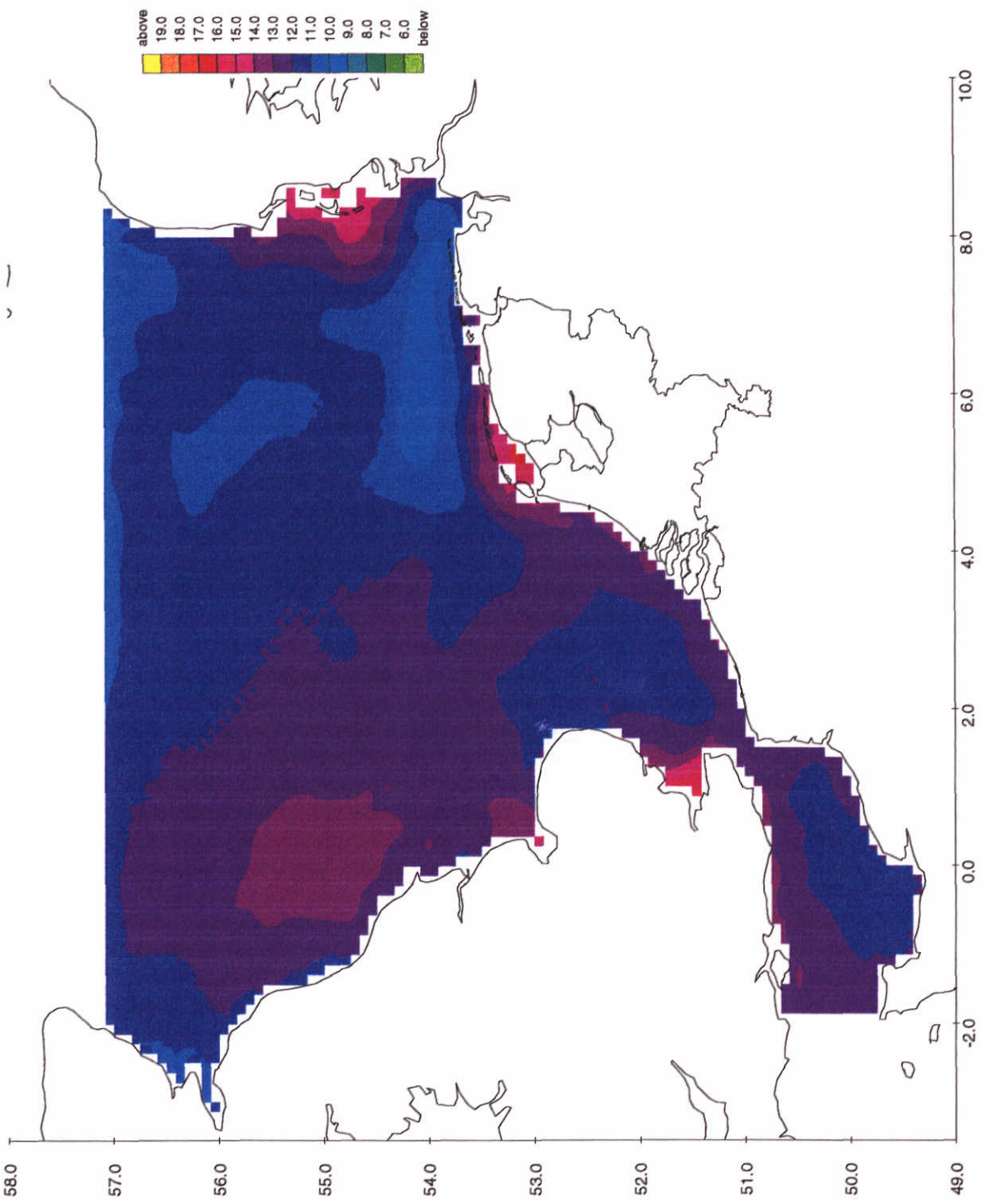

Model results of SST obtained with TRIWAQ/TEM
Date : 1989/05/29 13:00

1998-12-14
12:35:45

DELFT HYDRAULICS

Z-2506

Fig. 4.12

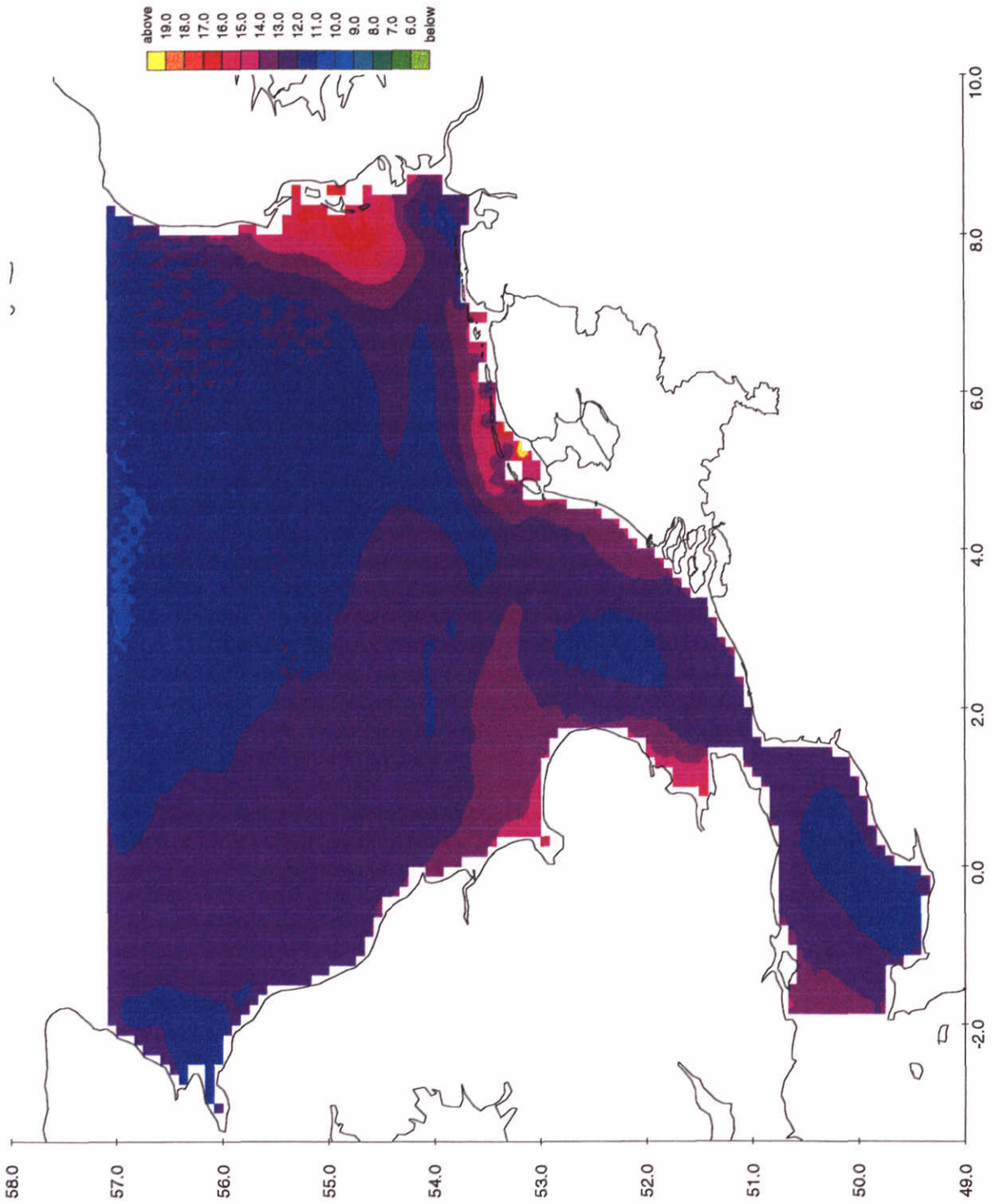

Model results of SST obtained with TRIWAQ/TEM
Date : 1989/06/02 13:00

1998-12-14
12:35:48

DELFT HYDRAULICS

Z-2506

Fig. 4.13

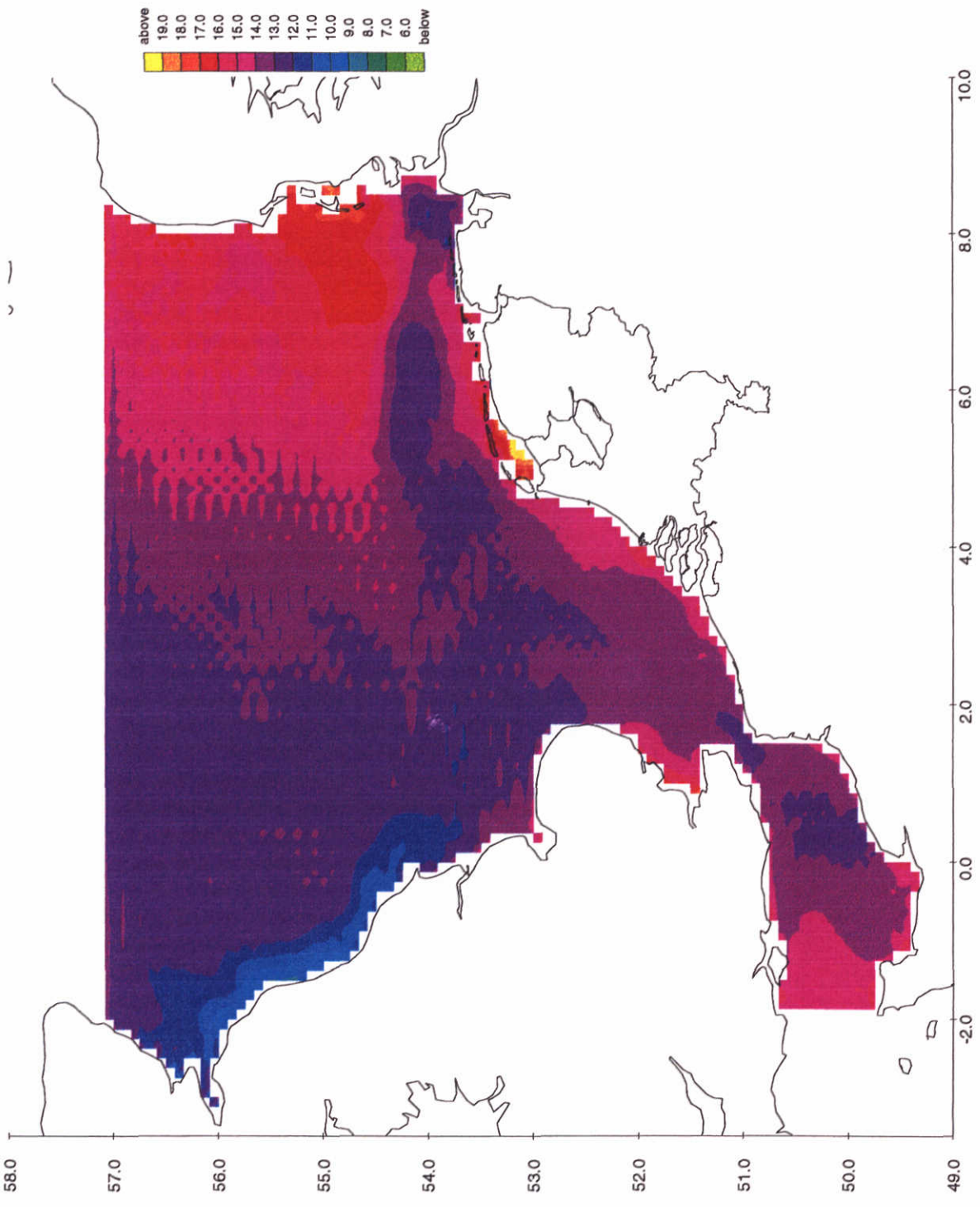

Model results of SST obtained with TRIWAQ/TEM
Date : 1989/06/12 13:00

1998-12-14
12:35:50

DELFT HYDRAULICS | Z-2506 | Fig. 4.14

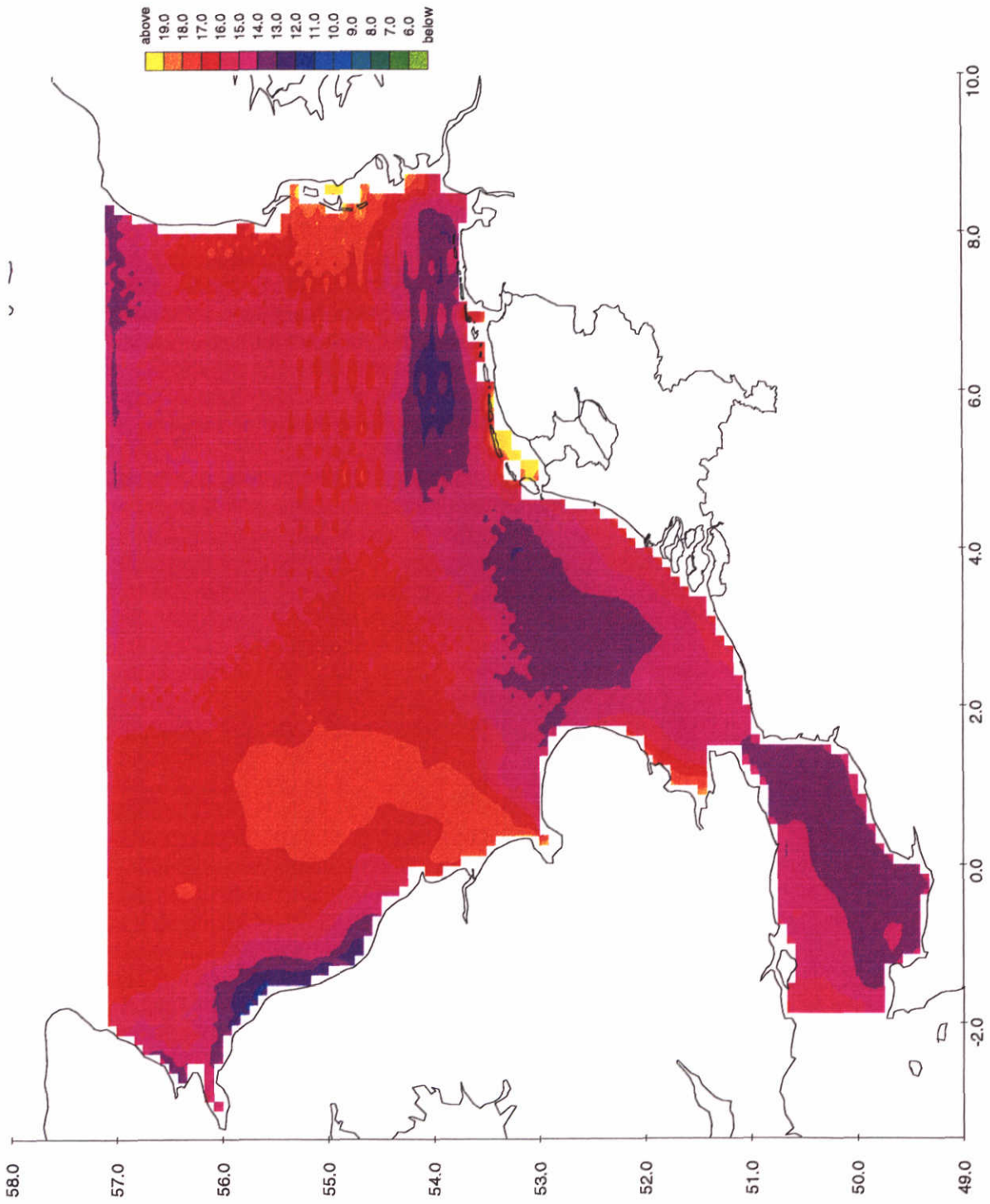

Model results of SST obtained with TRIWAQ/TEM
Date : 1989/06/18 13:00

1998-12-14
12:35:52

DELFT HYDRAULICS

Z-2506

Fig. 4.15

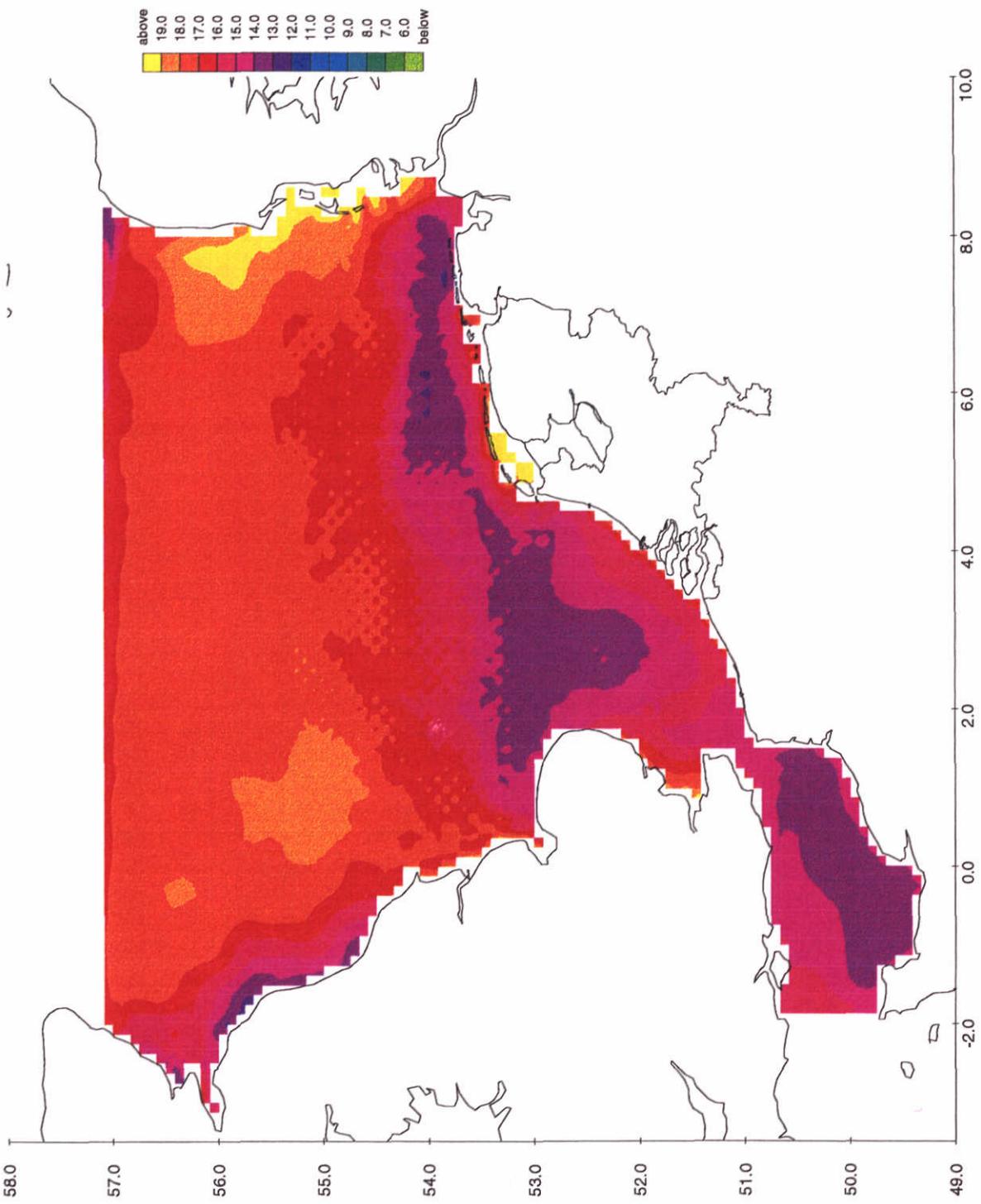

Model results of SST obtained with TRIWAQ/TEM
Date : 1989/06/19 13:00

1998-12-14
12:35:55

DELFT HYDRAULICS

Z-2506

Fig. 4.16

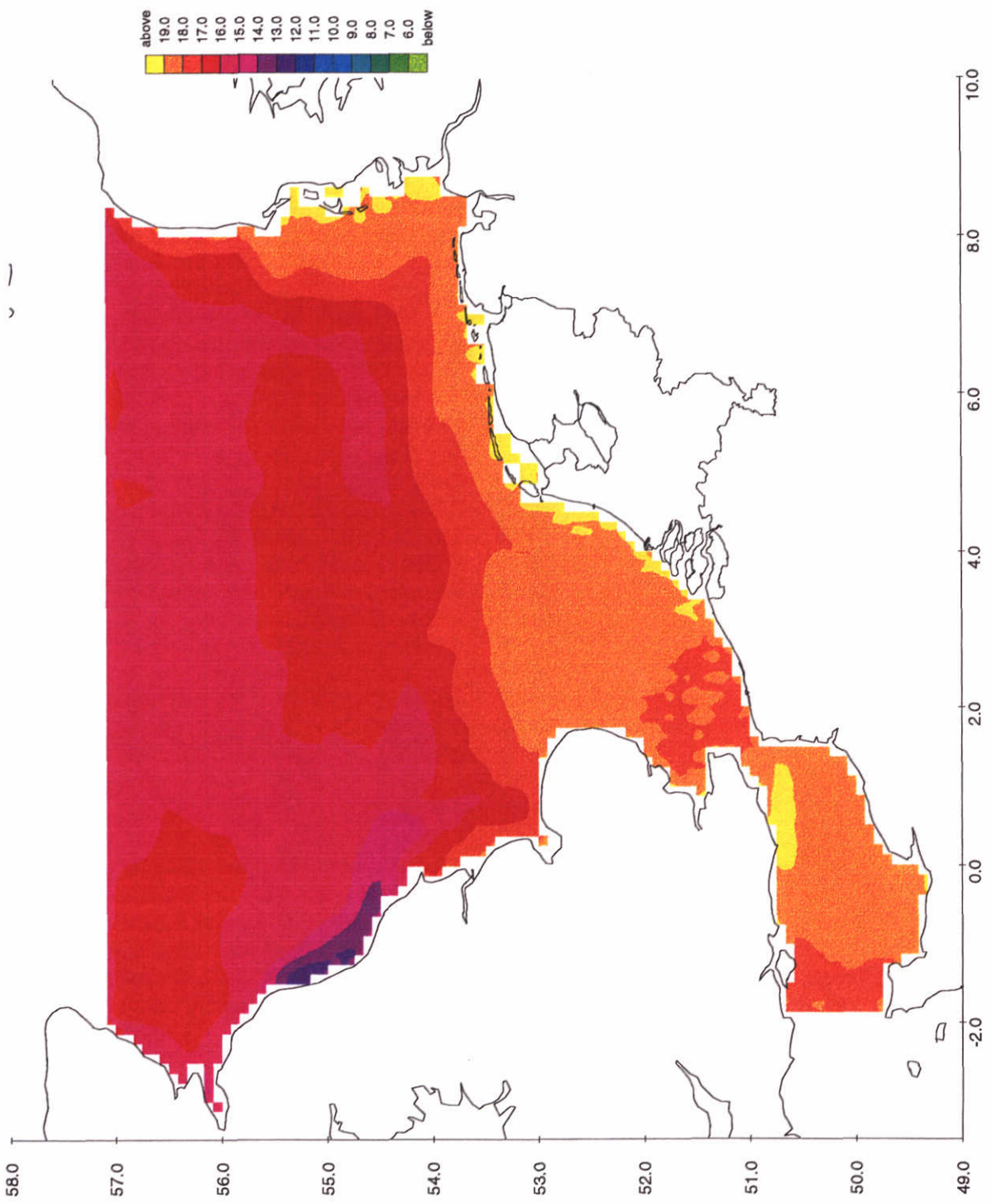

Model results of SST obtained with TRIWAQ/TEM
Date : 1989/08/18 13:00

1998-12-14
12:35:57

DELFT HYDRAULICS

Z-2506

Fig. 4.17

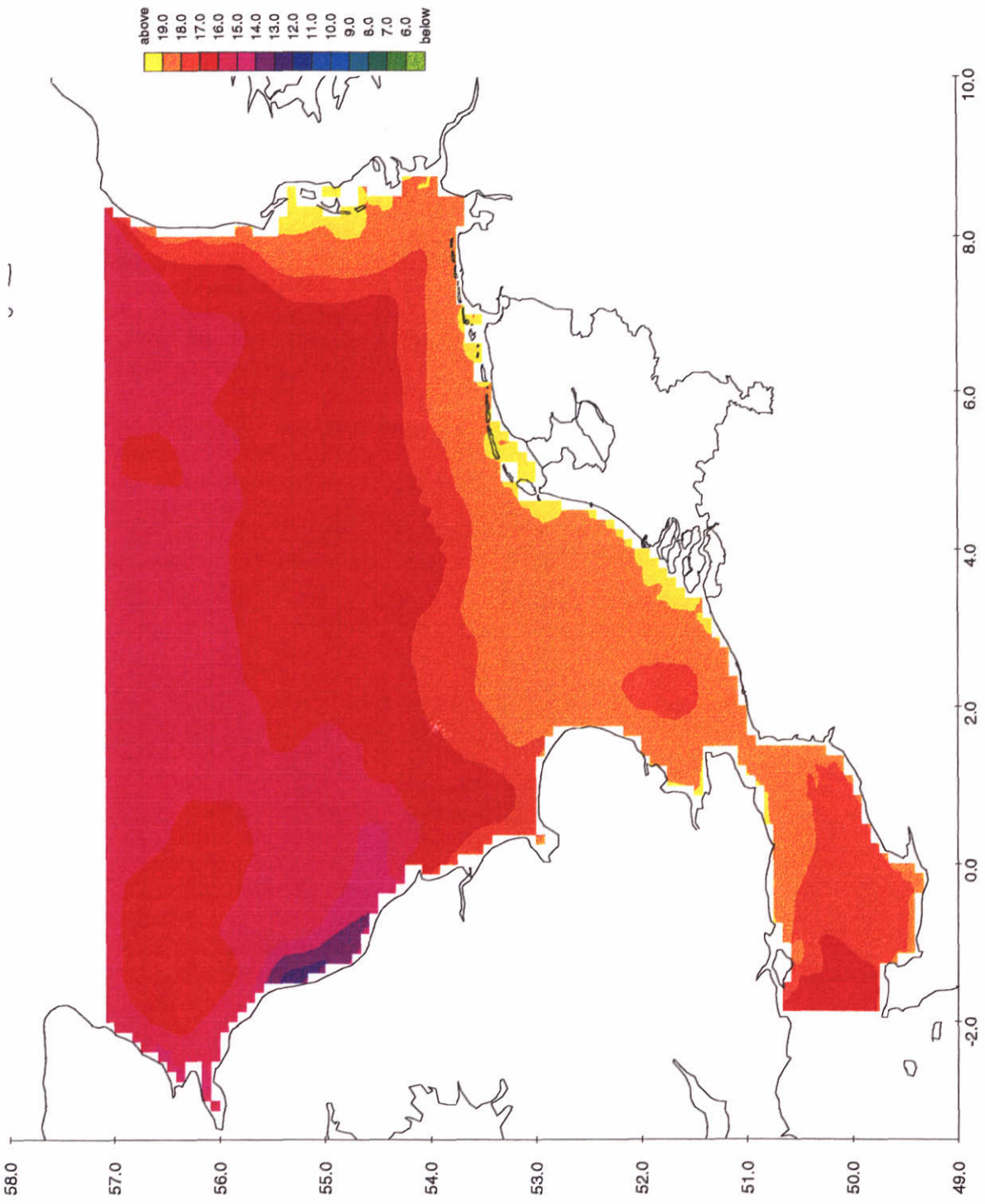

Model results of SST obtained with TRIWAQ/TEM
Date : 1989/08/23 13:00

1998-12-14
12:35:59

DELFT HYDRAULICS

Z-2506

Fig. 4.18

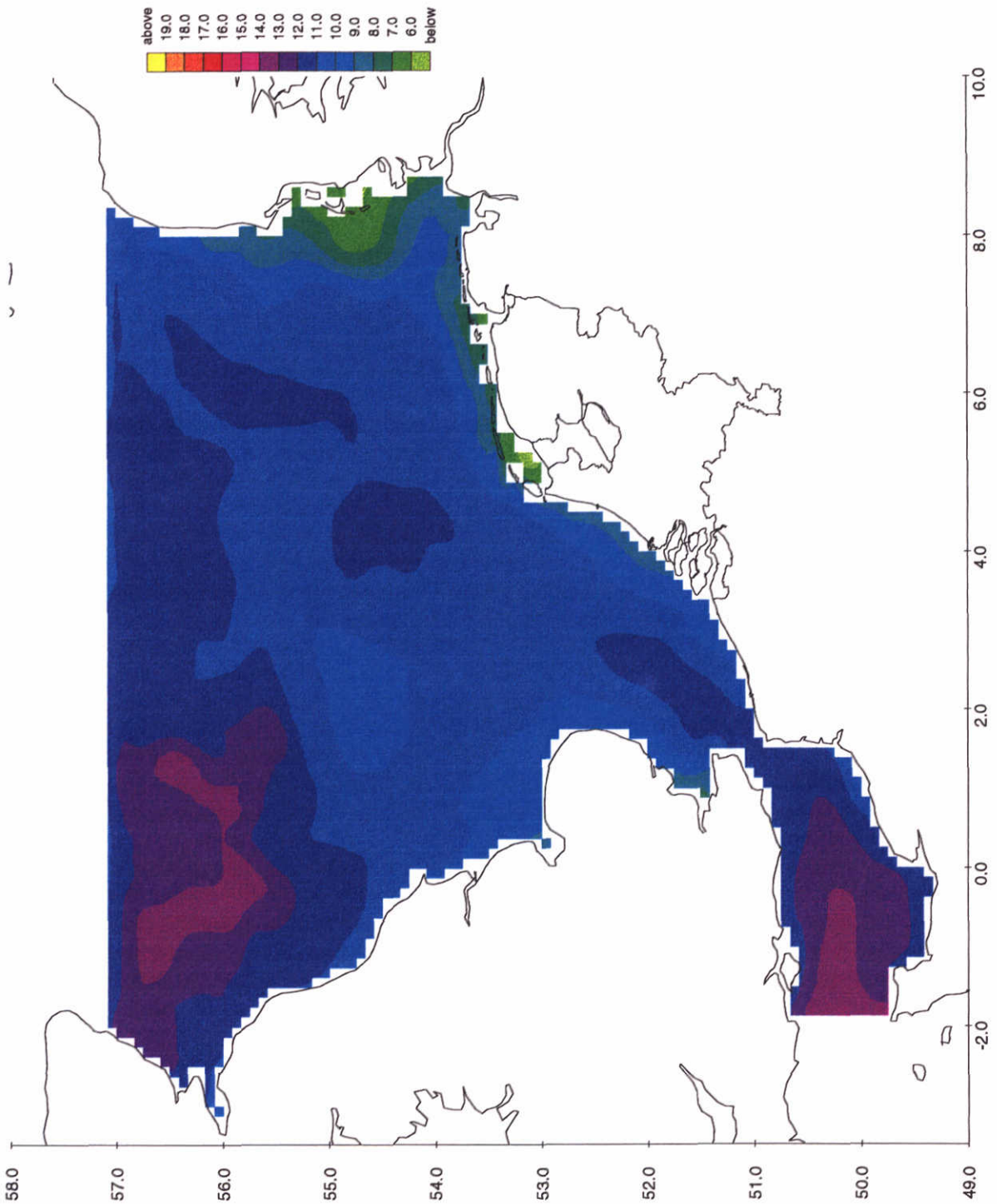

Model results of SST obtained with TRIWAQ/TEM
Date : 1989/11/29 13:00

1998-12-14
12:36:02

DELFT HYDRAULICS

Z-2506

Fig. 4.19

WL | delft hydraulics

Rotterdamseweg 185
postbus 177
2600 MH Delft
telefoon 015 285 85 85
telefax 015 285 85 82
e-mail info@wldelft.nl
internet www.wldelft.nl

Rotterdamseweg 185
p.o. box 177
2600 MH Delft
The Netherlands
telephone +31 15 285 85 85
telefax +31 15 285 85 82
e-mail info@wldelft.nl
internet www.wldelft.nl